CAIO IGOR GONÇALVES CHINELATO

Safe control systems with control barrier function

São Paulo
2022

CAIO IGOR GONÇALVES CHINELATO

Safe control systems with control barrier function

Corrected Version

Thesis presented to the Escola Politécnica da Universidade de São Paulo to obtain the degree of Doctor of Science.

São Paulo
2022

CAIO IGOR GONÇALVES CHINELATO

Safe control systems with control barrier function

Corrected Version

Thesis presented to the Escola Politécnica da Universidade de São Paulo to obtain the degree of Doctor of Science.

Concentration area:

3139 - System engineering

Advisor:

Prof. Dr. Bruno Augusto Angélico

São Paulo
2022

Este exemplar foi revisado e corrigido em relação à versão original, sob responsabilidade única do autor e com a anuência de seu orientador.

São Paulo, 26 de Abril de 2022

Assinatura do autor: 

Assinatura do orientador: 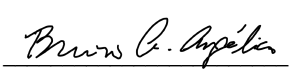

Catalogação-na-publicação

Chinelato, Caio Igor Gonçalves
Safe control systems with control barrier function / C. I. G. Chinelato, B. A. Angélico -- versão corr. -- São Paulo, 2022.
146 p.

Tese (Doutorado) - Escola Politécnica da Universidade de São Paulo. Departamento de Engenharia de Telecomunicações e Controle.

1.Control barrier function 2.Safety 3.Robust control 4.Quadratic programming I.Universidade de São Paulo. Escola Politécnica. Departamento de Engenharia de Telecomunicações e Controle II.t. III.Angélico, Bruno Augusto

ACKNOWLEDGMENTS

To Prof. Dr. Bruno Augusto Angélico, who introduced me the research topic treated in this thesis, and helped me in theoretical analysis, insights, results and publications.

To my parents and friends for supporting me in difficult moments.

To the Laboratório de Controle Aplicado (LCA) of the Escola Politécnica da Universidade de São Paulo (EPUSP) for the availability of experimental resources to obtain the results.

To all professors of Electrical Engineering and Mechanical Engineering graduate programs of EPUSP that teach me fundamental concepts used in the thesis.

To Instituto Federal de São Paulo (IFSP) - Campus São Paulo for giving me support to the PhD.

To Gabriel Pereira das Neves, Mateus Mussi Brugnolli and all the other members of the LCA that helped me in insights, practical experiments and publications.

RESUMO

Este trabalho apresenta abordagens para o controle seguro de sistemas dinâmicos com funções de barreira de controle (CBFs). O sistema deve satisfazer objetivos de estabilidade/rastreamento e restrições de segurança. Os objetivos de estabilidade/rastreamento podem ser satisfeitos através de uma função de Lyapunov de controle (CLF) ou uma lei de controle nominal, como descrito na literatura clássica de controle. Restrições de segurança são especificadas em termos da invariância de um conjunto e verificadas através de CBFs. A existência de uma CBF satisfazendo condições especificas implica na invariância do conjunto e segurança do sistema. A estrutura de controle considerada unifica os objetivos de estabilidade/rastreamento, expressos como uma CLF ou uma lei de controle nominal, e as restrições de segurança, expressas como uma CBF, através de uma programação quadrática (QP). Se os objetivos de estabilidade/rastreamento e as restrições de segurança estão em conflito, a estrutura de controle pondera estes requisitos no sentido da segurança ser sempre priorizada. Inicialmente, uma revisão de literatura com trabalhos relacionados à segurança de sistemas dinâmicos e CBF é apresentada e a formulação básica da estrutura de controle considerada é descrita por CBFs representadas por restrições de segurança de grau relativo unitário. Posteriormente, tópicos avançados são apresentados, tais como CBFs representadas por restrições de segurança de alto grau relativo, CBFs robustas, uma solução explícita sem QP e CBFs de tempo discreto (DCBFs). As principais contribuições deste trabalho são novas formulações para CBFs robustas, onde funções de barreira de controle exponenciais robustas (RECBFs) e funções de barreira de controle com modos deslizantes (SMCBFs) são propostas, a aplicação experimental de uma solução explícita para lidar com restrições de segurança de alto grau relativo e robustas, e aplicações práticas não exploradas na literatura até o momento. Os experimentos são organizados de forma que todos os tópicos tratados na revisão de literatura e as contribuições do trabalho sejam mostrados. Os resultados são apresentados experimentalmente em um pêndulo roda de reação e um pêndulo de Furuta, e numericamente em um sistema de levitação magnética (MAGLEV) com múltiplas entradas e múltiplas saídas (MIMO) e no controle de cruzeiro adaptativo (ACC) aplicado a veículos automotivos. Em todos os casos, os objetivos de estabilidade/rastreamento e as restrições de segurança são satisfeitos.

Palavras-Chave – Função de barreira de controle, Segurança, Controle robusto, Programação quadrática.

ABSTRACT

This work presents approaches for the safe control of dynamical systems with control barrier functions (CBFs). The system must satisfy stability/tracking objectives and safety constraints. Stability/tracking objectives can be satisfied through a control Lyapunov function (CLF) or a nominal control law, as described in classical control literature. Safety constraints are specified in terms of a set invariance and verified through CBFs. The existence of a CBF satisfying specific conditions implies in set invariance and system safety. The control framework considered unifies stability/tracking objectives, expressed as a CLF or a nominal control law, and safety constraints, expressed as a CBF, through quadratic programming (QP). If stability/tracking objectives and safety constraints are in conflict, the control framework mediates these requirements, in the sense that safety is always prioritized. Initially, a literature review with works related to the safety of dynamical systems and CBF is presented and the basic formulation of the considered control framework is described by CBFs represented by relative-degree one safety constraints. Posteriorly, advanced topics are presented, such as CBFs represented by high relative-degree safety constraints, robust CBFs, an explicit solution without QP and discrete-time CBFs (DCBFs). The main contributions of this work are new formulations for robust CBFs, where robust exponential control barrier functions (RECBFs) and sliding mode control barrier functions (SMCBFs) are proposed, the experimental application of an explicit solution to deal with high relative-degree and robust safety constraints, and practical applications not explored in the literature so far. The experiments are organized so that all the topics described in the literature review and the work contributions be covered. The results are presented experimentally in a reaction wheel pendulum and a Furuta pendulum, and numerically in a Multiple-Input-Multiple-Output (MIMO) magnetic levitation system (MAGLEV) and adaptive cruise control (ACC) applied to automotive vehicles. In all cases, stability/tracking objectives and safety constraints are satisfied.

Keywords – Control barrier function, Safety, Robust control, Quadratic programming.

LIST OF FIGURES

LIST OF ABBREVIATIONS

LCA	Laboratório de Controle Aplicado
EPUSP	Escola Politécnica da Universidade de São Paulo
IFSP	Instituto Federal de São Paulo
CBF	Control Barrier Function
RCBF	Reciprocal Control Barrier Function
ZCBF	Zeroing Control Barrier Function
ECBF	Exponential Control Barrier Function
CLF	Control Lyapunov Function
ESCLF	Exponentially Stabilizing Control Lyapunov Function
DESCLF	Discrete-time Exponentially Stabilizing Control Lyapunov Function
DCBF	Discrete-time Control Barrier Function
DECBF	Discrete-time Exponential Control Barrier Function
SMC	Sliding Mode Control
HOCBF	High Order Control Barrier Function
RECBF	Robust Exponential Control Barrier Function
SMCBF	Sliding Mode Control Barrier Function
DCLF	Discrete-time Control Lyapunov Function
QP	Quadratic Programming
NLP	Nonlinear Programming
VIOL	Virtual Input-Output Linearization
ADAS	Advanced Driver Assistance Systems
CC	Cruise Control
ACC	Adaptive Cruise Control
CACC	Cooperative Adaptive Cruise Control
CA	Collision Avoidance
SISO	Single-Input-Single-Output

MIMO	Multiple-Input-Multiple-Output
MPC	Model Predictive Control
MAGLEV	Magnetic Levitation
DOF	Degrees-of-Freedom
PD	Proportional-Derivative
PI	Proportional-Integral
PID	Proportional-Integral-Derivative
LQR	Linear Quadratic Regulator
PWM	Pulse Width Modulation
EMF	Electromotive-Force
CoM	Center of Mass
LMI	Linear Matrix Inequalities

LIST OF SYMBOLS

t	Time
x	System states
x_k	System states (discrete-time)
y	System outputs - time
Y	System outputs - frequency
u	System inputs
u_k	System inputs (discrete-time)
u^*	Final QP-based controller
u_k^*	Final QP-based controller (discrete-time)
u_{no}	Nominal control law
u_{no_d}	Nominal control law (discrete-time)
e_u	Error between u and u_{no}
f	System locally Lipschitz function (real dynamics)
g	System locally Lipschitz function (real dynamics)
$\bar{f}$	System locally Lipschitz function (nominal dynamics)
$\bar{g}$	System locally Lipschitz function (nominal dynamics)
f_d	System locally Lipschitz function (discrete-time)
g_d	System locally Lipschitz function (discrete-time)
B	RCBF
h	ZCBF
h_d	DCBF
C	Safe set
C_d	Safe set (discrete-time)
D	Set related to the states
D_d	Set related to the states (discrete-time)
U	Set related to the inputs

U_d	Set related to the inputs (discrete-time)
V	CLF
V_d	DCLF
γ	Constant related to the CBF
γ_d	Constant related to the DCBF
c_1	Constant related to the CLF
c_2	Constant related to the CLF
c_V	Constant related to the CLF
K_{clf}	Set related to the CLF
ψ_0	Function related to the CLF
ψ_1	Function related to the CLF
ε_{clf}	Constant related to the CLF
δ_{clf}	Constant related to the CLF
γ_{clf}	Constant related to the CLF
a	Constant related to the CLF
b	Constant related to the CLF
k_{so}	Function related to the CLF
c_{1_d}	Constant related to the DCLF
c_{2_d}	Constant related to the DCLF
c_{V_d}	Constant related to the DCLF
α_h	Function related to the ZCBF
α_B	Function related to the RCBF
α_1	Function related to the RCBF
α_2	Function related to the RCBF
κ	Class of functions
a_κ	Constant related to the class of functions κ
K_{zcbf}	Set related to the ZCBF
K_{rcbf}	Set related to the RCBF
δ	Relaxation parameter

δ_d	Relaxation parameter (discrete-time)
p_δ	Weight on the relaxation parameter
p_{δ_d}	Weight on the relaxation parameter (discrete-time)
H	Cost function related to the QP-based controller
F	Cost function related to the QP-based controller
u_h	Human operator control input
u_{cbf}	Control input related to the CBF
I_h	Function related to the explicit solution
J_h	Function related to the explicit solution
K_h	Project parameter related to the explicit solution
C_h	Project parameter related to the explicit solution
z_h	Function related to the explicit solution
k_h	Function related to the explicit solution
v_{he}	Function related to the explicit solution
s_h	Variable related to the explicit solution
L_h	Constant related to the explicit solution
g_b	Safety constraint
γ_b	Constant related to the safety constraint g_b
r	Safety constraint relative-degree
μ_b	Virtual control input related to the ECBF
F_b	Matrix related to the ECBF
G_b	Vector related to the ECBF
C_b	Vector related to the ECBF
η_b	Vector related to the ECBF
K_b	Vector related to the ECBF
p_b	Vector of poles related to the ECBF
p_{b_i}	Poles related to the ECBF
A_b	Matrix related to the ECBF
I_e	Function related to the explicit solution

J_e	Function related to the explicit solution
C_e	Project parameter related to the explicit solution
ψ_{h_r}	Series of functions related to the HOCBF
α_{h_r}	Class κ functions related to the HOCBF
C_{h_r}	Series of sets related to the HOCBF
O_h	Remaining Lie derivatives and partial derivatives related to the HOCBF
K_{hocbf}	Set related to the HOCBF
k_{b_r}	Constants related to the ECBF
μ_c	Virtual control input related to the CLF
Δ_1^b	Model uncertainty related to the RECBF
Δ_2^b	Model uncertainty related to the RECBF
$\Delta_{1,max}^b$	Bound of model uncertainty related to the RECBF
$\Delta_{2,max}^b$	Bound of model uncertainty related to the RECBF
ψ_0^{bv}	Function related to the RECBF
ψ_1^{bv}	Function related to the RECBF
$\psi_{0,bv}^{max}$	Function related to the RECBF
$\psi_{1,bv}^{p}$	Function related to the RECBF
$\psi_{1,bv}^{n}$	Function related to the RECBF
$\psi_{0,bv}^{p}$	Function related to the RECBF
$\psi_{0,bv}^{n}$	Function related to the RECBF
A_r	Function related to the RECBF
b_r	Function related to the RECBF
$\bar{\mu}_b$	Nominal virtual control input
Δ	Model uncertainty related to the SMCBF
$\Delta_{\max}$	Bound of the model uncertainty related to the SMCBF
S_{cbf}	Sliding surface related to the SMCBF
s_{cbf}	Scalar equation related to the SMCBF
λ_{cbf}	Constant related to the SMCBF

h_d	CBF desired value
$\tilde{h}$	CBF error
η_{cbf}	Constant related to the SMCBF
O_{cbf}	Remaining derivatives related to the SMCBF
μ_{eq}	Equivalent control related to the SMCBF
K_{smc}	Gain related to the SMCBF
Φ	Boundary layer thickness related to the SMCBF
α	Pendulum angle (reaction wheel pendulum) [rad]
θ	Wheel angle (reaction wheel pendulum) [rad]
τ	Torque (reaction wheel pendulum) [N·m]
L_r	Lagrangian (reaction wheel pendulum) [J]
K_r	Kinetic energy (reaction wheel pendulum) [J]
V_r	Potential energy (reaction wheel pendulum) [J]
d_{rw}	Number of generalized coordinates or degrees-of-freedom (reaction wheel pendulum)
q_{r_i}	Generalized coordinates (reaction wheel pendulum)
τ_{r_i}	Generalized forces (torques) (reaction wheel pendulum)
m_p	Pendulum mass (reaction wheel pendulum) [kg]
m_r	Reaction wheel mass (reaction wheel pendulum) [kg]
J_p	Pendulum moment of inertia (reaction wheel pendulum) [kg·m^2]
J_r	Reaction wheel moment of inertia (reaction wheel pendulum) [kg·m^2]
l_p	Pendulum length (reaction wheel pendulum) [m]
l_{cp}	Distance to the pendulum center of mass (reaction wheel pendulum) [m]
g	Gravitational acceleration constant [m/s^2]
R_{m_r}	Motor armature resistance (reaction wheel pendulum) [Ω]
i_{m_r}	Motor current (reaction wheel pendulum) [A]
V_{m_r}	Motor voltage (reaction wheel pendulum) [V]
PWM_r	Pulse width modulation signal (reaction wheel pendulum)

K_{e_r}	Back electromotive-force constant (reaction wheel pendulum) [V/(rad/s)]
K_{t_r}	Motor torque constant (reaction wheel pendulum) [N·m/V]
x_{cr}	System states (reaction wheel pendulum)
x_{cr}^*	Equilibrium point (reaction wheel pendulum)
u_{cr}	System input (reaction wheel pendulum)
A_{cr}	State matrix (reaction wheel pendulum)
B_{cr}	Input matrix (reaction wheel pendulum)
f_{cr}	Function related to the reaction wheel pendulum
g_{cr}	Function related to the reaction wheel pendulum
Q_{cr}	Positive-semidefinite matrix related to the continuous-time LQR (reaction wheel pendulum)
R_{cr}	Positive-definite matrix related to the continuous-time LQR (reaction wheel pendulum)
K_{cr}	Gain matrix related to the continuous-time LQR (reaction wheel pendulum)
α_{ref}	Reference Input (reaction wheel pendulum) [rad]
α_{max}	CBF bound (reaction wheel pendulum) [rad]
α_{ini}	Initial pendulum angle (reaction wheel pendulum) [rad]
$u_{no_{cr}}$	Nominal control input (reaction wheel pendulum)
h_{cr}	CBF (reaction wheel pendulum)
$c_{1_{cr}}$	Constant related to the CBF (reaction wheel pendulum)
$c_{2_{cr}}$	Constant related to the CBF (reaction wheel pendulum)
$\alpha_{h_{cr}}$	Function related to the CBF (reaction wheel pendulum)
γ_{cr}	Constant related to the CBF (reaction wheel pendulum)
Δ_{cr}	Encoder resolution (reaction wheel pendulum)
$K_{b_{cr}}$	Vector related to the ECBF (reaction wheel pendulum)
A_c	State matrix related to the continuous-time LQR
B_c	Input matrix related to the continuous-time LQR
K_c	Gain matrix related to the continuous-time LQR
J_c	Performance index related to the continuous-time LQR

Q_c	Positive-semidefinite matrix related to the continuous-time LQR
R_c	Positive-definite matrix related to the continuous-time LQR
P_c	Positive-definite matrix related to the continuous-time LQR
x_{dr_k}	System states (reaction wheel pendulum) - discrete-time
$x^*_{dr_k}$	Equilibrium point (reaction wheel pendulum) - discrete time
u_{dr_k}	System input (reaction wheel pendulum) - discrete time
G_{dr}	State matrix (reaction wheel pendulum) - discrete time
H_{dr}	Input matrix (reaction wheel pendulum) - discrete time
f_{dr}	Function related to the reaction wheel pendulum - discrete time
g_{dr}	Function related to the reaction wheel pendulum - discrete time
T_{dr}	Sampling time (reaction wheel pendulum)
Q_{dr}	Positive-semidefinite matrix related to the discrete-time LQR (reaction wheel pendulum)
R_{dr}	Positive-definite matrix related to the discrete-time LQR (reaction wheel pendulum)
K_{dr}	Gain matrix related to the discrete-time LQR (reaction wheel pendulum)
$u_{no_{dr}}$	Nominal control input (reaction wheel pendulum) - discrete time
h_{dr}	DCBF (reaction wheel pendulum)
A_{dcbf}	Function related to the DCBF (reaction wheel pendulum)
b_{dcbf}	Function related to the DCBF (reaction wheel pendulum)
γ_{dr}	Constant related to the DCBF (reaction wheel pendulum)
G_d	State matrix related to the discrete-time LQR
H_d	Input matrix related to the discrete-time LQR
K_d	Gain matrix related to the discrete-time LQR
J_k	Performance index related to the discrete-time LQR
Q_d	Positive-semidefinite matrix related to the discrete-time LQR
R_d	Positive-definite matrix related to the discrete-time LQR
P_d	Symmetric matrix related to the discrete-time LQR
θ_{0_F}	Arm angle (Furuta pendulum) [rad]

θ_{1_F}	Pendulum angle (Furuta pendulum) [rad]
τ_{m_F}	Torque (Furuta pendulum) [N·m]
m_{0_F}	Arm mass (Furuta pendulum) [kg]
m_{1_F}	Pendulum mass (Furuta pendulum) [kg]
l_{0_F}	Arm length (Furuta pendulum) [m]
l_{1_F}	Pendulum length (Furuta pendulum) [m]
r_F	Radius from fixed axis to pendulum (Furuta pendulum) [m]
d_F	Radius related to center of mass (Furuta pendulum) [m]
L_F	Lagrangian (Furuta pendulum) [J]
K_{0_F}	Kinetic energy of the arm (Furuta pendulum) [J]
K_{1_F}	Kinetic energy of the pendulum (Furuta pendulum) [J]
V_F	Total potential energy (Furuta pendulum) [J]
Q_{0_F}	Generalized force (torque) (Furuta pendulum)
Q_{1_F}	Generalized force (torque) (Furuta pendulum)
I_{0_F}	Moment of inertia of the arm (Furuta pendulum) [kg·m^2]
I_{1_F}	Moment of inertia of the pendulum (Furuta pendulum) [kg·m^2]
R_{m_F}	Motor armature resistance (Furuta pendulum) [Ω]
i_{m_F}	Motor current (Furuta pendulum) [A]
V_{m_F}	Motor voltage (Furuta pendulum) [V]
PWM_F	Pulse width modulation signal (Furuta pendulum)
K_{e_F}	Back electromotive-force constant (Furuta pendulum) [V/(rad/s)]
K_{t_F}	Motor torque constant (Furuta pendulum) [N·m/V]
b_{0_F}	Viscous damping of motor shaft and gearbox (Furuta pendulum) [N·m/rad/s]
b_{1_F}	Viscous damping of pendulum bearing and encoder coupling (Furuta pendulum) [N·m/rad/s]
x_F	System states (Furuta pendulum)
x_F^*	Equilibrium point (Furuta pendulum)
$\theta_{1_F}^*$	Equilibrium point (Furuta pendulum)
u_F	System input (Furuta pendulum)

A_F	State matrix (Furuta pendulum)
B_F	Input matrix (Furuta pendulum)
f_F	Function related to the Furuta pendulum
g_F	Function related to the Furuta pendulum
Q_F	Positive-semidefinite matrix related to the LQR (Furuta pendulum)
R_F	Positive-definite matrix related to the LQR (Furuta pendulum)
K_F	Gain matrix related to the LQR (Furuta pendulum)
$\theta_{0_{Fref}}$	Reference Input (Furuta pendulum) [rad]
$\theta_{1_{Fref}}$	Reference Input (Furuta pendulum) [rad]
$\theta_{1_{Fmax}}$	CBF bound (Furuta pendulum) [rad]
$\theta_{1_{ini}}$	Initial pendulum angle (Furuta pendulum) [rad]
u_{no_F}	Nominal control input (Furuta pendulum)
u_{cbf_F}	Control input related to the CBF (Furuta pendulum)
h_F	CBF (Furuta pendulum)
K_{b_F}	Vector related to the ECBF (Furuta pendulum)
C_{e_F}	Project parameter related to the explicit solution (Furuta pendulum)
λ_{cbf_F}	Constant related to the SMCBF (Furuta pendulum)
η_{cbf_F}	Constant related to the SMCBF (Furuta pendulum)
Φ_F	Boundary layer thickness related to the SMCBF (Furuta pendulum)
K_{smc_F}	Gain related to the SMCBF (Furuta pendulum)
Δ_F	Model uncertainty related to the SMCBF (Furuta pendulum)
$\Delta_{F_{max}}$	Bound of the model uncertainty related to the SMCBF (Furuta pendulum)
V_1	Voltage (MAGLEV) [V]
V_2	Voltage (MAGLEV) [V]
V_3	Voltage (MAGLEV) [V]
i_1	Current (MAGLEV) [A]
i_2	Current (MAGLEV) [A]

i_3	Current (MAGLEV) [A]
F_1	Attractive force (MAGLEV) [N]
F_2	Attractive force (MAGLEV) [N]
F_3	Attractive force (MAGLEV) [N]
r_1	Plate position (MAGLEV) [m]
r_2	Plate position (MAGLEV) [m]
r_3	Plate position (MAGLEV) [m]
X_V	Plate coordinate axis (MAGLEV)
X_p	Plate coordinate axis (MAGLEV)
X_r	Plate coordinate axis (MAGLEV)
O	Plate origin (MAGLEV)
x_v	Vertical gap length (MAGLEV) [m]
θ_p	Pitching angle (MAGLEV) [rad]
θ_r	Rotating angle (MAGLEV) [rad]
M	Mass of the plate (MAGLEV) [kg]
J_{pm}	Moment of inertia around the origin in pitching direction (MAGLEV) [kg·m^2]
J_{rm}	Moment of inertia around the origin in rolling direction (MAGLEV) [kg·m^2]
d_{ml}	Distance between the origin and the center of gravity (MAGLEV) [m]
l_{1g}	Plate parameter (MAGLEV) [m]
l_{2g}	Plate parameter (MAGLEV) [m]
l_{3g}	Plate parameter (MAGLEV) [m]
k_1	Constant related to the electromagnet (MAGLEV) [N·m^2/V]
k_2	Constant related to the electromagnet (MAGLEV) [N·m^2/V]
k_3	Constant related to the electromagnet (MAGLEV) [N·m^2/V]
x_{ml}	State vector (MAGLEV)
w_{ml}	Input vector (MAGLEV)
y_{ml}	Output vector (MAGLEV)

f_{ml}	Function related to the MAGLEV
g_{ml}	Function related to the MAGLEV
o_{ml}	Function related to the MAGLEV
u_{ml}	Voltage command signals (MAGLEV)
r_{1_d}	Reference Input (MAGLEV) [m]
$r_{1_{\max}}$	CBF bound (MAGLEV) [m]
$r_{1_{rs}}$	CBF bound (MAGLEV) [m]
r_{1_b}	CBF bound (MAGLEV) [m]
r_{1_0}	Plate initial position (MAGLEV) [m]
r_{2_d}	Reference Input (MAGLEV) [m]
$r_{2_{\max}}$	CBF bound (MAGLEV) [m]
$r_{2_{rs}}$	CBF bound (MAGLEV) [m]
r_{2_b}	CBF bound (MAGLEV) [m]
r_{2_0}	Plate initial position (MAGLEV) [m]
r_{3_d}	Reference Input (MAGLEV) [m]
$r_{3_{\max}}$	CBF bound (MAGLEV) [m]
$r_{3_{rs}}$	CBF bound (MAGLEV) [m]
r_{3_b}	CBF bound (MAGLEV) [m]
r_{3_0}	Plate initial position (MAGLEV) [m]
$w_{no_{ml}}$	Nominal control input (MAGLEV)
f_{ml_y}	Function related to the MAGLEV
g_{ml_y}	Function related to the MAGLEV
S_{ml_c}	Sliding surface related to the SMC (MAGLEV)
s_{ml_c}	Scalar equation related to the SMC (MAGLEV)
λ_{ml_c}	Constant related to the SMC (MAGLEV)
y_{ml_d}	Reference vector (MAGLEV)
$\tilde{y}_{ml}$	Output error (MAGLEV)
η_{ml_c}	Constant related to the SMC (MAGLEV)
$w_{ml_{eq}}$	Equivalent control related to the SMC (MAGLEV)

$\bar{f}_{ml_y}$	Function related to the MAGLEV (nominal dynamics)
$\bar{g}_{ml_y}$	Function related to the MAGLEV (nominal dynamics)
K_{ml_c}	Gain related to the SMC (MAGLEV)
I	Identity matrix
Φ_{ml_c}	Boundary layer thickness related to the SMC (MAGLEV)
${w_{ml}}^*$	Final QP-based controller (MAGLEV)
h_{ml}	CBF (MAGLEV)
h_1	CBF (MAGLEV)
h_2	CBF (MAGLEV)
h_3	CBF (MAGLEV)
$\mu_{b_{ml}}$	Virtual control input (MAGLEV)
μ_{b_1}	Virtual control input (MAGLEV)
μ_{b_2}	Virtual control input (MAGLEV)
μ_{b_3}	Virtual control input (MAGLEV)
η_{b_1}	Vector related to the ECBF (MAGLEV)
η_{b_2}	Vector related to the ECBF (MAGLEV)
η_{b_3}	Vector related to the ECBF (MAGLEV)
K_{b_1}	Vector related to the ECBF (MAGLEV)
K_{b_2}	Vector related to the ECBF (MAGLEV)
K_{b_3}	Vector related to the ECBF (MAGLEV)
A_{r_1}	Function related to the RECBF (MAGLEV)
A_{r_2}	Function related to the RECBF (MAGLEV)
A_{r_3}	Function related to the RECBF (MAGLEV)
b_{r_1}	Function related to the RECBF (MAGLEV)
b_{r_2}	Function related to the RECBF (MAGLEV)
b_{r_3}	Function related to the RECBF (MAGLEV)
ψ^{max}_{0,bv_1}	Function related to the RECBF (MAGLEV)
ψ^{max}_{0,bv_2}	Function related to the RECBF (MAGLEV)
ψ^{max}_{0,bv_3}	Function related to the RECBF (MAGLEV)

ψ^{p}_{1,bv_1}	Function related to the RECBF (MAGLEV)
ψ^{n}_{1,bv_1}	Function related to the RECBF (MAGLEV)
ψ^{p}_{1,bv_2}	Function related to the RECBF (MAGLEV)
ψ^{n}_{1,bv_2}	Function related to the RECBF (MAGLEV)
ψ^{p}_{1,bv_3}	Function related to the RECBF (MAGLEV)
ψ^{n}_{1,bv_3}	Function related to the RECBF (MAGLEV)
$\Delta^{b}_{1_1,max}$	Bound of model uncertainty related to the RECBF (MAGLEV)
$\Delta^{b}_{2_1,max}$	Bound of model uncertainty related to the RECBF (MAGLEV)
$\Delta^{b}_{1_2,max}$	Bound of model uncertainty related to the RECBF (MAGLEV)
$\Delta^{b}_{2_2,max}$	Bound of model uncertainty related to the RECBF (MAGLEV)
$\Delta^{b}_{1_3,max}$	Bound of model uncertainty related to the RECBF (MAGLEV)
$\Delta^{b}_{2_3,max}$	Bound of model uncertainty related to the RECBF (MAGLEV)
s_{ml_s}	Sliding surface related to the SMCBF (MAGLEV)
Φ_{ml_s}	Boundary layer thickness related to the SMCBF (MAGLEV)
λ_{ml_s}	Matrix related to the SMCBF (MAGLEV)
η_{ml_s}	Vector related to the SMCBF (MAGLEV)
K_{ml_s}	Gain related to the SMCBF (MAGLEV)
$\Delta_{ml_{\max}}$	Bound of the model uncertainty related to the SMCBF (MAGLEV)
v_h	Host vehicle speed (ACC) - time [m/s]
V_h	Host vehicle speed (ACC) - frequency [m/s]
v_{h_0}	Host vehicle initial speed (ACC) [m/s]
a_h	Host vehicle acceleration (ACC) [m/s^2]
v_l	Leader vehicle speed (ACC) [m/s]
x_{l_0}	Leader vehicle initial position (ACC) [m]
x_{h_0}	Host vehicle initial position (ACC) [m]
x_r	Relative distance between the vehicles (ACC) [m]
v_r	Relative speed between the vehicles (ACC) [m/s]
v_c	Cruise speed (ACC) [m/s]

a_h^*	Desired acceleration/deceleration (ACC) [m/s^2]
u_{th}	Control signal provided to the throttle pedal (ACC) - time [%]
U_{th}	Control signal provided to the throttle pedal (ACC) - frequency [%]
u_{br}	Control signal provided to the brake pedal (ACC) [%]
$T_{d_{acc}}$	Sampling time (ACC) [s]
K_{sm}	Controller transfer function - Smith predictor (ACC)
G_n	Nominal system transfer function - Smith predictor (ACC)
G	Real system transfer function - Smith predictor (ACC)
r_e	Reference input - Smith predictor (ACC) - continuous-time
r_{e_k}	Reference input - Smith predictor (ACC) - discrete-time
R_e	Reference input - Smith predictor (ACC) - frequency
e_p	System error - Smith predictor (ACC) - continuous-time
e_{p_k}	System error - Smith predictor (ACC) - discrete-time
τ_d	Time delay - Smith predictor (ACC) [s]
$\hat{y}$	Predicted value for the system output - Smith predictor (ACC)
x_{acc}	System states (ACC) - continuous-time
x_{acc_k}	System states (ACC) - discrete-time
u_{acc}	System input (ACC) - continuous-time
u_{acc_k}	System input (ACC) - discrete-time
y_{acc}	System output (ACC) - continuous-time
y_{acc_k}	System output (ACC) - discrete-time
f_{acc}	Function related to the ACC - continuous-time
f_{acc_d}	Function related to the ACC - discrete-time
g_{acc}	Function related to the ACC - continuous-time
g_{acc_d}	Function related to the ACC - discrete-time
$u_{no_{acc}}$	Nominal control input (ACC)
V_{acc}	CLF (ACC)
h_{acc}	CBF (ACC)

h_{acc_k}	DCBF (ACC)
e_{acc}	Function related to the ACC - continuous-time
e_{acc_k}	Function related to the ACC - discrete-time
$\hat{y}_{acc}$	Predicted value for the system output - Smith predictor (ACC) - continuous-time
$\hat{y}_{acc_{k+\tau_d}}$	Predicted value for the system output - Smith predictor (ACC) - discrete-time
$K_{P_{acc}}$	Proportional gain (ACC)
$K_{I_{acc}}$	Integral gain (ACC)
τ_{th}	Desired time headway (ACC)
$\alpha_{h_{acc}}$	Function related to the CBF (ACC) - continuous-time
γ_{acc}	Constant related to the CBF (ACC) - continuous-time
$c_{V_{acc}}$	Constant related to the CLF (ACC) - continuous-time
δ_{acc}	Relaxation parameter (ACC) - continuous-time
$p_{\delta_{acc}}$	Weight on the relaxation parameter (ACC) - continuous-time
H_{acc}	Cost function related to the QP-based controller (ACC) - continuous-time
F_{acc}	Cost function related to the QP-based controller (ACC) - continuous-time
$\gamma_{d_{acc}}$	Constant related to the DCBF (ACC)
M_h	Host vehicle mass (ACC) [Kg]
F_r	Aerodynamic drag (ACC) [N]
F_w	Wheel force (ACC) [N]
μ_{acc}	Linearized control input (ACC)
T_a	Air temperature (ACC) [K]
C_{ad}	Air drag coefficient (ACC)
A_f	Effective vehicle cross-sectional area (ACC) [m^2]
P_{abs}	Environmental air absolute pressure (ACC) [Pa]
w_x	Longitudinal wind speed along earth-fixed X-axis (ACC) [m/s]
e_h	Acceleration error (ACC)
ϕ_{mf}	Unknown parts of the plant (model-free control)

$\hat{\phi}_{mf}$	Algebraic estimator (model-free control)
α_{mf}	Constant parameter (model-free control)
$\hat{\alpha}_{mf}$	Algebraic estimator (model-free control)
ν	System order (model-free control)
y_d	Set-point (model-free control)
e_{mf}	Error (model-free control)
c_{mf}	Constant related to the model-free control
τ_{mf}	Variable related to the model-free control
K_P	Proportional gain (model-free control)
T	Trapezoidal approximation window (model-free control)
N	Number of elements in the window (model-free control)
T_s	Sampling time (model-free control) [s]
a_{mf}	Constant related to the model-free control
b_{mf}	Constant related to the model-free control
f_{mf}	Function related to the model-free control
f_1	Function related to the model-free control
f_2	Function related to the model-free control
I_1	Function related to the model-free control
I_2	Function related to the model-free control
ϕ_{th}	Unknown parts of the plant (model-free control - throttle)
ϕ_{br}	Unknown parts of the plant (model-free control - brake)
α_{th}	Constant parameter (model-free control - throttle)
α_{br}	Constant parameter (model-free control - brake)
e_{th}	Error (model-free control - throttle)
e_{br}	Error (model-free control - brake)
$K_{P_{th}}$	Proportional gain (model-free control - throttle)
$K_{P_{br}}$	Proportional gain (model-free control - brake)

CONTENTS

1 INTRODUCTION

Two dual concepts related to control systems are liveness and safety. Liveness requires that "good" things eventually happen (ALPERN; SCHNEIDER, 1985). Asymptotic stability can be seen as an example of a liveness property in the sense that an asymptotically stable equilibrium point is eventually reached (AMES et al., 2019). Liveness can be mathematically related to a control Lyapunov function (CLF) or an arbitrary nominal control law. Safety requires that "bad" things do not happen (LAMPORT, 1977). Invariance can be seen as an example of a safety property in the sense that any trajectory starting inside an invariant set will never reach the complement of the set, describing the locus where "bad" things happen (AMES et al., 2019). Safety is represented by constraints in system states or outputs and can be mathematically related to a control barrier functions (CBF). Based on these definitions, it can be argued that safety has received much less attention in control theory than liveness (AMES et al., 2019).

Nowadays, safety is a fundamental concept in several engineering problems, such as control systems, robotics and automotive applications. Safety-critical systems are those that must satisfy control objectives (stability/tracking) and safety constraints, where the safety constraints must be prioritized. Several motivational examples can be considered as safety-critical systems:

- Dynamic balancing of a two-wheeled human transporter (*Segway*): The objective is to ensure safe operation of the system, i.e., the *Segway* does not tip over and always stays upright. A controller must be applied to track a reference input (stability/tracking objective) and to ensure that the *Segway* angular position (system state) never exceeds a predetermined bound (safety constraint);

- Adaptive cruise control (ACC) and lane keeping in automotive vehicles: In the ACC, a controlled vehicle tracks a cruise speed (stability/tracking objective), however when a leader vehicle with lower speed is detected, the controlled vehicle speed (system state) must be adapted in order to maintain a safe distance between the

vehicles (safety constraint). In lane keeping, the vehicle is controlled to stay within a lane identified by cameras (safety constraint);

- Dynamic walking of legged robots: Legged robots are able to locomote over discrete surfaces, such as a terrain with steeping stones with discrete gaps between the steps. Precisely stepping on the footholds is critical and missing the foothold, even by a few centimeters, may cause a dramatic fall of the robotic system. In this sense, the stepping stones can be related to safety constraints that must be strictly enforced (AMES et al., 2019);

The recent works that relate safety constraints and CBFs (AMES et al., 2017), (AMES; GRIZZLE; TABUADA, 2014) suggest that control design techniques based on CLFs can be suitably transposed to address safety considerations (AMES et al., 2019). Then, this work presents approaches for the safe control of dynamical systems with CBFs. The system must satisfy stability/tracking objectives and safety constraints. Stability/tracking objectives can be satisfied through a CLF or a nominal control law, as described in classical control literature. Safety constraints are specified in terms of a set invariance and verified through CBFs. The existence of a CBF satisfying specific conditions implies set invariance and system safety.

The control framework considered unifies stability/tracking objectives, expressed as a CLF or a nominal control law, and safety constraints, expressed as a CBF, through quadratic programming (QP). If stability/tracking objectives and safety constraints are in conflict, the control framework mediates these requirements, in the sense that safety is always prioritized.

1.1 Objective

The main objective is to develop robust CBFs for high relative-degree safety constraints.

Other objectives include:

- The experimental application of an explicit solution to deal with high relative-degree and robust safety constraints;
- Practical applications not explored in the literature so far;

1.2 Justification

Recent works show that CBFs can be applied to safety-critical systems, however they need to be validated in more applications to certify their effectiveness. Then, in this work, some applications are presented to show the effectiveness of the considered control framework and new contributions are described.

Besides that, robustness is an essential topic in safety-critical systems, because if disturbances and model uncertainties are not considered, the CBFs may not respect the safety constraints. Thus, robust CBFs must be studied and applied mainly when high relative-degree safety constraints are considered.

Finally, the considered control framework presents versatility, in the sense that can be applied in linear or nonlinear systems and can be combined with any nominal control law. So, the application possibilities become unlimited.

1.3 Contributions

The main work contributions are:

- The proposition of a robust exponential control barrier function (RECBF) when model uncertainties are considered. The results with the RECBF are verified numerically;
- The proposition of a sliding mode control barrier function (SMCBF) when model uncertainties are considered. The results with the SMCBF are verified numerically and experimentally;
- The experimental application of an explicit solution to deal with high relative-degree and robust safety constraints;
- ACC applied to a generic automotive vehicle considering an upper level controller (outer loop) and a lower level controller (inner loop). The results are presented numerically. The works presented in the literature related to this control strategy only consider the upper level controller;

1.4 Methodology

Initially, a literature review with works related to the safety of dynamical systems and CBF was realized aiming the understanding of theoretical aspects, such as the concepts of CLF and CBF, the basic formulation of the considered control framework for relative-degree one CBFs, high relative-degree CBFs, robust CBFs, an explicit solution to the control framework without QP and discrete-time CBFs (DCBFs).

After the literature review, some numerical tests with well-known systems were performed aiming the comprehension of practical aspects related to the implementation of the considered control framework.

The first results were obtained considering a reaction wheel pendulum (practical application not explored in the literature so far), whose results are presented numerically and experimentally in subsection 6.1. During the execution of the experiments, we observe that robustness is an essential topic in safety-critical systems, mainly in experimental applications were disturbances and model uncertainties exert great influence. Therefore, after obtain these results, the work focus was on theoretical and practical contributions to robust CBFs. So, we propose RECBF and SMCBF. In parallel, we adapt an explicit solution to the considered control framework without QP to deal with high relative-degree and robust safety constraints.

Then, new results were obtained considering a Furuta pendulum (practical application not explored in the literature so far), whose results are presented experimentally in subsection 6.2, and a Multiple-Input-Multiple-Output (MIMO) magnetic levitation system (MAGLEV), whose results are presented numerically in subsection 6.3. In these results, we apply RECBFs, SMCBFs and the explicit solution to deal with high relative-degree and robust safety constraints.

Finally, we obtain results with ACC applied to automotive vehicles, whose results are presented numerically in subsection 6.4. The control framework described in this work has already been applied to the ACC problem. However, the works presented in the literature related to this control strategy do not deal with input delay for the ACC problem and only consider the ACC upper level controller. Here, we consider an upper level controller and a lower level controller that will be described posteriorly.

This thesis is organized as follows: Chapter 2 presents a literature review with works related to the safety of dynamical systems, the definition of CLF and CBF, and the basic formulation of the considered control framework considering QP and an explicit solution.

High relative-degree CBFs, robust CBFs and DCBFs are described in Chapters 3, 4 and 5 respectively. In Chapter 6, the numerical/experimental results are presented. The conclusions and publications are presented in Chapter 7.

2 CONTROL BARRIER FUNCTION (CBF)

This chapter presents the basic concepts related to safety-critical systems and CBF. Initially, a literature review with works related to the safety of dynamical systems and CBF is presented, and posteriorly, the basic formulation of the considered control framework is described for CBFs represented by relative-degree one safety constraints.

2.1 Literature Review

The safety of dynamical systems is represented by constraints in system states or outputs and can be specified in terms of a set invariance (BLANCHINI, 1999). Set invariance is often established through the use of barrier functions (also known as barrier certificates), which in optimization problems, are added to cost functions to avoid undesirable regions (BOYD; VANDENBERGHE, 2004).

Considering an affine control system:

$$\dot{x} = f(x) + g(x)u, \tag{2.1}$$

where $f(x)$ and $g(x)$ are locally Lipschitz, $x \in D \subset \mathbb{R}^n$ are the states and $u \in U \subset \mathbb{R}^m$ are the inputs, there are two types of barrier functions: reciprocal barrier function $B(x)$ and zeroing barrier function $h(x)$. Let C be a set related to the system safety and defined by:

$$\begin{aligned} C &= \{x \in D \subset \mathbb{R}^n : h(x) \geq 0\}, \\ \partial C &= \{x \in D \subset \mathbb{R}^n : h(x) = 0\}, \\ \text{Int}(C) &= \{x \in D \subset \mathbb{R}^n : h(x) > 0\}, \end{aligned} \tag{2.2}$$

where ∂C is the set boundary, we have that $B(x) \to \infty$ as $x \to \partial C$ and $h(x) \to 0$ as $x \to \partial C$ (AMES et al., 2017).

The definition of forward invariance and safety are given respectively by:

Definition 2.1. *Let u be a feedback controller such that (2.1) is locally Lipschitz. For*

any initial condition $x_0 \in D$ there exists a maximum interval of existence $I(x_0)$ such that $x(t)$ is the unique solution to (2.1) on $I(x_0)$. The set C is forward invariant if for every $x_0 \in C$, $x(t) \in C$ for $x(0) = x_0$ and all $t \in I(x_0)$ (AMES et al., 2019).

Definition 2.2. *The system (2.1) is safe with respect to the set C if the set C is forward invariant (AMES et al., 2019).*

The first study to provide necessary and sufficient conditions for set invariance was described by Nagumo's Theorem in the 1940's:

Theorem 2.1. *Given a dynamical system $\dot{x} = f(x)$ with $x \in \mathbb{R}^n$, assuming that the safe set C is the superlevel set of a smooth function $h : \mathbb{R}^n \to \mathbb{R}$, i.e., $C = \{x \in \mathbb{R}^n : h(x) \geq 0\}$, and that $\frac{\partial h}{\partial x}(x) \neq 0$ for all x such that $h(x) = 0$, then C is an invariant set if $\dot{h}(x) \geq 0 \; \forall \; x \in \partial C$ (AMES et al., 2019; NAGUMO, 1942).*

In the 2000's, barrier functions were introduced to prove the safety of nonlinear and hybrid systems using Nagumo's Theorem (PRAJNA; JADBABAIE, 2004), (PRAJNA, 2006), (PRAJNA; RANTZER, 2005).

Nagumo's Theorem gives necessary and sufficient conditions for set invariance considering the boundary of the set. To ensure safety over the entire set, a "Lyapunov-like" approach was proposed in (TEE; GE; TAY, 2009), where a positive definite barrier Lyapunov function $B(x)$ is proposed to guarantee output tracking while preventing output constraint violation for nonlinear systems. The barrier Lyapunov function tends to infinity when it approaches the constraint limits (TEE; GE; TAY, 2009).

The first definition of CBF is presented in (WIELAND; ALLGOWER, 2007). This work presents a safe controller that combines the Sontag's universal control formula (SONTAG, 1989) and a barrier function $B(x)$ to ensure system safety. Based on this idea, (ROMDLONY; JAYAWARDHANA, 2016) propose the concept of control Lyapunov barrier function, where the Sontag's universal control formula is applied to design a feedback control law that satisfies simultaneously stability/tracking objectives, expressed as a CLF, and safety constraints, expressed as a CBF.

Freeman and Kokotovic propose a QP-based controller to satisfy stability/tracking objectives expressed as CLFs (FREEMAN; KOKOTOVIC, 1996). The inequality constraint on the QP is obtained through the CLF's Lie derivatives. Inspired on this idea, (AMES; GRIZZLE; TABUADA, 2014) propose a feedback design problem that unifies stability/tracking objectives, expressed as a CLF and safety constraints, expressed as a CBF, in the sense that safety is always guaranteed. In this approach, a QP-based

controller mediates two inequalities constraints associated with the CLF and the CBF. Relaxation is used to make the stability/tracking objectives as a soft constraint in the QP, while safety is kept as a hard constraint. Then, stability/tracking objectives and safety constraints do not need to be simultaneously met. On the other hand, the formulation proposed in (ROMDLONY; JAYAWARDHANA, 2016) is only applicable when the two objectives can be simultaneously met (XU et al., 2015). More complete and detailed versions of (AMES; GRIZZLE; TABUADA, 2014) can be seen in (AMES et al., 2019) and (AMES et al., 2017). It is important to highlight that we specify the stability/tracking objectives as a soft constraint in the QP. This does not mean that system stability is not considered when the CBF hard constraint is acting because, in this case, the forward invariance of C is ensured as will be described posteriorly and forward invariance is related to the asymptotic stability of C (XU et al., 2015).

The works (TEE; GE; TAY, 2009), (WIELAND; ALLGOWER, 2007) and (ROMDLONY; JAYAWARDHANA, 2016) impose that $\dot{B}(x) \leq 0$. This condition is more restrictive and stronger than necessary because imposes invariance of all sublevel sets. In (AMES; GRIZZLE; TABUADA, 2014), this condition was modified to $\dot{B}(x) \leq \frac{\gamma}{B(x)}$, where γ is a positive constant. This new condition, proposed by (KONG et al., 2013), only requires a single sublevel set to be invariant, allowing $\dot{B}(x)$ to grow when it is far away from the boundary of the set and stop growing when it approaches the boundary of the set. This condition enlarges the set of controls that can guarantee the invariance of a given set and makes the problem less restrictive (XU, 2018).

Besides that, in the approach of (AMES; GRIZZLE; TABUADA, 2014), the stability/tracking objectives can be expressed as any linear or nonlinear nominal control law, such as proportional-integral-derivative (PID), linear quadratic regulator (LQR), feedback linearization and others, making the control design more versatile (AMES et al., 2019), (RAUSCHER; KIMMEL; HIRCHE, 2016), (GURRIET et al., 2018).

Considering these advantages, the approach of (AMES; GRIZZLE; TABUADA, 2014) has been shown more effective and general, and several applications using this methodology are proposed in the literature, such as ACC (MEHRA et al., 2015), lane keeping (XU et al., 2017), bipedal walking robot (NGUYEN; SCREENATH, 2015), robotic manipulator (RAUSCHER; KIMMEL; HIRCHE, 2016), two-wheeled human transporter (*Segway*) (GURRIET et al., 2018), quadrotors (WU; SREENATH, 2016) and multi-robot systems (WANG; AMES; EGERSTEDT, 2017); thus, this approach is considered in this work.

Model predictive control (MPC) is an example of a controller that considers an opti-

mization problem and state constraints, similarly to described in the approach of (AMES; GRIZZLE; TABUADA, 2014). However, MPC needs predictions of future states to generate the control input and safety constraints are usually enforced as distance constraints defined under Euclidean norms, which for some problems are only solved using a large horizon (ZENG; ZHANG; SREENATH, 2021). Thus, MPC increases the computational complexity and presents feasibility problems in the optimization for some situations. Some works described that these issues can be solved integrating MPC and CBF. In (ZENG; ZHANG; SREENATH, 2021), MPC and DCBF are unified and applied to an obstacle avoidance problem. The work (SON; NGUYEN, 2019) incorporates continuous-time CBF into a nonlinear MPC framework. The objectives are to ensure safety in infinite prediction horizon, improve nonlinear MPC performance and reduce computational burden. The work (ROSOLIA; AMES, 2021) proposes a control design that express CBF as a low level control and the MPC as a high level planning.

2.2 Control Lyapunov Function (CLF)

One of the modern control design tools for the stabilization of nonlinear systems is the application of CLFs. As previously described, the main ideas to obtain safe controllers with CBFs are inspired in concepts related to CLFs. In (WIELAND; ALLGOWER, 2007) and (ROMDLONY; JAYAWARDHANA, 2016), the Sontag's universal control formula is applied and in (AMES; GRIZZLE; TABUADA, 2014), the QP-based controller introduced by Freeman and Kokotovic is applied. As this work considers the approach proposed by (AMES; GRIZZLE; TABUADA, 2014), in this section, the QP-based controller presented by Freeman and Kokotovic is described. The Sontag's universal control formula is shown in Appendix A.

Initially, we define Lie derivative:

Definition 2.3. *Let $V : \mathbb{R}^n \to \mathbb{R}$ be a smooth scalar function, and $f : \mathbb{R}^n \to \mathbb{R}^n$ be a smooth vector field on $\mathbb{R}^n$, then the Lie derivative of V with respect to f is a scalar function defined by $L_f V = \nabla V f$ (SLOTINE; LI, 1991).*

The main idea is that a feedback controller u can stabilize the system (2.1) if it satisfies

$$\dot{V}(x) = L_f V(x) + L_g V(x) u \leq -c_V V(x), \tag{2.3}$$

where c_V is a positive constant and $V(x)$ is an exponentially stabilizing control Lyapunov function (ESCLF) for the system (2.1), referred in this work simply as CLF, defined as:

Definition 2.4. *A continuously differentiable function $V(x) : \mathbb{R}^n \to \mathbb{R}$ is an ESCLF if there exist positive constants $c_1, c_2, c_V > 0$ such that for all x, the following inequalities hold (AMES et al., 2014), (AMES et al., 2017):*

$$c_1 \|x\|^2 \leq V(x) \leq c_2 \|x\|^2, \tag{2.4}$$

$$\inf_{u \in U} \left[L_f V(x) + L_g V(x) u + c_V V(x) \right] \leq 0. \tag{2.5}$$

The existence of an ESCLF yields a family of controllers that exponentially stabilize the system to the zero dynamics (AMES et al., 2017). In particular, consider the set

$$K_{clf}(x) = \left\{ u \in U : L_f V(x) + L_g V(x) u + c_V V(x) \leq 0 \right\}. \tag{2.6}$$

It follows that a locally Lipschitz controller $u(x)$ satisfies

$$u(x) \in K_{clf}(x) \Rightarrow \|x(t)\| \leq \sqrt{\frac{c_2}{c_1}} e^{-\frac{c_V}{2} t} \|x(0)\|, \tag{2.7}$$

i.e., inequality constraints on CLF's Lie derivatives are imposed to obtain entire classes of controllers that stabilize the system (2.1) and c_V is the design parameter related to the convergence rate to the stabilization.

Freeman and Kokotovic propose the QP-based controller $u^*(x)$, defined pointwise as the element of $K_{clf}(x)$ having minimum Euclidean norm, such as (FREEMAN; KOKOTOVIC, 1996):

$$\begin{aligned} u^*(x) = & \underset{u \in \mathbb{R}^m}{\arg\min} \ \tfrac{1}{2} u^T u \\ s.t. \ & \psi_0(x) + \psi_1^T(x) u \leq 0, \end{aligned} \tag{2.8}$$

where

$$\begin{aligned} \psi_0(x) &= L_f V(x) + c_V V(x), \\ \psi_1(x) &= L_g V(x)^T. \end{aligned} \tag{2.9}$$

The closed-form solution of the QP (2.8) is given by (AMES et al., 2014):

$$u^*(x) = \begin{cases} -\frac{\psi_0(x)\psi_1(x)}{\psi_1(x)^T \psi_1(x)} & if \ \ \psi_0(x) > 0 \\ 0 & if \ \ \psi_0(x) \leq 0. \end{cases} \tag{2.10}$$

These controllers have been applied and executed experimentally to achieve bipedal walking on a human-sized robot (GALLOWAY et al., 2015), for example.

2.3 CBF - Definition

As previously mentioned, the safety of dynamical systems is represented by constraints in system states or outputs and can be specified in terms of a set C defined by (2.2). The system is safe with respect to the set C if the set C is forward invariant, as described Definitions 2.1 and 2.2. If $B(x)$ or $h(x)$ satisfies "Lyapunov-like" conditions, then forward invariance of C is guaranteed (AMES et al., 2019).

The main idea is that a feedback controller u can render the set C forward invariant if it allows $\dot{B}(x)$ to grow when it is far away from the boundary of the set C, i.e.,

$$\dot{B}(x) = L_f B(x) + L_g B(x)u \leq \frac{\gamma}{B(x)}, \tag{2.11}$$

or it allows $\dot{h}(x)$ to decrease when it is far away from the boundary of the set C, i.e.,

$$\dot{h}(x) = L_f h(x) + L_g h(x)u \geq -\gamma h(x), \tag{2.12}$$

where γ is a positive constant and the conditions (2.11) and (2.12) are proposed by (KONG et al., 2013) as previously described. As shown for CLFs, in CBFs, inequality constraints on the CBF's Lie derivatives are imposed to obtain entire classes of controllers that render the set C forward invariant.

Some works apply $B(x)$, such as (AMES et al., 2017), (MEHRA et al., 2015) and (RAUSCHER; KIMMEL; HIRCHE, 2016), and other works apply $h(x)$, such as (XU et al., 2017) and (GURRIET et al., 2018). The work (AMES et al., 2017) suggests that unbounded function values may be undesirable when real-time/embedded implementations are considered. Therefore, as $B(x)$ tends to infinity as its argument approaches the boundary of C, $h(x)$ may be a more reasonable choice for some applications, and the definitions and the controllers are described in this work considering $h(x)$. The equivalent definitions and controllers considering $B(x)$ are described in Appendix B.

Next, we formalize the definitions of ZCBF and describe the feedback controller u that render the set C forward invariant.

Definition 2.5. *A continuous function $\alpha_h : [0, a_\kappa) \to [0, \infty)$ for some $a_\kappa > 0$ is said to belong to class κ if it is strictly increasing and $\alpha_h(0) = 0$ (AMES et al., 2017).*

Definition 2.6. *Consider the control system (2.1) and a set C defined by (2.2) for a continuously differentiable function $h(x) : \mathbb{R}^n \to \mathbb{R}$. The function $h(x)$ is called a ZCBF defined on set D (defined in (2.1)) with $C \subseteq D \subset \mathbb{R}^n$, if there exists an extended class κ*

function α_h such that (AMES et al., 2017)

$$\sup_{u \in U} \left[L_f h(x) + L_g h(x) u + \alpha_h(h(x)) \right] \geq 0, \forall x \in D. \tag{2.13}$$

Given a ZCBF $h(x)$, for all $x \in D$, define the set (AMES et al., 2017)

$$K_{zcbf}(x) = \left\{ u \in U : L_f h(x) + L_g h(x) u + \alpha_h(h(x)) \geq 0 \right\}. \tag{2.14}$$

Considering control values in this set, the forward invariance of C is guaranteed by the following corollary:

Corollary 2.1. *Consider a set C defined by (2.2) and let $h(x)$ be a ZCBF for the system (2.1). Then any Lipschitz continuous controller $u : D \to U$ such that $u(x) \in K_{zcbf}(x)$ will render the set C forward invariant (AMES et al., 2017).*

Typically, it is considered $\alpha_h(h(x)) = \gamma h(x)$ as described in (2.12).

It is important to highlight that the safe set C (2.2), the ZCBF $h(x)$ and the RCBF $B(x)$ are defined considering only the states x. However, the works (HUANG; YONG; CHEN, 2021) and (HUANG; YONG; CHEN, 2019) define the concept of control-dependent invariant set and control-dependent barrier function, where the safe set and the CBF are defined considering the states x and the inputs u simultaneously.

2.4 Control Framework

This section presents the control framework proposed by (AMES; GRIZZLE; TABUADA, 2014) that unifies the stability/tracking objectives, expressed as a CLF or a nominal control law u_{no}, and the safety constraints, expressed as a CBF, through QP. Figs. 1a and 1b present a synthesized description of the control framework when stability/tracking objectives are expressed as a CLF and as a nominal control law u_{no} respectively. The expression for the final QP-based controller $\mathbf{u}^*$ will be described in the next subsections.

Figure 1: Synthesized description of the control framework.

(a) Stability/tracking objectives expressed as a CLF.

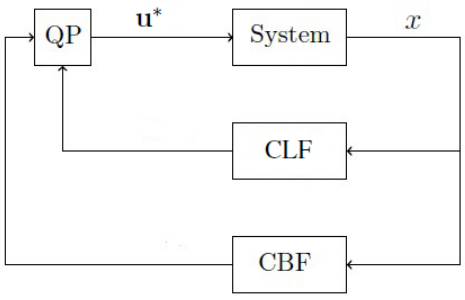

(b) Stability/tracking objectives expressed as a nominal control law u_{no}.

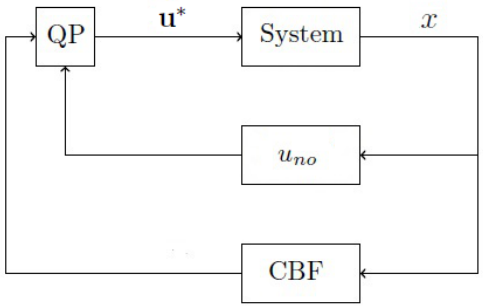

Source: Author.

2.4.1 Unifying CLF and CBF Through Quadratic Programming (QP)

Given a CBF $h(x)$ associated with a set C defined by (2.2) and a CLF $V(x)$, they can be integrated into a single controller through a QP such as (AMES et al., 2017):

$$\begin{aligned} \mathbf{u}^*(x) = & \underset{\mathbf{u}=(u,\delta)\in\mathbb{R}^m\times\mathbb{R}}{\arg\min} \ \tfrac{1}{2}\mathbf{u}^T H(x)\mathbf{u} + F(x)^T\mathbf{u} \\ s.t. \ & L_f V(x) + L_g V(x)u + c_V V(x) - \delta \leq 0, \\ & L_f h(x) + L_g h(x)u + \alpha_h(h(x)) \geq 0, \end{aligned} \tag{2.15}$$

where the constraints related to CLF and CBF are described in (2.5) and (2.13), respectively, $H(x) \in \mathbb{R}^{(m+1)\times(m+1)}$ and $F(x) \in \mathbb{R}^{m+1}$. The matrix $H(x)$ is constituted by the penalty weight p_δ that multiplies the relaxation parameter δ in order to make the stability/tracking objectives as a soft constraint in the QP, while safety is kept as a hard constraint. The parameter c_V is related to the convergence rate to the stabilization while the CLF is acting to satisfy the stability/tracking objectives. Typically, it is considered $\alpha_h(h(x)) = \gamma h(x)$ and γ specifies how far from the barrier limit the CBF acts to satisfy the safety constraints. Therefore, the design parameters are p_δ, c_V and γ. The controller (2.15) is graphically represented in Fig. 1a.

As described in (AMES; GRIZZLE; TABUADA, 2014) and (MEHRA et al., 2015), magnitude constraints for the input u can also be applied in the QP-based controller (2.15). In this case, an additional relaxation parameter must be considered.

The following Theorem provides a sufficient condition for $\mathbf{u}^*(x)$ in (2.15) to be locally Lipschitz continuous in Int(C), thereby guaranteeing local existence and uniqueness of solutions to the closed-loop system, and the applicability of Corollary 2.1 (AMES et al.,

2017).

Theorem 2.2. *Suppose that the following functions are all locally Lipschitz: the vector fields f and g in the control system (2.1), the gradients of h and V, and the cost function terms $H(x)$ and $F(x)$ in (2.15). Then $\mathbf{u}^*(x)$ in (2.15) is locally Lipschitz continuous for $x \in \text{Int}(C)$ (AMES et al., 2017) and renders the set C defined by (2.2) forward invariant.*

2.4.2 Unifying Nominal Control Law and CBF Through QP

Another approach for the control framework unifies stability/tracking objectives, expressed as any linear or nonlinear nominal control law, and safety constraints, represented by a CBF, through QP. This approach makes the control design more versatile (AMES et al., 2019), (RAUSCHER; KIMMEL; HIRCHE, 2016), (GURRIET et al., 2018).

Suppose any linear or nonlinear nominal control law u_{no}, such as a PID, a LQR or a feedback linearization, for the control system (2.1). The idea here is to consider that the safety constraint modifies the nominal control law in a minimal way, just when the states are approaching the border of the safe set, so that the final control u satisfies the Corollary 2.1. Therefore, the final controller is formulated as an optimization problem minimizing the error (RAUSCHER; KIMMEL; HIRCHE, 2016)

$$e_u = u_{no} - u. \tag{2.16}$$

The squared norm of the error

$$\|e_u\|^2 = u^T u - 2u_{no}^T u + u_{no}^T u_{no} \tag{2.17}$$

is considered as the objective function. The last term of (2.17) is neglected, since it is constant in a minimization process with respect to u. Thus, we can consider the following QP-based controller (AMES et al., 2019), (RAUSCHER; KIMMEL; HIRCHE, 2016):

$$\begin{aligned} &\mathbf{u}^*(x) = \underset{u \in \mathbb{R}^m}{\arg\min}\ u^T u - 2u_{no}^T u \\ &s.t.\ \ L_f h(x) + L_g h(x) u + \alpha_h(h(x)) \geq 0, \end{aligned} \tag{2.18}$$

where the constraint related to the CBF is defined in (2.13) and typically, $\alpha_h(h(x)) = \gamma h(x)$. A block diagram of this scheme is represented in Fig. 1b. It is important to highlight that the relaxation parameter δ is unnecessary since the nominal control law u_{no} is on the objective function and there are no constraints related to stability/tracking objectives.

Similarly to described in the last subsection, the following theorem provides a sufficient condition for $\mathbf{u}^*(x)$ in (2.18) to be locally Lipschitz, thereby guaranteeing local existence and uniqueness of solutions to the closed-loop system, and the applicability of Corollary 2.1.

Theorem 2.3. *Consider the control system (2.1), a locally Lipschitz nominal control law u_{no}, and a CBF h associated with a set C defined by (2.2). Supposing that the system (2.1) is controllable within the entire constrained space and the set C is not empty, then $\mathbf{u}^*(x)$ in (2.18) is Lipschitz continuous and renders the set C defined by (2.2) forward invariant (RAUSCHER; KIMMEL; HIRCHE, 2016).*

2.4.3 QP Problem Solutions

It is important to highlight how to solve the QP problem for simulations and practical embedded applications. In (AMES et al., 2017), a closed-form solution for the QP (2.15) is proposed. However, in most cases, numerical methods are applied. Matlab functions such as *fmincon* or *quadprog* can be applied for simulations. For practical embedded applications, packages such as *CVXGEN* can be considered (MATTINGLEY; BOYD, 2012). *CVXGEN* generates custom code using an online interface with no software installation. With minimal effort, turn a mathematical problem description into a high speed solver. Besides that, in (HILDRETH, 1957), Hildreth's QP procedure is proposed, which is a simple and practical numerical method that can be applied for simulations and practical embedded applications.

2.5 Explicit Solution

This section presents an explicit solution proposed in (IGARASHI; TEZUKA; NAKAMURA, 2019). This approach considers a safety assist control with a human operation. The stability/tracking objectives are expressed as a human operator control input and the safety constraints are expressed as a CBF. In this control framework, QP is not used and the final control is obtained as an explicit solution. It is important to highlight that the human operator control input can be considered as a nominal control law.

The inputs of the dynamical system (2.1) are represented by $u = u_h + u_{cbf}$, where u_h is the human operator control input and u_{cbf} is a control input related to the CBF. As described above, in this work, u_h is considered as a nominal control law u_{no}. The block diagram of the explicit solution is described in Fig. 2.

Figure 2: Block diagram of the explicit solution.

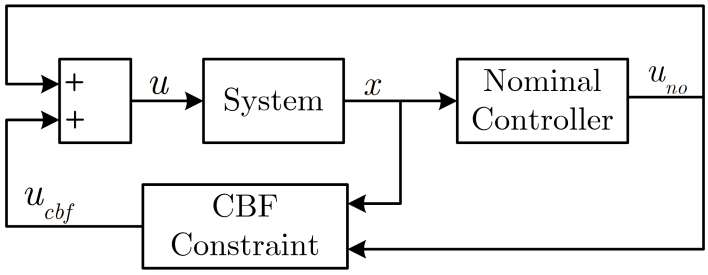

Source: Author.

The work (IGARASHI; TEZUKA; NAKAMURA, 2019) express the safety constraint as a RCBF $B(x)$, however, in this work, the explicit solution is adapted to express the safety constraint as a ZCBF $h(x)$. Thus, the control input u_{cbf} can be obtained by (IGARASHI; TEZUKA; NAKAMURA, 2019):

$$u_{cbf} = \begin{cases} -\frac{I_h(x,u_{no})-J_h(x)}{\|L_g h(x)\|^2}(L_g h(x))^T & if \;\; I_h(x,u_{no}) < J_h(x) \\ 0 & if \;\; I_h(x,u_{no}) \geq J_h(x), \end{cases} \tag{2.19}$$

where functions $I_h : \mathbb{R}^n \times \mathbb{R}^m \to \mathbb{R}$ and $J_h : \mathbb{R}^n \to \mathbb{R}$ are defined by:

$$\begin{aligned} I_h(x,u_{no}) &= L_f h(x) + L_g h(x) u_{no}, \\ J_h(x) &= K_h h(x) + C_h, \end{aligned} \tag{2.20}$$

where K_h and C_h are design parameters. Equation (2.19) is an explicit solution to the QP-based controller (2.18) considering $u = u_{no} + u_{cbf}$. The Appendix C describes how the explicit solution is obtained considering the RCBF $B(x)$.

The results obtained with the explicit solution are very similar to the results obtained with the QP-based control framework. However, the explicit solution is computationally advantageous, because the QP does not need to be solved at each sampling time. The disadvantage is that the explicit solution cannot be applied to multiple CBFs.

It is important to highlight that the results presented in (IGARASHI; TEZUKA; NAKAMURA, 2019) are verified only numerically and, in this work, the results are verified both numerically and experimentally.

3 HIGH RELATIVE-DEGREE CBF

Initially, the definition of relative-degree is presented.

Definition 3.1. *The relative-degree of a continuously differentiable function* $h(x) : \mathbb{R}^n \to \mathbb{R}$ *with respect to system (2.1) is the number of times we need to differentiate it along the dynamics of (2.1) until control* u *explicitly shows (KHALIL, 2002), (XIAO; BELTA, 2019).*

The control framework described in the last chapter is only applicable for relative-degree one safety constraints. However, in several systems, high relative-degree safety constraints (greater that one) are considered. In this case, as $L_g h(x) = 0$, the QP described in (2.15) or in (2.18) cannot be solved. Some solutions are presented in the literature to deal with high relative-degree safety constraints.

Consider a relative-degree two safety constraint $g_b(x)$. The work (WU; SCREENATH, 2015) proposes a simple and practical solution that considers the CBF

$$h(x, \dot{x}) = \gamma_b g_b(x) + \dot{g}_b(x, \dot{x}), \tag{3.1}$$

where $\gamma_b > 0$. This new CBF uses the constraint $g_b(x)$ and has relative-degree one. A similar solution can be seen in (TAYLOR et al., 2020). This solution has the limitation to be applied only for relative-degree two safety constraints. In (HSU; XU; AMES, 2015), a backstepping-based method is applied to arbitrary high relative-degree safety constraints.

In (NGUYEN; SREENATH, 2016a), the concept of exponential control barrier function (ECBF) is introduced as a way to systematically enforce high relative-degree safety constraints. (NGUYEN; SREENATH, 2016a) employs a virtual input-output linearization (VIOL) and applies a pole placement controller in the virtual control input to drive the CBF to zero. In (XIAO; BELTA, 2019), a simpler and more general formulation of CBF to deal with high relative-degree safety constraints, called high order control barrier function (HOCBF), is proposed. The HOCBFs are determined by a set of class κ functions given in Definition 2.5. The general form of these HOCBFs is associated with the forward

invariance of the intersection of a series of sets and can be adapted to different types of systems and constraints. (XIAO; BELTA, 2019) show that HOCBF can be related to ECBF. HOCBF is defined in Appendix D.

3.1 Exponential CBF (ECBF)

The concept of ECBF is introduced in (NGUYEN; SREENATH, 2016a), where in the final control framework, the stability/tracking objectives are expressed as a CLF and the ECBF is derived based on the RCBF $B(x)$. However, in this work, the formulation of (NGUYEN; SREENATH, 2016a) is adapted in order to express the stability/tracking objectives as a nominal control law, such as in (2.18), and the ECBF is derived based on the ZCBF $h(x)$, such as in (AMES et al., 2019). The term ECBF is used since the resulting CBF constraint is an exponential function of the initial condition (NGUYEN; SREENATH, 2016a).

In (AMES et al., 2014), a systematic procedure using input-output linearization to design CLFs for regulating outputs with arbitrary relative-degree is described. This procedure could be applied to design CBFs for constraints with arbitrary relative-degree r. However, this procedure is not directly feasible to $\dot{h}(x,u) = L_f h(x) + L_g h(x)u$, because the term $(L_g h(x))^{-1}$ must be applied, and $L_g h(x)$ is a vector when $m > 1$ in (2.1), and obviously not invertible (NGUYEN; SREENATH, 2016a). The work (NGUYEN; SREENATH, 2016a) introduces the notion of VIOL wherein an invertible decoupling matrix is not required. Considering a virtual control input μ_b defined as

$$h^{(r)}(x,u) = L_f^r h(x) + L_g L_f^{r-1} h(x)u := \mu_b, \tag{3.2}$$

such that the input-output linearized system becomes (NGUYEN; SREENATH, 2016a)

$$\begin{aligned} \dot{\eta}_b(x) &= F_b \eta_b(x) + G_b \mu_b, \\ h(x) &= C_b \eta_b(x), \end{aligned} \tag{3.3}$$

where $\eta_b(x)$ is defined as

$$\eta_b(x) := \begin{bmatrix} h(x) \\ \dot{h}(x) \\ \ddot{h}(x) \\ \vdots \\ h^{(r-1)}(x) \end{bmatrix} = \begin{bmatrix} h(x) \\ L_f h(x) \\ L_f^2 h(x) \\ \vdots \\ L_f^{(r-1)} h(x) \end{bmatrix}, \tag{3.4}$$

$F_b \in \mathbb{R}^{r\times r}$, $G_b \in \mathbb{R}^{r\times 1}$ are defined as

$$F_b = \begin{bmatrix} 0 & 1 & 0 & \cdots & 0 \\ 0 & 0 & 1 & \cdots & 0 \\ \vdots & \vdots & \vdots & \ddots & \vdots \\ 0 & 0 & 0 & \cdots & 1 \\ 0 & 0 & 0 & \cdots & 0 \end{bmatrix}, G_b = \begin{bmatrix} 0 \\ 0 \\ \vdots \\ 0 \\ 1 \end{bmatrix}, \tag{3.5}$$

and C_b is defined as

$$C_b = \begin{bmatrix} 1 & 0 & \cdots & 0 \end{bmatrix}. \tag{3.6}$$

If we want to drive $h(x)$ to zero, the work (NGUYEN; SREENATH, 2016a) proposes to design the ECBF with a pole placement controller $\mu_b = -K_b\eta_b$, with all negative real poles $p_b = -\begin{bmatrix} p_{b_1} & p_{b_2} & \cdots & p_{b_r} \end{bmatrix}$, where $p_{b_i} > 0,\ i = 1, \cdots, r$; thus, $h(x(t)) = C_b e^{A_b t}\eta_b(x_0)$, where the closed-loop matrix $A_b = F_b - G_b K_b$ with all negative real eigenvalues and x_0 is the initial condition. Moreover, if $\mu_b \geq -K_b\eta_b$, then $h(x(t)) \geq C_b e^{A_b t}\eta_b(x_0)$ (AMES et al., 2019).

We now can define the ECBF:

Definition 3.2. *Given a set C defined by (2.2) for a r-times continuously differentiable function $h(x) : \mathbb{R}^n \to \mathbb{R}$, then $h(x)$ is an ECBF if there exists a row vector $K_b \in \mathbb{R}^r$ such that for the control system (2.1) (NGUYEN; SREENATH, 2016a), (AMES et al., 2019),*

$$\sup_{u\in U}\left[L_f^r h(x) + L_g L_f^{r-1} h(x)u + K_b\eta_b(x)\right] \geq 0 \tag{3.7}$$

$\forall x \in \mathrm{Int}(C)$ results in $h(x(t)) \geq C_b e^{A_b t}\eta_b(x_0) \geq 0$, whenever $h(x_0) \geq 0$, and $\eta_b(x)$ is defined in (3.4).

Given an ECBF $h(x)$, we can implement a controller that enforces the condition given in Definition 3.2 by extending the QP-based controller presented in (2.15). So, a CLF $V(x)$ and an ECBF $h(x)$ can be unified using QP considering the following controller (AMES et al., 2019):

$$\begin{aligned} \mathbf{u}^*(x) = & \underset{(u,\mu_b,\delta)\in\mathbb{R}^{m+2}}{\arg\min} \ \tfrac{1}{2}u^T H(x)u + p_\delta\delta^2 \\ s.t. \ & L_f V(x) + L_g V(x)u + c_V V(x) - \delta \leq 0, \\ & L_f^r h(x) + L_g L_f^{r-1} h(x)u = \mu_b, \\ & \mu_b \geq -K_b\eta_b(x), \end{aligned} \tag{3.8}$$

where p_δ is the weight on the relaxation parameter δ.

Similarly to (2.18), a nominal control law u_{no} and an ECBF $h(x)$ can be unified using QP considering the following controller (AMES et al., 2019), (NGUYEN; SREENATH, 2016a):

$$\begin{aligned} \mathbf{u}^*(x) = & \underset{(u,\mu_b)\in\mathbb{R}^{m+1}}{\arg\min} \; u^T u - 2u_{no}^T u \\ s.t. \;\; & L_f^r h(x) + L_g L_f^{r-1} h(x) u = \mu_b, \\ & \mu_b \geq -K_b \eta_b(x). \end{aligned} \tag{3.9}$$

Remark 3.1. *Note that when the relative-degree $r = 1$, $K_b\eta_b(x)$ in (3.7) reduces to $\gamma h(x)$ with $\gamma > 0$. Thus, the Definition 2.6 defines a relative-degree one ECBF when $\alpha_h(h(x)) = \gamma h(x)$. In this sense, the Definition 3.2 is a generalization of the definition of CBFs for higher relative-degree functions $h(x)$ (AMES et al., 2019).*

Finally, the explicit solution (2.19) can be adapted to represent the safety constraint as an ECBF $h(x)$, such as

$$u_{cbf} = \begin{cases} -\frac{I_e(x,u_{no}) - J_e(x)}{\left\| L_g L_f^{r-1} h(x) \right\|^2} (L_g L_f^{r-1} h(x))^T & if \;\; I_e(x,u_{no}) < J_e(x) \\ 0 & if \;\; I_e(x,u_{no}) \geq J_e(x), \end{cases} \tag{3.10}$$

where functions $I_e : \mathbb{R}^n \times \mathbb{R}^m \to \mathbb{R}$ and $J_e : \mathbb{R}^n \to \mathbb{R}$ are defined by

$$\begin{aligned} I_e(x,u_{no}) &= L_f^r h(x) + L_g L_f^{r-1} h(x) u_{no}, \\ J_e(x) &= -K_b \eta_b(x) + C_e, \end{aligned} \tag{3.11}$$

where C_e is a design parameter. Equation (3.10) is an explicit solution to the QP-based controller (3.9) considering $u = u_{no} + u_{cbf}$.

4 ROBUST CBF

In this chapter, the control framework previously described is reformulated considering robustness issues. Robustness is an essential topic in safety-critical systems, because if disturbances and model uncertainties are not considered, the CBFs may not respect the safety constraints. Robust CBFs are studied in (XU et al., 2015), (KOLATHAYA; AMES, 2019), (NGUYEN; SREENATH, 2016b), (NGUYEN; SREENATH, 2020) and (JANKOVIC, 2018).

In (XU et al., 2015), the robustness of the CBF under model perturbation is investigated. This work verifies forward invariance of the set C, shown in (2.2), considering perturbations in the system (2.1). If the model perturbation has a H_∞ norm less than a determined constant value, input-to-state stability property of the set C is verified, the set is asymptotically stable and the system is robust. However, this work only describes robustness analysis and does not develop the design of a robust controller. The design of a safe robust controller is described in (KOLATHAYA; AMES, 2019) and (JANKOVIC, 2018), considering disturbances, and in (NGUYEN; SREENATH, 2016b) and (NGUYEN; SREENATH, 2020), considering model uncertainties. In this work, two safe robust controllers to deal with model uncertainties are proposed.

The first safe robust controller proposed in this work is an extension of the formulation proposed in (NGUYEN; SREENATH, 2016b) and (NGUYEN; SREENATH, 2020), where it is only considered relative-degree one safety constraints. However, in this work, this formulation is adapted in order to consider high relative-degree safety constraints expressed as robust exponential control barrier functions (RECBFs). Besides that, the stability/tracking objectives are expressed as a nominal control law, whereas in (NGUYEN; SREENATH, 2016b) and (NGUYEN; SREENATH, 2020), the stability/tracking objectives are expressed as a CLF.

The design of the second safe robust controller is an extension of the methodology proposed in (NGUYEN; SREENATH, 2016a) for ECBF, where a VIOL is employed and a pole placement controller is applied in the virtual control input to drive the CBF to

zero. However, here a sliding mode control (SMC) is applied in the virtual control input to deal with model uncertainties. We define this approach as sliding mode control barrier function (SMCBF), in contrast to ECBF.

4.1 Robust Exponential CBF (RECBF)

The design of the control framework with robust CBF and considering model uncertainties is described in (NGUYEN; SREENATH, 2016b) and (NGUYEN; SREENATH, 2020), where in the final control framework, stability/tracking objectives are expressed as a CLF and the robust CBF is derived based on the RCBF $B(x)$. The final QP-based controller is reformulated considering the effects of model uncertainties in CLFs and CBFs. However, in this work, the QP-based controller is adapted in order to express stability/tracking objectives as a nominal control law and to consider high relative-degree safety constraints expressed as RECBFs. We consider that $f(x)$ and $g(x)$ in (2.1) represent the real dynamics and are not exactly known. However, the controller's design is based on the nominal dynamics $\bar{f}(x)$ and $\bar{g}(x)$.

In (NGUYEN; SREENATH, 2016b) and (NGUYEN; SREENATH, 2020), a systematic procedure using input-output linearization is described to design CLFs considering model uncertainties. This scheme generates a control input μ_c. The effect of uncertainty for the CLF with respect to μ_c is linear, time-invariant and state-independent, so the uncertainty can be evaluated based on the difference between the real and the nominal model. This procedure could be applied to design CBFs considering model uncertainties. However, the effect of uncertainties for CBF constraints with respect to the control input is nonlinear, not static and not directly feasible to $\dot{h}(x,u) = L_f h(x) + L_g h(x)u$, because the term $(L_g h(x))^{-1}$ must be applied, and $L_g h(x)$ is a vector when $m > 1$ in (2.1), and obviously not invertible (NGUYEN; SREENATH, 2016b). Thus, the same approach cannot be applied. In order to address this issue, the work (NGUYEN; SREENATH, 2016b) suggests the same VIOL described in section 3.1 for ECBFs.

The effect of uncertainties in VIOL (3.2) can be described such as

$$h^{(r)}(x, \Delta_1^b, \Delta_2^b, \mu_b) = \mu_b + \Delta_1^b + \Delta_2^b \mu_b, \tag{4.1}$$

where Δ_1^b and Δ_2^b are related to the model uncertainties (NGUYEN; SREENATH, 2016b), (NGUYEN; SREENATH, 2020). The ECBF condition described in (3.9) then becomes

$$\psi_0^{bv} + \psi_1^{bv}(\mu_b + \Delta_1^b + \Delta_2^b \mu_b) \geq 0, \tag{4.2}$$

where $\psi_0^{bv} = K_b\eta_b(x)$ and $\psi_1^{bv} = 1$.

Assuming that model uncertainty is bounded, i.e.,

$$\left|\Delta_1^b\right| \leq \Delta_{1,max}^b,\ \left|\Delta_2^b\right| \leq \Delta_{2,max}^b, \tag{4.3}$$

the robust version of the ECBF constraints will then become

$$\psi_{0,bv}^{max} + \psi_{1,bv}^{p}(x)\mu_b \geq 0, \tag{4.4}$$

$$\psi_{0,bv}^{max} + \psi_{1,bv}^{n}(x)\mu_b \geq 0, \tag{4.5}$$

where $\psi_{0,bv}^{max} := \max(\psi_{0,bv}^{p}, \psi_{0,bv}^{n})$, $\psi_{0,bv}^{p} := \psi_0^{bv} + \psi_1^{bv}\Delta_{1,max}^b$, $\psi_{0,bv}^{n} := \psi_0^{bv} - \psi_1^{bv}\Delta_{1,max}^b$, $\psi_{1,bv}^{p} := \psi_1^{bv}(I + \Delta_{2,max}^b)$ and $\psi_{1,bv}^{n} := \psi_1^{bv}(I - \Delta_{2,max}^b)$ (NGUYEN; SREENATH, 2016b).

Applying the robust ECBF constraints (4.4) and (4.5) in the control framework (3.9), we obtain the final robust control framework

$$\begin{aligned} \mathbf{u}^*(x) = & \underset{(u,\mu_b)\in\mathbb{R}^{m+1}}{\arg\min}\ u^T u - 2u_{no}^T u \\ s.t.\ & A_r(x)u + b_r(x) = \mu_b, \\ & \psi_{0,bv}^{max} + \psi_{1,bv}^{p}(x)\mu_b \geq 0, \\ & \psi_{0,bv}^{max} + \psi_{1,bv}^{n}(x)\mu_b \geq 0, \end{aligned} \tag{4.6}$$

where $A_r = L_g L_f^{r-1} h(x)$ and $b_r = L_f^r h(x)$. This formulation can be applied to high relative-degree safety constraints considering model uncertainties. It is important to highlight that this formulation is obtained considering the control framework (3.9), where the stability/tracking objectives are expressed as a nominal control law u_{no}, however the formulation can be adapted to the control framework (3.8), where the stability/tracking objectives are expressed as a CLF $V(x)$.

4.2 Sliding Mode CBF (SMCBF)

Considering the virtual input-output linearized system (3.3), the basic idea here is to design the CBF with a SMC applied to the virtual control input μ_b in order to deal with model uncertainties instead of applying a pole placement controller as described for the ECBF. We consider that $f(x)$ and $g(x)$ in (2.1) represent the real dynamics and are not exactly known. However, the controller's design is based on the nominal dynamics $\bar{f}(x)$ and $\bar{g}(x)$, and the nominal VIOL, defined by (3.2), is described as

$$\bar{\mu}_b := L_{\bar{f}}^r h(x) + L_{\bar{g}} L_{\bar{f}}^{r-1} h(x) u. \tag{4.7}$$

Thus, the effect of model uncertainties in VIOL can be described as

$$h^{(r)}(x, \Delta, \bar{\mu}_b) = \bar{\mu}_b + \Delta, \tag{4.8}$$

where Δ is related to the difference between the real dynamics and the nominal dynamics in the Lie derivatives of the VIOL, i.e., the model uncertainties. We assume that Δ is bounded, i.e.,

$$|\Delta| \leq \Delta_{\max}. \tag{4.9}$$

Consider a time-varying surface S_{cbf} in state-space $\mathbb{R}^n$ defined by the scalar equation $s_{cbf}(x,t) = 0$, where

$$s_{cbf}(x,t) = \left(\frac{d}{dt} + \lambda_{cbf}\right)^{r-1} \tilde{h}, \tag{4.10}$$

h_d is the CBF desired value, $\tilde{h} = h - h_d$ and λ_{cbf} is a strictly positive constant. The problem of tracking $h = h_d$ is equivalent to that of remaining on the surface S_{cbf} for all $t > 0$. Furthermore, $s_{cbf} = 0$ represents a linear differential equation whose unique solution is $\tilde{h} = 0$, given that $h_d(0) = h(0)$; thus, the problem of tracking h_d can be reduced to that of keeping the scalar quantity s_{cbf} to zero (KHALIL, 2002), (SLOTINE; LI, 1991). We consider $h_d \geq 0$ since we want to guarantee that $h \geq 0$.

The problem of keeping s_{cbf} at zero can be achieved by choosing a control law such that s_{cbf} satisfies

$$\frac{1}{2}\frac{d}{dt}s_{cbf}^2 \leq -\eta_{cbf}\left|s_{cbf}\right|, \tag{4.11}$$

being η_{cbf} a strictly positive constant. The condition (4.11), called sliding condition, demonstrates that, once on the surface, the system trajectories remains it, i.e., the surface is an invariant set. Therefore, model uncertainties and disturbances can be tolerated. S_{cbf} is denominated sliding surface, and the system's behaviour once on the surface is called sliding mode (UTKIN; GULDNER; SHI, 2009), (SLOTINE; LI, 1991).

In the SMC design, a feedback control law, called equivalent control, is determined to maintain the system in sliding mode, i.e., $\dot{s}_{cbf} = 0$. However, in order to deal with model uncertainties and disturbances, the control law has to be discontinuous across S_{cbf} (KHALIL, 2002), (SLOTINE; LI, 1991).

Using (4.8), we obtain

$$\dot{s}_{cbf} = h^{(r)} - h_d^{(r)} + O_{cbf}(\lambda_{cbf}, \tilde{h}) = \bar{\mu}_b + \Delta - h_d^{(r)} + O_{cbf}(\lambda_{cbf}, \tilde{h}), \tag{4.12}$$

where $O_{cbf}(\lambda_{cbf}, \tilde{h})$ denotes the remaining derivatives of $\tilde{h}$ with degree less than or equal

to $r-1$.

The equivalent control μ_{eq} designed using the nominal dynamics and that would achieve $\dot{s}_{cbf}=0$ is given by

$$\mu_{eq}=h_d^{(r)}-O_{cbf}(\lambda_{cbf},\tilde{h}). \tag{4.13}$$

The control law given by

$$\mu_b=\mu_{eq}-K_{smc}\,\mathrm{sgn}(s_{cbf}), \tag{4.14}$$

where sgn is the sign function, will drive h to h_d despite the bounded uncertainty Δ in (4.8) by choosing K_{smc} large enough. Using (4.12) and the sliding condition (4.11), we obtain

$$\frac{1}{2}\frac{d}{dt}s_{cbf}^2=\dot{s}_{cbf}s_{cbf}=\Delta s_{cbf}-K_{smc}\left|s_{cbf}\right|\leq-\eta_{cbf}\left|s_{cbf}\right|, \tag{4.15}$$

and K_{smc} that satisfies the sliding condition (4.11) is then given by

$$K_{smc}\geq\Delta+\eta_{cbf}. \tag{4.16}$$

The discontinuous term in (4.14) generates a control switching that is necessarily imperfect, because switching is not instantaneous, and the value of s_{cbf} is not known with infinite precision and is never exactly zero. This can lead to "chattering", i.e., undesirable high-frequency oscillation. To avoid "chattering", a boundary layer is applied in the neighboring of the sliding surface and the saturation function replaces the sign function (UTKIN; GULDNER; SHI, 2009), (SLOTINE; LI, 1991), such as

$$\mu_b=\mu_{eq}-K_{smc}\,\mathrm{sat}(s_{cbf}/\Phi), \tag{4.17}$$

where

$$\mathrm{sat}(s_{cbf}/\Phi)=\begin{cases}s_{cbf}/\Phi,\ \text{if}\ \ |s_{cbf}|\leq\Phi\\ \mathrm{sgn}(s_{cbf}/\Phi),\ \text{if}\ \ |s_{cbf}|>\Phi,\end{cases} \tag{4.18}$$

and Φ is the boundary layer thickness.

We now can define the SMCBF:

Definition 4.1. *Consider the control system (2.1) and a set C defined by (2.2) for a r-times continuously differentiable function $h(x):\mathbb{R}^n\to\mathbb{R}$, then $h(x)$ is an SMCBF if it satisfies*

$$\sup_{u\in U}\left[L_f^r h(x)+L_gL_f^{r-1}h(x)u-\mu_{eq}+K_{smc}\,\mathrm{sat}(s_{cbf}/\Phi)\right]\geq 0. \tag{4.19}$$

Similarly to (2.18), a nominal control law u_{no} and a SMCBF $h(x)$ can be unified using QP considering the following controller:

$$\begin{aligned} \mathbf{u}^*(x) = & \underset{(u,\mu_b)\in\mathbb{R}^{m+1}}{\arg\min} \; u^T u - 2u_{no}^T u \\ s.t. \;\; & L_f^r h(x) + L_g L_f^{r-1} h(x) u = \mu_b \\ & \mu_b \geq \mu_{eq} - K_{smc}\,\mathrm{sat}(s_{cbf}/\Phi). \end{aligned} \tag{4.20}$$

It is important to highlight that this formulation is obtained considering the stability/tracking objectives expressed as a nominal control law u_{no}, however the formulation can be adapted to consider the stability/tracking objectives expressed as a CLF $V(x)$.

Finally, the explicit solution (2.19) can be adapted to represent the safety constraint as a SMCBF $h(x)$, such as

$$u_{cbf} = \begin{cases} -\frac{I_e(x,u_{no})-J_e(x)}{\left\|L_g L_f^{r-1} h(x)\right\|^2}(L_g L_f^{r-1} h(x))^T & if \;\; I_e(x,u_{no}) < J_e(x) \\ 0 & if \;\; I_e(x,u_{no}) \geq J_e(x), \end{cases} \tag{4.21}$$

where functions $I_e : \mathbb{R}^n \times \mathbb{R}^m \to \mathbb{R}$ and $J_e : \mathbb{R}^n \to \mathbb{R}$ are defined by

$$\begin{aligned} I_e(x,u_{no}) &= L_f^r h(x) + L_g L_f^{r-1} h(x) u_{no}, \\ J_e(x) &= \mu_{eq} - K_{smc}\,\mathrm{sat}(s_{cbf}/\Phi) + C_e, \end{aligned} \tag{4.22}$$

where C_e is a design parameter. Equation (4.21) is an explicit solution to the QP-based controller (4.20) considering $u = u_{no} + u_{cbf}$.

5 DISCRETE-TIME CBF (DCBF)

The control framework proposed in the last chapters, developed for continuous-time systems, is extended to discrete-time systems in (AGRAWAL; SREENATH, 2017) and (TAKANO; OYAMA; YAMAKITA, 2018). In discrete-time, the stability/tracking objectives and the safety constraints are integrated through a general nonlinear programming (NLP) (and potentially non-convex), and under certain conditions, the optimization problem can be described as a convex QP. In (AGRAWAL; SREENATH, 2017), the stability/tracking objectives are expressed as a discrete-time CLF (DCLF) and in (TAKANO; OYAMA; YAMAKITA, 2018), as a nominal control law. Figs. 3a and 3b present a synthesized description of the control framework when stability/tracking objectives are expressed as a DCLF and as a nominal control law u_{no_d} respectively. The expression for the final NLP-based controller $\mathbf{u}_k^*$ will be described posteriorly.

Figure 3: Synthesized description of the discrete-time control framework.

(a) Stability/tracking objectives expressed as a DCLF.

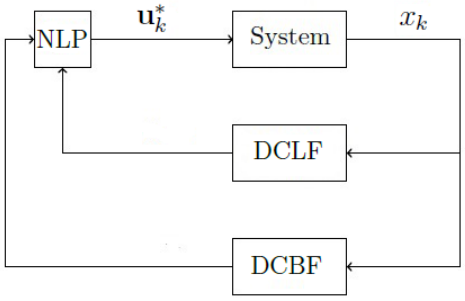

(b) Stability/tracking objectives expressed as a nominal control law u_{no_d}.

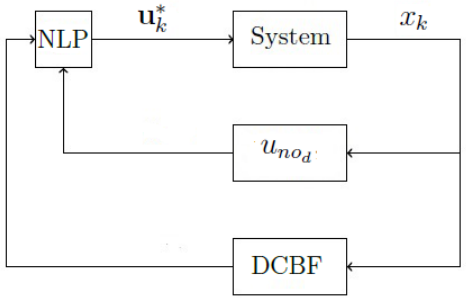

Source: Author.

In discrete-time, the system described in (2.1) is represented as

$$x_{k+1} = f_d(x_k) + g_d(x_k)u_k, \tag{5.1}$$

with states $x(k) = x_k \in D_d \subset \mathbb{R}^n$ and inputs $u(k) = u_k \in U_d \subset \mathbb{R}^m$.

In the following sections, the concepts of DCLF, DCBF and the control framework

described in the last chapters for discrete-time are presented.

5.1 Discrete-Time CLF (DCLF)

In this section, DCLF is defined.

Definition 5.1. *A map $V_d : D_d \to \mathbb{R}$ is a discrete-time exponentially stabilizing control Lyapunov function (DESCLF), referred in this work simply as DCLF, for the discrete-time control system (5.1) if there exists (AGRAWAL; SREENATH, 2017), (ZENG; ZHANG; SCREENATH, 2021):*

1. *positive constants c_{1_d} and c_{2_d} such that*

$$c_{1_d} \|x_k\|^2 \leq V_d(x_k) \leq c_{2_d} \|x_k\|^2, \tag{5.2}$$

and

2. *a control input $u_k : D_d \to U_d$, $\forall x_k \in D_d$ and $c_{V_d} > 0$ such that*

$$\Delta V_d(x_k, u_k) + c_{V_d} V_d(x_k) \leq 0, \tag{5.3}$$

where $\Delta V_d(x_k, u_k) := V_d(x_{k+1}) - V_d(x_k)$.

Similarly to (2.8) for the continuous-time systems, the DCLF condition (5.3) can be enforced through a constrained optimization problem (AGRAWAL; SREENATH, 2017):

$$\begin{aligned} u_k^* = & \underset{u_k \in D_d}{\arg\min}\ u_k^T u_k \\ s.t.\ & \Delta V_d(x_k, u_k) + c_{V_d} V_d(x_k) \leq 0. \end{aligned} \tag{5.4}$$

5.2 DCBF - Definition

Such as for continuous-time in (2.2), we define a safe set C_d (AGRAWAL; SREENATH, 2017):

$$\begin{aligned} C_d &= \{x_k \in D_d \subset \mathbb{R}^n : h_d(x_k) \geq 0\}, \\ \partial C_d &= \{x_k \in D_d \subset \mathbb{R}^n : h_d(x_k) = 0\}, \end{aligned} \tag{5.5}$$

for a function $h_d(x_k) : \mathbb{R}^n \to \mathbb{R}$. Then, the DCBF can be defined (TAKANO; OYAMA; YAMAKITA, 2018):

Definition 5.2. *$h_d(x_k)$ is a DCBF for the discrete-time control system (5.1) if it satisfies:*

1. $h_d(x_0) \geq 0$, *where* x_0 *is the initial state,*

2. $\Delta h_d(x_k, u_k) + \gamma_d h_d(x_k) \geq 0,\ \gamma_d > 0,$ *where* $\Delta h_d(x_k, u_k) := h_d(x_{k+1}) - h_d(x_k)$.

This essentially means that the control input u_k maintains $h_d \geq 0$ given that $h_d(x_0) \geq 0$. In other words, u_k keeps the trajectory x_k of the system within the safe set C_d, given the initial state x_0 lies in the C_d (AGRAWAL; SREENATH, 2017).

5.3 Unifying DCLF and DCBF Through Nonlinear Programming (NLP)

Stability/tracking objectives, represented by a DCLF $V_d(x_k)$, and safety constraints, represented by a DCBF $h_d(x_k)$, can be unified through the following NLP (AGRAWAL; SREENATH, 2017), (ZENG; ZHANG; SCREENATH, 2021):

$$\begin{aligned} \mathbf{u}_k^* = & \underset{\mathbf{u_k}=(u_k,\delta_d)\in\mathbb{R}^{m+1}}{\arg\min} \ \mathbf{u}_k^T \mathbf{u}_k + p_{\delta_d}\delta_d^2 \\ s.t. \ & \Delta V_d(x_k, u_k) + c_{V_d} V_d(x_k) - \delta_d \leq 0 \\ & \Delta h_d(x_k, u_k) + \gamma_d h_d(x_k) \geq 0, \end{aligned} \tag{5.6}$$

where the constraints related to the DCLF and DCBF are given in Definition 5.1 and Definition 5.2 respectively. The term p_{δ_d} is the penalty weight on the relaxation parameter δ_d used to make the stability/tracking objectives as a soft constraint in the QP, while safety is kept as a hard constraint. The parameter c_{V_d} is related to the convergence rate to the stabilization while the DCLF is acting to satisfy the stability/tracking objectives and γ_d specifies how far from the barrier limit the DCBF acts to satisfy the safety constraints. Therefore, the design parameters are p_{δ_d}, c_{V_d} and γ_d. The controller (5.6) is graphically represented in Fig. 3a.

5.4 Unifying Nominal Control Law and DCBF Through NLP

Stability/tracking objectives, represented by a nominal control law u_{no_d}, and safety constraints, represented by a DCBF $h_d(x_k)$, can be unified through the following NLP (TAKANO; OYAMA; YAMAKITA, 2018):

$$\begin{aligned} \mathbf{u}_k^* = & \underset{u_k\in\mathbb{R}^m}{\arg\min} \ u_k^T u_k - 2u_{no_d}^T u_k \\ s.t. \ & \Delta h_d(x_k, u_k) + \gamma_d h_d(x_k) \geq 0, \end{aligned} \tag{5.7}$$

where the constraint related to the DCBF is given in Definition 5.2. The controller (5.7) is graphically represented in Fig. 3b. It is important to highlight that the relaxation parameter δ_d is unnecessary since the nominal control law u_{no_d} is on the objective function and there are no constraints related to stability/tracking objectives.

6 NUMERICAL/EXPERIMENTAL RESULTS

In this chapter, the numerical/experimental results are presented. The experiments are organized so that all the topics described in the literature review and the work contributions were covered.

6.1 Reaction Wheel Pendulum

For the reaction wheel pendulum, a LQR is applied as a nominal control law to satisfy the stability objective. The LQR is described in Appendix E. Initially, the safety constraint is represented as a relative-degree one CBF. The control framework is applied as described in (2.18). Posteriorly, the safety constraint is represented as a relative-degree two CBF. The control framework is applied considering an ECBF, as described in (3.9). Finally, the discrete-time control framework is applied, as described in (5.7), considering a discrete-time LQR and a DCBF. The results are presented numerically and experimentally. It is important to highlight that there are few studies dealing with DCBFs in the literature and the results in (AGRAWAL; SREENATH, 2017) and (TAKANO; OYAMA; YAMAKITA, 2018) are verified only numerically while here the results are verified numerically and experimentally.

6.1.1 System Modeling

The reaction wheel pendulum is an inverted pendulum balanced by an actuated rotating reaction wheel (*flywheel*). This system can reflect different typical problems in control, such as nonlinearities, robustness, stabilization and under actuation, thus being an attractive and useful system for research and advanced education. Several engineering problems can be approximately modeled as an inverted pendulum, such as rocket launch, *Segway* and bipedal robot (BLOCK; ASTROM; SPONG, 2007).

Reaction wheels are actuators commonly used in aerospace applications, such as in

spacecrafts (YANG, 2017) and satellites (CHOU et al., 2011), to control the attitude without the use of thrusters. In robotics, reaction wheels have been also applied in bipedal walking robots (BROWN; SCHMIEDELER, 2016) and to some variations of the reaction wheel pendulum (MUEHLEBACH; D'ANDREA, 2017), (TÜRKMEN et al., 2017), (HAN; LEE, 2015), (NEVES; ANGÉLICO; AGULHARI, 2019).

The schematic diagram and the prototype of the reaction wheel pendulum developed at Laboratório de Controle Aplicado (LCA)- Escola Politécnica da Universidade de São Paulo (EPUSP) are presented in Figs. 4a and 4b respectively. The system is constituted by an inverted pendulum that is balanced by an actuated reaction wheel. α is the pendulum angle, θ is the wheel angle and τ is the torque acting on the reaction wheel. The angles are measured with two encoders and the reaction wheel is actuated by a permanent-magnet DC motor.

Figure 4: Reaction wheel pendulum developed at LCA-EPUSP.

(a) Schematic diagram. (b) Prototype.

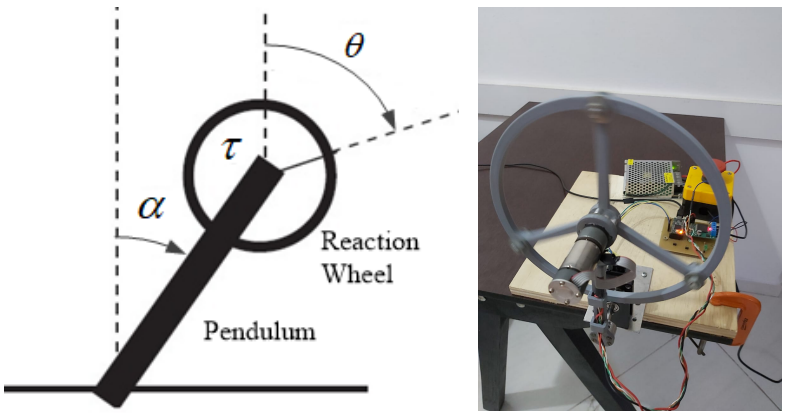

Source: Author.

The equations of motion can be derived using the Lagrangian method. The Lagrange's equations are described as

$$\frac{d}{dt}\left(\frac{\partial L_r}{\partial \dot{q}_{r_i}}\right) - \frac{\partial L_r}{\partial q_{r_i}} = \tau_{r_i}, \quad i = 1, ..., d_{rw}, \tag{6.1}$$

where $L_r = K_r - V_r$ is the system Lagrangian, K_r is the total kinetic energy, V_r is the total potential energy, d_{rw} is the number of generalized coordinates or degrees-of-freedom, q_{r_i} represents the generalized coordinates and τ_{r_i} represents the generalized forces (torques).

For the reaction wheel pendulum, the generalized coordinates are α and θ ($d_{rw} = 2$), and the generalized torques are $+\tau$, imposed by the DC motor and acting on the reaction wheel, and $-\tau$, which is the reaction torque acting on the pendulum.

The system kinetic energy K_r is the sum of the pendulum kinetic energy and the reaction wheel kinetic energy:

$$K_r = \frac{1}{2}\left(m_p l_{cp}^2 + J_p\right)\dot{\alpha}^2 + \frac{1}{2}m_r l_p^2 \dot{\alpha}^2 + \frac{1}{2}J_r(\dot{\theta}+\dot{\alpha})^2, \tag{6.2}$$

where m_p and m_r are the pendulum and the reaction wheel masses, J_p and J_r are the pendulum and the reaction wheel moments of inertia, l_p is the pendulum length and l_{cp} is the distance to the pendulum center of mass.

Assuming that the system potential energy V_r is due to gravity only, we have

$$V_r = m_p g l_{cp}\cos\alpha + m_r g l_p \cos\alpha, \tag{6.3}$$

where g is the gravitational acceleration constant.

Applying (6.2) and (6.3) in (6.1), the following equations of motion can be obtained:

$$(m_p l_{cp}^2 + m_r l_p^2 + J_p + J_r)\ddot{\alpha} + J_r\ddot{\theta} + (m_p g l_{cp} + m_r g l_p)\sin\alpha = -\tau, \tag{6.4}$$

$$J_r(\ddot{\alpha}+\ddot{\theta}) = \tau. \tag{6.5}$$

The reaction wheel is actuated by a permanent-magnet DC motor. The motor equation is given by:

$$R_{m_r} i_{m_r} + K_{e_r}\dot{\theta} = V_{m_r}, \tag{6.6}$$

where i_{m_r} is the motor current, V_{m_r} is the motor voltage, R_{m_r} is the armature resistance and K_{e_r} is the back electromotive-force (EMF) constant. Since we consider a 12 V DC motor and a control input using a pulse width modulation (PWM) signal $PWM_r \in [-1, 1]$, which includes the duty-cycle and the rotation direction, we apply the following relation:

$$V_{m_r} = 12\ PWM_r. \tag{6.7}$$

Thus, the motor torque τ can be obtained by:

$$\tau = K_{t_r} i_{m_r} = \frac{K_{t_r}}{R_{m_r}}(12\ PWM_r - K_{e_r}\dot{\theta}), \tag{6.8}$$

where K_{t_r} is the motor torque constant. With this relation, the input is expressed as PWM_r.

The numerical values of the parameters are $m_p = 0.117$kg, $m_r = 0.119$kg, $J_p = 6.2533\times10^{-4}$kg·m^2, $J_r = 9.4559\times10^{-4}$kg·m^2, $l_p = 0.14298$m, $l_{cp} = 0.0987$m, $g = 9.81$m/s^2, $K_{t_r} = 0.0601$N·m/V, $K_{e_r} = 0.1836$V/(rad/s) and $R_{m_r} = 2.44\Omega$.

6.1.2 Continuous-Time Results

The behavior of the reaction wheel pendulum with the proposed control framework is verified through numerical simulations with MATLAB/Simulink and experimentally using the prototype shown in Fig. 4b. The system is controlled by a development board Teensy 3.2, which has a 32 bits ARM Cortex-M4 microcontroller with 256 Kbytes of flash memory and 64 Kbytes of RAM. The pendulum angle α and the wheel angle θ are measured with encoders[1], while the pendulum velocity $\dot{\alpha}$ and the wheel velocity $\dot{\theta}$ are obtained by Euler backward approximations. The reaction wheel is actuated by a 12 V permanent-magnet DC motor and the motor driver is a H-bridge model VNH5019.

The reaction wheel pendulum has an unstable equilibrium point on its upright position. Several control strategies presented in the literature have been applied to stabilize this system, such as proportional-derivative (PD) control (BLOCK; ASTROM; SPONG, 2007), pole placement method (JEPSEN et al., 2009), feedback linearization (SPONG; CORKE; LOZANO, 2001) and SMC (RIZAL et al., 2018), (TRENTIN et al., 2020). These works are proposed to satisfy a stability objective, i.e, to stabilize the system at the equilibrium point, but safety constraints are not considered. So, the control framework described in this work is applied to simultaneously satisfy a stability objective and a safety constraint. Since the focus is on safety, a simple LQR is applied as a nominal control law for stabilizing the pendulum. The safety constraint, expressed as a CBF, is considered to guarantee that the pendulum angular position never exceeds a predetermined bound.

In order to design the LQR to stabilize the system, the nonlinear model is linearized around the equilibrium point, resulting in:

$$\dot{x}_{cr} = A_{cr}x_{cr} + B_{cr}u_{cr}, \tag{6.9}$$

where $x_{cr} = \begin{bmatrix}\alpha & \dot{\alpha} & \dot{\theta}\end{bmatrix}^T$, $u_{cr} = PWM_r$, A_{cr} is the state matrix, B_{cr} is the input matrix and the equilibrium point is $x^*_{cr} = [0 \;\; 0 \;\; 0]^T$ (pendulum at upright position). It is important to highlight that (6.9) can be related to (2.1), where $f_{cr}(x_{cr}) = A_{cr}x_{cr}$ and $g_{cr}(x_{cr}) = B_{cr}$. The numerical values of matrices A_{cr} and B_{cr} are:

$$A_{cr} = \begin{bmatrix} 0 & 1 & 0 \\ 66.7479 & 0 & 1.0774 \\ -66.7479 & 0 & -5.8606 \end{bmatrix}, B_{cr} = \begin{bmatrix} 0 \\ -70.4050 \\ 382.9616 \end{bmatrix}. \tag{6.10}$$

[1]The resolution of the reaction wheel encoder is equal to $2\pi/230.7$ (230.7 pulses/revolution), while for the pendulum encoder, it is equal to $2\pi/2048$ (2048 pulses/revolution).

The continuous-time LQR, whose formulation is described in (E.2), is designed considering

$$Q_{cr} = \begin{bmatrix} 4.5837 & 0 & 0 \\ 0 & 3.2058 & 0 \\ 0 & 0 & 0.0071 \end{bmatrix}, \; R_{cr} = 30, \tag{6.11}$$

resulting in

$$K_{cr} = \begin{bmatrix} -3.906 & -0.599 & -0.0569 \end{bmatrix}. \tag{6.12}$$

We propose an experiment whereby the pendulum angle α should track a reference input α_{ref} composed of short-time pulses. This is considered in order to verify the effect of the CBF, i.e., with the final control framework, the pendulum is expected not to exit the safe set. Initially, only LQR is applied. When a reference input is considered, the nominal control input (E.2) becomes

$$u_{no_{cr}} = -K_{cr}x_{cr} + K_{cr_{11}}\alpha_{ref}, \tag{6.13}$$

where $K_{cr_{11}} = -3.906$.

Posteriorly, the control framework that unifies the nominal LQR (6.13) and the continuous-time CBF through the QP shown in (2.18) is applied to guarantee that $|\alpha|$ never exceeds a predetermined bound α_{max}. For doing so, the CBF must be chosen in order to satisfy the safe set (2.2). This can be solved applying the following relative-degree one CBF:

$$h_{cr}(x_{cr}) = c_{1_{cr}}\left[\alpha_{max}^2 - \alpha^2 - c_{2_{cr}}\dot{\alpha}^2\right], \tag{6.14}$$

where $c_{1_{cr}}$ and $c_{2_{cr}}$ are constants determined empirically. A similar CBF can be found in (TAYLOR et al., 2020) applied to a *Segway*. The term $c_{2_{cr}}\dot{\alpha}^2$ scales the importance of the velocity $\dot{\alpha}$. If a small value is set to $c_{2_{cr}}$, so that the velocity exerts little influence, it can be observed that $h_{cr}(x) \geq 0$ happens only when $|\alpha| < \alpha_{max}$, so the safe set (2.2) is satisfied.

The QP (2.18) is implemented using Hildreth's QP procedure (HILDRETH, 1957). The algorithm is embedded in the Teensy 3.2 board. We consider $\alpha_{h_{cr}}(h_{cr}(x_{cr})) = \gamma_{cr}h_{cr}(x_{cr})$, where γ_{cr} is a positive constant. Initially, the numerical values considered for the CBF (6.14) and the QP (2.18) are $\alpha_{max} = 0.087$rad (5°), $c_{1_{cr}} = 0.5$, $c_{2_{cr}} = 0.001$ and $\gamma_{cr} = 55$. The amplitude of the pulses (0.2s) in α_{ref} is ± 0.140rad ($\pm 8°$). This amplitude was chosen because, after several experimental tests, we verify that this value is adequate to ensure the stabilization of the pendulum with the LQR, and higher values can turn the system unstable. Lower values for the bound α_{max} were tested, however due

to practical issues related to sensor imprecision, unmodeled dynamics, and angular speed estimators, the safety constraint was not respected. When the value of γ_{cr} is increased, the CBF acts close to the barrier limit α_{max}, and if γ_{cr} is increased considerably, the safety constraint is not respected. When the value of γ_{cr} is reduced, the CBF becomes more conservative, acting far from the barrier limit α_{max}. The constant $c_{1_{cr}}$ exerts little influence and it is set according to (TAYLOR et al., 2020). We also observed that using higher values for $c_{2_{cr}}$ make the CBF more conservative, and lower values have little influence.

Numerical simulations are performed in MATLAB/Simulink. In order to make the simulation more realistic, the actuator dead-zone and measurement noise are added to the encoder output. Dead-zone is experimentally identified as equal to 0.13 (in duty-cycle of PWM). The measurement noise is modeled as a random variable uniformly distributed in $(-\Delta_{cr}/2,\ \Delta_{cr}/2)$, where Δ_{cr} is the resolution of each encoder. With this approach, the measurement noise represents the quantization noise of the encoders.

Simulation results are presented in Figs. 5 for LQR, and 6 for LQR with CBF. We assume that the pendulum starts at an initial angular position $\alpha_{ini} = 0.069$rad (4°). A reference α_{ref} with short pulses (0.2s) with amplitude ±0.140rad (±8°) is applied. The results show that the LQR is able to stabilize the system. When the LQR is combined with the CBF, in the final control framework, it is possible to see that the safety constraint is respected, i.e, $|\alpha|$ never exceeds α_{max} and the CBF $h_{cr}(x)$ respects the safe set (2.2).

Figure 5: Numerical simulation (reaction wheel pendulum) - LQR without CBF.

(a) Pendulum angle α. (b) Pendulum velocity $\dot{\alpha}$.

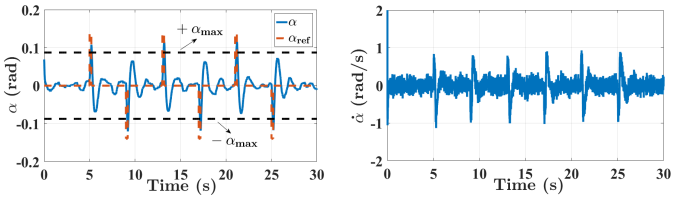

(c) Wheel velocity $\dot{\theta}$. (d) Control input u_{cr}.

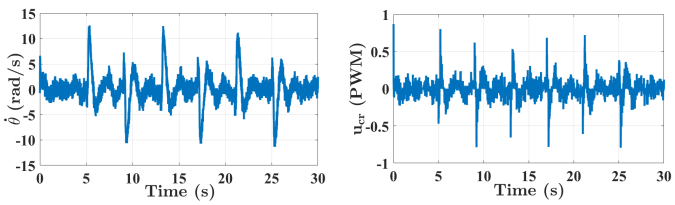

Source: Author.

Figure 6: Numerical simulation (reaction wheel pendulum) - LQR with CBF.

(a) Pendulum angle α. (b) Pendulum velocity $\dot{\alpha}$.

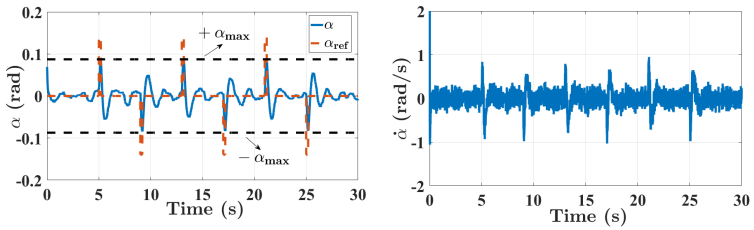

(c) Wheel velocity $\dot{\theta}$. (d) Control input u_{cr}.

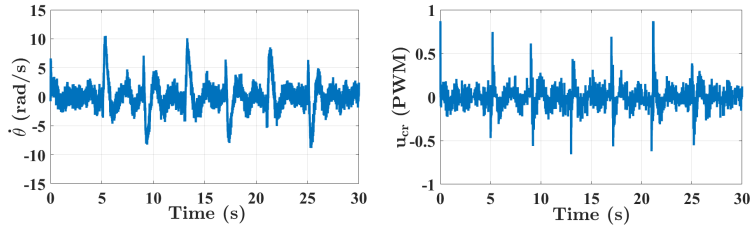

(e) CBF h_{cr}.

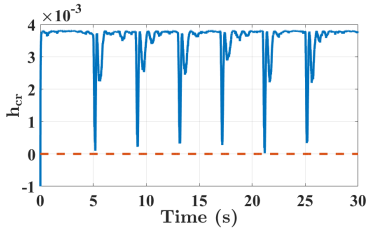

Source: Author.

The experimental results with the prototype are presented in Figs. 7 and 8. In Fig. 7, only LQR is considered. It is possible to see that the controller performs well, keeping the system balanced and trying to track the short pulses. In Fig. 8, the final control framework is applied. Using the parameter $\gamma_{cr} = 55$, such as in the simulations, the CBF acts very close to the barrier bound α_{max}, and it was observed in previous experiments that some values of $|\alpha|$ somewhat exceeded α_{max}, mainly due to sensor imprecision, unmodeled dynamics, and angular speed estimators. Hence, for the experiments, a more conservative barrier with $\gamma_{cr} = 1$ is considered, so that the safety constraint is respected. In Fig. 8, initially, $|\alpha|$ exceeds α_{max}, since the CBF is programmed to act only after the transient response due to the initial condition (we consider $5s$). Posteriorly, it is possible to see that the safety constraint is respected, i.e, $|\alpha|$ never exceeds α_{max} and the CBF $h_{cr}(x)$ respects the safe set (2.2). It is important to highlight that the control input u_{cr} is zero between $0s$ and $5s$, because the microcontroller was programmed, in this experiment, only to display u_{cr}, and in this interval, only the nominal control input $u_{no_{cr}}$ is acting in the system.

Figure 7: Experimental result (reaction wheel pendulum) - LQR without CBF.

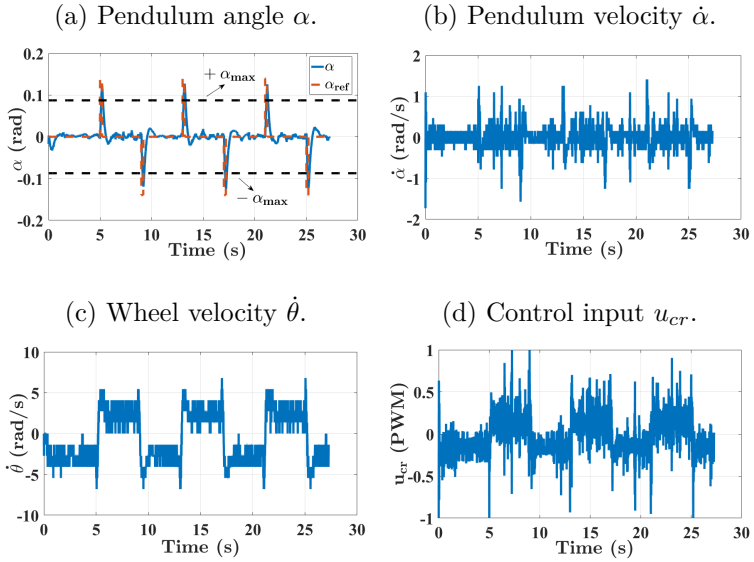

Source: Author.

Figure 8: Experimental result (reaction wheel pendulum) - LQR with CBF.

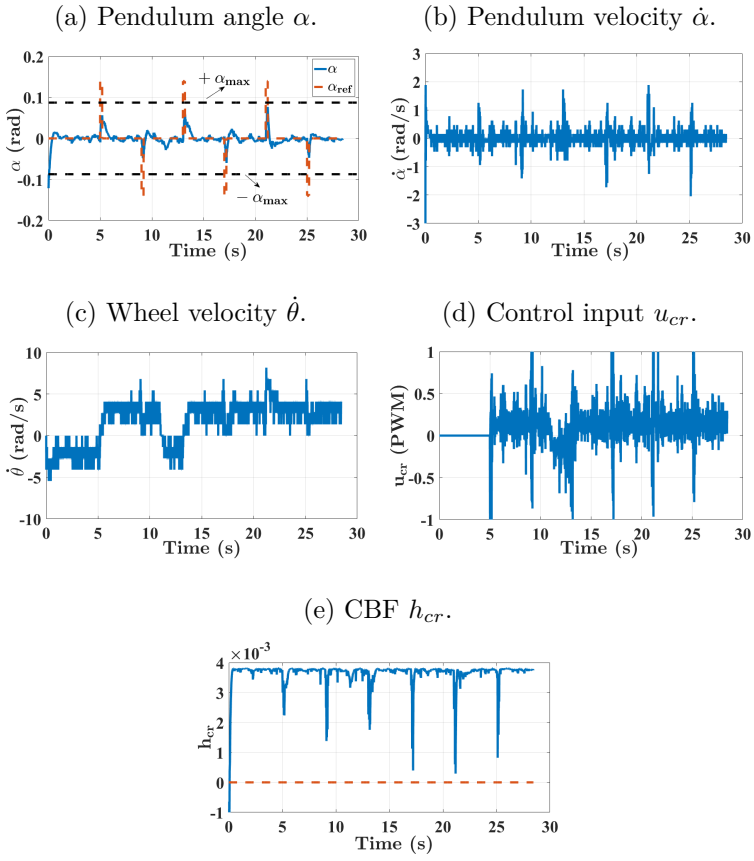

Source: Author.

6.1.2.1 ECBF

In the subsection 6.1.2, it is applied the relative-degree one safety constraint (6.14). However, the problem can also be solved applying a relative-degree two safety constraint, such as:

$$h_{cr}(x_{cr}) = \alpha_{max}^2 - \alpha^2. \tag{6.15}$$

As described in chapter 3, when high relative-degree safety constraints are considered, ECBFs must be applied. Thus, the QP-based controller described in (3.9) is applied. The nominal control law $u_{no_{cr}}$ is the LQR defined in (6.13). The QP is solved using Hildreth's QP procedure again.

The simulation results are presented in Fig. 9. The parameters for the ECBF (6.15) and the QP (3.9) are $\alpha_{max} = 0.087$rad (5°) and $K_{b_{cr}} = [2000 \quad 100]$. When the LQR is combined with the ECBF in the final control framework, it is possible to see that the safety constraint is respected, i.e, $|\alpha|$ never exceeds α_{max} and the ECBF $h_{cr}(x)$ respects the safe set (2.2).

Figure 9: Numerical simulation (reaction wheel pendulum) - LQR with ECBF.

(a) Pendulum angle α. (b) Pendulum velocity $\dot{\alpha}$.

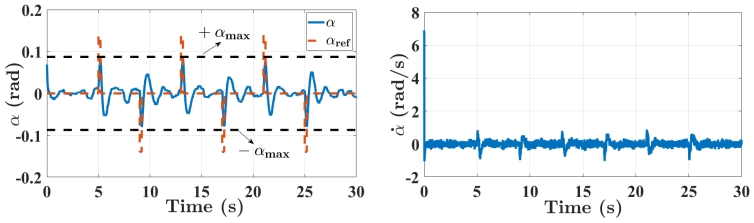

(c) Wheel velocity $\dot{\theta}$. (d) Control input u_{cr}.

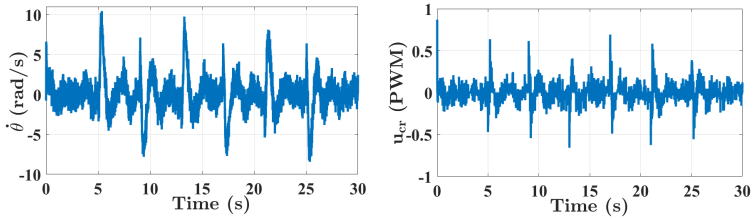

(e) ECBF h_{cr}.

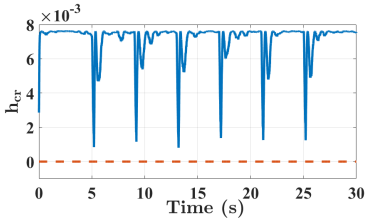

Source: Author.

6.1.3 Discrete-Time Results

In discrete-time, the linearized continuous-time model (6.9) is represented as

$$x_{dr_{k+1}} = G_{dr} x_{dr_k} + H_{dr} u_{dr_k}, \tag{6.16}$$

where $x_{dr_k} = \begin{bmatrix} \alpha_k & \dot{\alpha}_k & \dot{\theta}_k \end{bmatrix}^T$, $u_{dr_k} = PWM_{r_k}$, G_{dr} is the state matrix, H_{dr} is the input matrix and the equilibrium point is $x^*_{dr_k} = [0 \ 0 \ 0]^T$. It is important to highlight that (6.16) can be related to (5.1), where $f_{dr}(x_k) = G_{dr} x_{dr_k}$ and $g_{dr}(x_k) = H_{dr}$.

The linearized continuous-time model (6.9) is discretized considering a sampling time $T_{dr} = 0.02s$. The numerical values of the matrices G_{dr} and H_{dr} obtained are:

$$G_{dr} = \begin{bmatrix} 1.013 & 0.02009 & 0.0002078 \\ 1.327 & 1.013 & 0.02043 \\ -1.265 & -0.01287 & 0.8893 \end{bmatrix}, H_{dr} = \begin{bmatrix} -0.01358 \\ -1.335 \\ 7.233 \end{bmatrix}. \tag{6.17}$$

In this case, the weighting matrices of the LQR are set as

$$Q_{dr} = \begin{bmatrix} 0.0057 & 0 & 0 \\ 0 & 0.0040 & 0 \\ 0 & 0 & 0.0001 \end{bmatrix}, \ R_{dr} = 0.2800, \tag{6.18}$$

such that

$$K_{dr} = \begin{bmatrix} -3.3908 & -0.4475 & -0.0351 \end{bmatrix}. \tag{6.19}$$

The same setup of the continuous-time experiments are considered here. Initially, only the LQR is applied. When a reference input is considered, the control input (E.7) becomes

$$u_{no_{dr}} = -K_{dr} x_{dr_k} + K_{dr_{11}} \alpha_{ref}, \tag{6.20}$$

where $K_{dr_{11}} = -3.3908$.

Posteriorly, the control framework that unifies the LQR and the DCBF through the NLP shown in (5.7) is applied to guarantee that $|\alpha_k|$ never exceeds a predetermined bound α_{max}. The DCBF must be chosen in order to satisfy the safe set (5.5). This can be solved applying the following DCBF:

$$\begin{aligned} h_{dr_k}(x_{dr_k}) &= \alpha_{max} - \alpha_k, \ \alpha_k \geq 0, \\ h_{dr_k}(x_{dr_k}) &= \alpha_{max} + \alpha_k, \ \alpha_k < 0. \end{aligned} \tag{6.21}$$

It can be observed that $h_{dr}(x_{dr_k}) \geq 0$ is satisfied only when $|\alpha| < \alpha_{max}$, so the safe set

(5.5) is satisfied.

It is important to highlight that the DCBF (6.21) and the discrete-time system (6.16) are both linear, so the general NLP (5.7) can be described as a QP. Considering

$$\begin{aligned} h_{dr_{k+1}}(x_{dr_k}, u_{dr_k}) &= \alpha_{max} - \alpha_{k+1},\ \alpha_k \geq 0, \\ h_{dr_{k+1}}(x_{dr_k}, u_{dr_k}) &= \alpha_{max} + \alpha_{k+1},\ \alpha_k < 0, \end{aligned} \tag{6.22}$$

the NLP (5.7) can be described as the QP

$$\begin{aligned} \mathbf{u}^*_{dr_k} &= \underset{u_{dr_k} \in \mathbb{R}^m}{\arg\min}\ u^T_{dr_k} u_{dr_k} - 2u^T_{no_{dr}} u_{dr_k} \\ s.t.\ & A_{dcbf} u_{dr_k} \leq b_{dcbf}, \end{aligned} \tag{6.23}$$

where

$$\begin{aligned} &A_{dcbf} = -0.01358, b_{dcbf} = \alpha_{max} - 1.013\alpha_k - 0.02009\dot{\alpha}_k \\ &-0.0002078\dot{\theta}_k - h_{dr_k}(x_{dr_k}) + \gamma_{dr} h_{dr_k}(x_{dr_k}),\ \alpha_k \geq 0, \\ &A_{dcbf} = 0.01358, b_{dcbf} = \alpha_{max} + 1.013\alpha_k + 0.02009\dot{\alpha}_k \\ &+0.0002078\dot{\theta}_k - h_{dr_k}(x_{dr_k}) + \gamma_{dr} h_{dr_k}(x_{dr_k}),\ \alpha_k < 0. \end{aligned} \tag{6.24}$$

The QP (6.23) is solved using Hildreth's QP procedure again, which is also embedded in the Teensy 3.2 board. Initially, the numerical values considered for the DCBF (6.21) and the QP (6.23) are $\alpha_{max} = 0.087$rad (5°), $\gamma_{dr} = 0.25$ and the reference input α_{ref} is the same used in the continuous-time system. When the value of γ_{dr} is increased, the DCBF acts close to the barrier limit α_{max}, and if γ_{dr} is increased considerably, the safety constraint is not respected. When the value of γ_{dr} is reduced, the DCBF becomes more conservative, acting far from the barrier limit α_{max}.

Numerical simulations with MATLAB/Simulink are presented in Figs. 10 and 11. In order to make the simulation more realistic, the actuator dead-zone and measurement noise are added to the encoder output such as in the continuous-time results. In Fig. 10, only the LQR is considered, while in Fig. 11, the final control framework with the DCBF is applied. It is also possible to see that the LQR performs well and when it is used with the DCBF, the safety constraint is also satisfied and the DCBF $h_{dr_k}(x_{dr_k})$ respects the safe set (5.5).

Figure 10: Numerical simulation (reaction wheel pendulum) - LQR without DCBF.

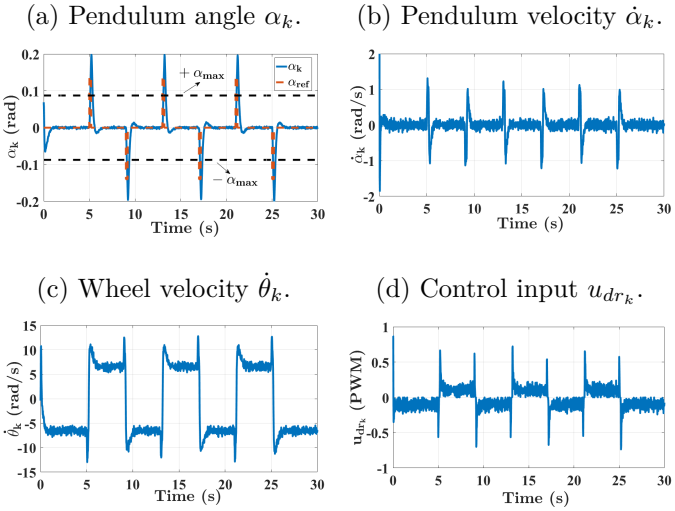

Source: Author.

Figure 11: Numerical simulation (reaction wheel pendulum) - LQR with DCBF.

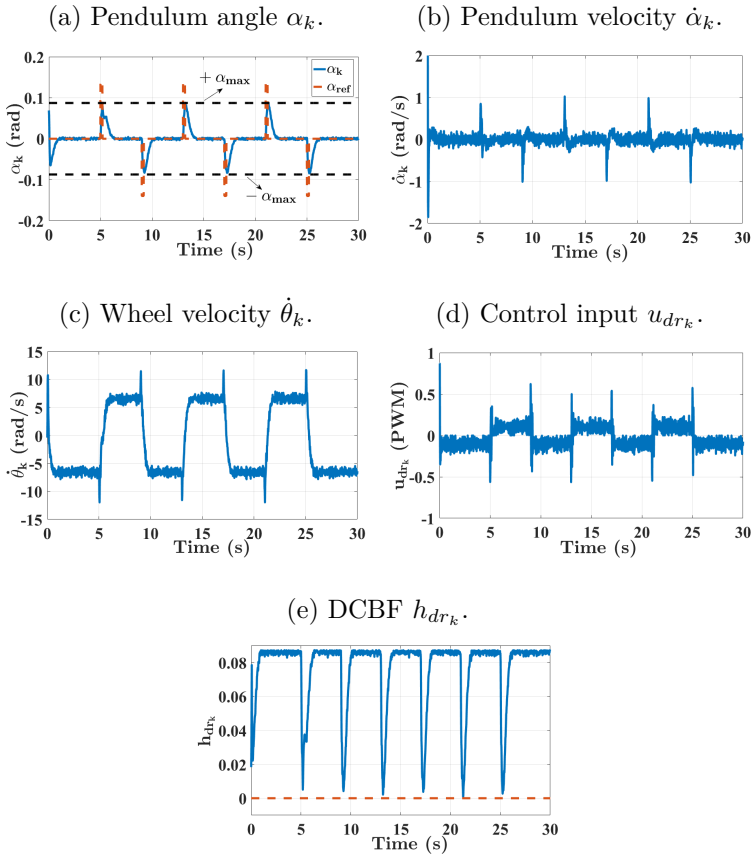

Source: Author.

Experimental results are presented in Figs. 12 for LQR, and in 13 for LQR with DCBF. Again, the system shown to be well stabilized and the DCBF is able to guarantee

the invariance of the safe set. For the same reasons presented in the continuous-time case, a more conservative DCBF is used with $\gamma_{dr} = 0.1$. In discrete-time, the results are somewhat better than in the continuous-time. One reason why this happened is that, in discrete-time, the effect of the zero-order hold in the practical implementation is included in the model (6.16). As in the continuous-time case, the control input u_{dr_k} is zero between $0s$ and $5s$, because the microcontroller was programmed, in this experiment, only to display u_{dr_k}, and in this interval, only the nominal control input $u_{no_{dr}}$ is acting in the system.

Figure 12: Experimental result (reaction wheel pendulum) - LQR without DCBF.

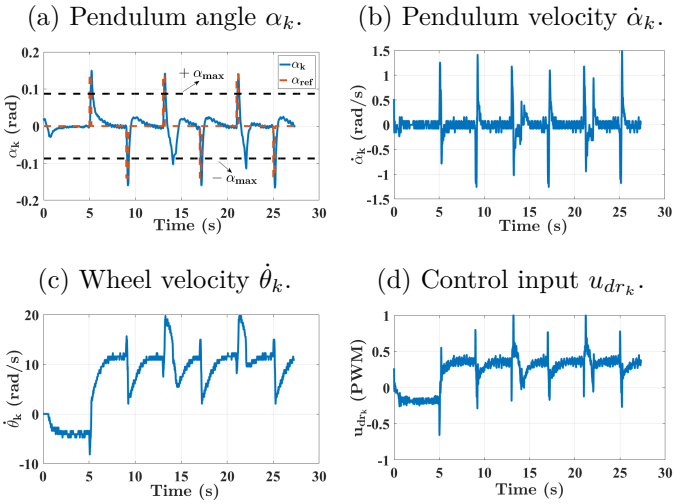

Source: Author.

Figure 13: Experimental result (reaction wheel pendulum) - LQR with DCBF.

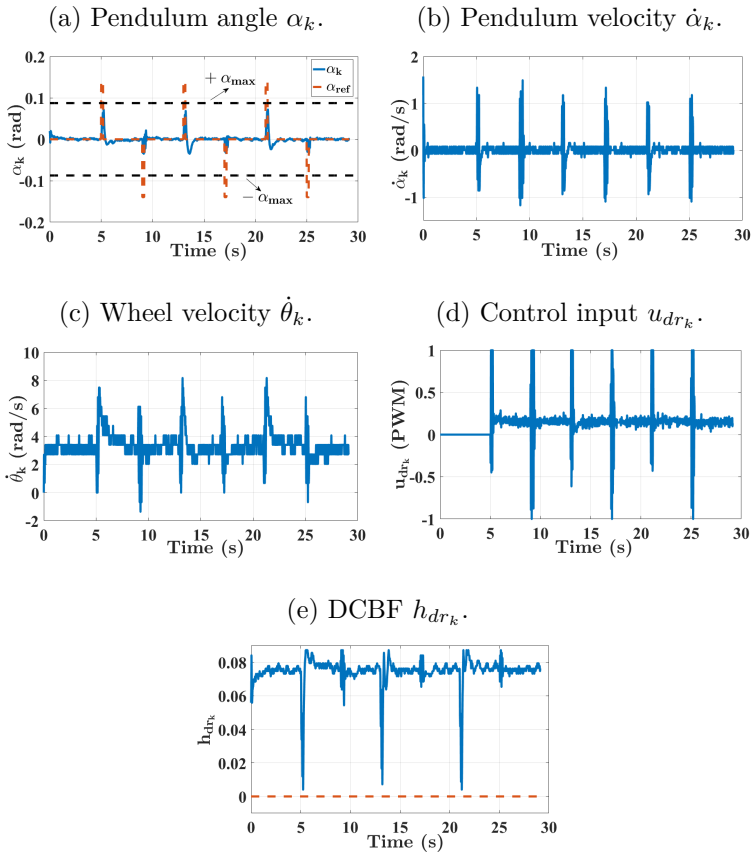

Source: Author.

6.2 Furuta Pendulum

For the Furuta pendulum, a LQR is applied as a nominal control law to satisfy the stability/tracking objective. Initially, the safety constraint is represented as an ECBF. The control framework is applied using the explicit solution without QP as described in (3.10). Posteriorly, model uncertainties are considered and the safe robust controller with SMCBF is applied. The control framework is applied using the explicit solution without QP as described in (4.21). The results are presented experimentally.

6.2.1 System Modeling

Furuta pendulum, introduced in (FURUTA; YAMAKITA; KOBAYASHI, 1992), is nonlinear, has two degrees-of-freedom (DOF) and consists of an arm rotating in the horizontal plane and a pendulum rotating in the vertical plane. The system has only one actuator that provides torque input at the arm. Furuta pendulum dynamics has analogy with more complex systems, such as walking robots and rocket thrusters.

The schematic diagram and the prototype of the Furuta pendulum developed at LCA-EPUSP are presented in Figs. 14a and 14b respectively. θ_{0_F} is the arm angle, θ_{1_F} is the pendulum angle and τ_{m_F} is the torque acting on the arm. The angles are measured with two encoders and the arm is actuated by a permanent-magnet DC motor. The pendulum parameters are arm mass m_{0_F}, pendulum mass m_{1_F}, arm length $2l_{0_F}$, pendulum length $2l_{1_F}$, radius from fixed axis to pendulum r_F and center of mass (CoM) of the arm w.r.t. fixed axis d_F.

Figure 14: Furuta pendulum developed at LCA-EPUSP.

(a) Schematic diagram. (b) Prototype.

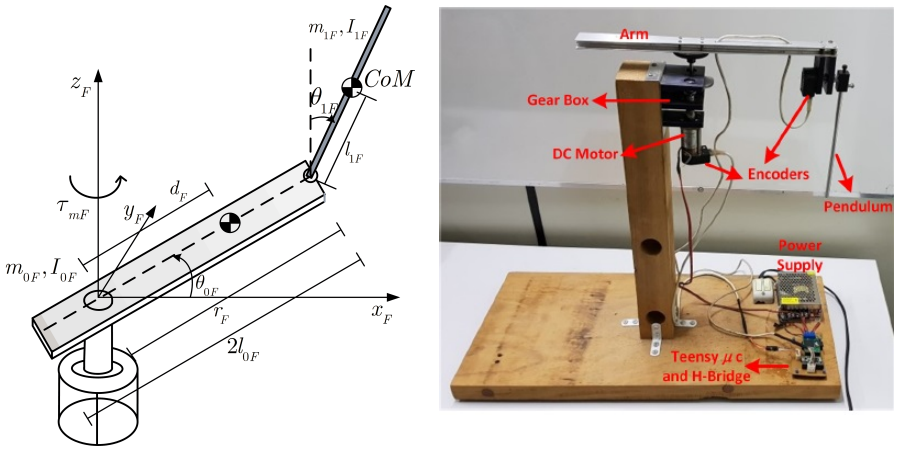

Source: Author.

The dynamic equations of the system are defined using the Lagrangian method:

$$\frac{d}{dt}\left(\frac{\partial L_F}{\partial \dot{\theta}_{i_F}}\right) - \frac{\partial L_F}{\partial \theta_{i_F}} = Q_{i_F}, \quad i = 0, 1 \tag{6.25}$$

where $L_F = K_{0_F} + K_{1_F} - V_F$ is the system Lagrangian, K_{0_F} is the kinetic energy of the arm, K_{1_F} is the kinetic energy of the pendulum, V_F is the total potential energy, θ_{0_F} and θ_{1_F} are the generalized coordinates and Q_{0_F} and Q_{1_F} are the generalized forces (torques).

The potential energy V_F can be described using the displacement of the CoM of the pendulum, such as

$$V_F = m_{1_F} g l_{1_F} \cos(\theta_{1_F}). \tag{6.26}$$

The kinetic energy of the arm K_{0_F} is composed only by the rotation. Hence,

$$K_{0_F} = \frac{I_{0_F} \dot{\theta}_{0_F}^2}{2}, \tag{6.27}$$

where the inertia I_{0_F} is given by

$$I_{0_F} = \frac{m_{0_F} (2l_{0_F})^2}{12} + m_{0_F} d_F^2. \tag{6.28}$$

The kinetic energy of the pendulum K_{1_F} can be described using its rotation, the velocity of the CoM in the x_F-direction and in y_F-direction (ANGÉLICO; BRUGNOLLI; NEVES, 2019), such as

$$K_{1_F} = \frac{I_{1_F}\dot{\theta}_{1_F}^2}{2} + \frac{m_{1_F}}{2}\left(l_{1_F}^2\dot{\theta}_{1_F}^2 + r_F^2\dot{\theta}_{0_F}^2 + l_{1_F}^2\dot{\theta}_{0_F}^2\sin^2(\theta_{1_F}) + 2r_F l_{1_F}\dot{\theta}_{0_F}\dot{\theta}_{1_F}\cos(\theta_{1_F})\right), \tag{6.29}$$

where the inertia I_{1_F} is given by

$$I_{1_F} = \frac{m_{1_F}(2l_{1_F})^2}{12}. \tag{6.30}$$

The rotation arm is actuated by a permanent-magnet DC motor. The motor equation is given by:

$$R_{m_F} i_{m_F} + K_{e_F}\dot{\theta}_{0_F} = V_{m_F}, \tag{6.31}$$

where i_{m_F} is the motor current, V_{m_F} is the motor voltage, R_{m_F} is the armature resistance and K_{e_F} is the back EMF constant. Since we consider a 12 V DC motor and a control input using a PWM signal $PWM_F \in [-1, 1]$, which includes the duty-cycle and the rotation direction, we apply the following relation:

$$V_{m_F} = 12\ PWM_F. \tag{6.32}$$

Thus, the motor torque τ_{m_F} can be obtained by:

$$\tau_{m_F} = K_{t_F} i_{m_F} = \frac{K_{t_F}}{R_{m_F}}(12\ PWM_F - K_{e_F}\dot{\theta}_{0_F}), \tag{6.33}$$

where K_{t_F} is the motor torque constant. With this relation, the input is expressed as PWM_F.

Lastly, the generalized forces Q_{0_F} and Q_{1_F} of (6.25) are defined as external forces and reaction forces with relation to each generalized variable θ_{0_F} and θ_{1_F}:

$$Q_{0_F} = \tau_{m_F} - b_{0_F}\dot{\theta}_{0_F}, \tag{6.34}$$

$$Q_{1_F} = -b_{1_F}\dot{\theta}_{1_F}, \tag{6.35}$$

where b_{0_F} is the viscous damping of motor shaft and gearbox, and b_{1_F} is the viscous damping of pendulum bearing and encoder coupling.

The numerical values of the parameters are $m_{0_F} = 0.393$kg, $m_{1_F} = 0.068$kg, $2l_{0_F} = 0.365$m, $2l_{1_F} = 0.207$m, $r_F = 0.210$m, $d_F = 0.022$m, $g = 9.81\text{m}/s^2$, $K_{t_F} = 0.02$N·m/A, $K_{e_F} = 0.08$V·s/rad, $R_{m_F} = 2.4\Omega$, $b_{0_F} = 10^{-4}$(N·m)/(rad/s) and $b_{1_F} = 10^{-6}$(N·m)/(rad/s).

6.2.2 ECBF - Explicit Solution

The behavior of the Furuta pendulum with the proposed control framework is verified experimentally using the prototype shown in Fig. 14b. The arm is actuated by a 12 V permanent-magnet DC motor and equipped with an incremental encoder used to measure the arm angle θ_{0_F}. The motor driver is a H-bridge model VNH5019. The pendulum angle θ_{1_F} is measured through another incremental encoder. The arm velocity $\dot{\theta}_{0_F}$ and the pendulum velocity $\dot{\theta}_{1_F}$ are obtained by Euler backward approximations. The system is controlled by a development board Teensy 3.2.

Furuta pendulum is related to three classical control objectives: swing-up, stabilization and trajectory tracking (AVELAR; VALENZUELA, 2016). In swing-up objective, the pendulum starts at the downward stable equilibrium point and must be taken to the upward unstable equilibrium point (HERA et al., 2009). In stabilization objective, the pendulum must be regulated at the upward unstable equilibrium point. In trajectory tracking objective, the arm must track a desired trajectory while the pendulum remains regulated at the upward unstable equilibrium point. These objectives can be solved using several control strategies such as SMC (PARK; CHWA, 2009), neural network control (VALENZUELA et al., 2016), feedback linearization (AVELAR; VALENZUELA, 2016) and Fuzzy (DANG et al., 2014). These works consider stability/tracking objectives, however safety constraints are not taken into account. So, the control framework described in this work is applied to simultaneously satisfy stability/tracking objectives and safety constraints when model uncertainties are considered. Since the focus is on safety, a simple LQR is considered as the nominal control law to reach the stability/tracking objectives in the Furuta pendulum. The safety constraint is considered to guarantee that the pendulum angular position never exceeds a predetermined bound.

In order to design the LQR to stabilize the system, the nonlinear model is linearized around the equilibrium point, resulting in:

$$\dot{x}_F = A_F x_F + B_F u_F, \tag{6.36}$$

where $x_F = \begin{bmatrix}\theta_{0_F} & \theta_{1_F} & \dot{\theta}_{0_F} & \dot{\theta}_{1_F}\end{bmatrix}^T$, $u_F = PWM_F$, A_F is the state matrix, B_F is the input matrix and the equilibrium point is $x_F^* = [0 \;\; 0 \;\; 0 \;\; 0]^T$ (pendulum at upright position). It is important to highlight that (6.36) can be related to (2.1), where $f_F(x_F) = A_F x_F$ and

$g_F(x_F) = B_F$. The numerical values of the matrices A_F and B_F are:

$$A_F = \begin{bmatrix} 0 & 0 & 1 & 0 \\ 0 & 0 & 0 & 1 \\ 0 & -19.8123 & -0.1446 & 0.0003 \\ 0 & 101.2361 & 0.22 & -0.0015 \end{bmatrix}, B_F = \begin{bmatrix} 0 \\ 0 \\ 18.8571 \\ -28.6956 \end{bmatrix}. \tag{6.37}$$

The LQR, whose formulation is described in (E.2), is designed considering

$$Q_F = \begin{bmatrix} 32.8281 & 0 & 0 & 0 \\ 0 & 131.3123 & 0 & 0 \\ 0 & 0 & 1.3131 & 0 \\ 0 & 0 & 0 & 8.2070 \end{bmatrix}, \; R_F = 1000, \tag{6.38}$$

resulting in

$$K_F = \begin{bmatrix} -0.1812 & -8.8716 & -0.2146 & -0.9226 \end{bmatrix}. \tag{6.39}$$

We propose an experiment whereby the arm angle θ_{0_F} should track a reference input $\theta_{0_{Fref}}$ and the pendulum angle θ_{1_F} should be regulated at the upward unstable equilibrium point $\theta_{1_{Fref}} = \theta^*_{1_F} = 0$rad (0°), while short pulses (0.2s) with amplitude ±0.052rad (±3°) are applied in $\theta_{1_{Fref}}$ to verify the effect of the CBF, i.e., θ_{1_F} is expected not to exit the safe set (2.2) when the CBF is applied. This amplitude was chosen because, after several experimental tests, we verify that this value is adequate to ensure the stabilization of the pendulum with the LQR, and higher values can turn the system unstable. The safety constraint is considered to guarantee that the pendulum angular position $|\theta_{1_F}|$ never exceeds a predetermined bound $\theta_{1_{Fmax}} = 0.061$rad (3.5°). Lower values for this bound were tested, however due to practical issues related to sensor imprecision and angular speed estimators, the safety constraint was not respected. It is important to highlight that the LQR is designed with an integrator aiming that θ_{0_F} track $\theta_{0_{Fref}}$ and the arm mass m_{0_F} is increased 65.14% to verify the control framework robustness.

Initially, only the LQR is applied and the CBF is not considered. The experimental results are presented in Fig. 15. In all experiments, the pendulum is assumed to start approximately at an initial angular position $\theta_{1_{ini}} = 0$rad (0°). The results show that the LQR is able to stabilize the system at the equilibrium point even with the increase in the mass m_{0_F} and the application of the pulses in $\theta_{1_{Fref}}$. However, as the CBF is not considered, the safety constraint is not respected.

Figure 15: LQR without the ECBF considering the real system dynamics (Furuta pendulum).

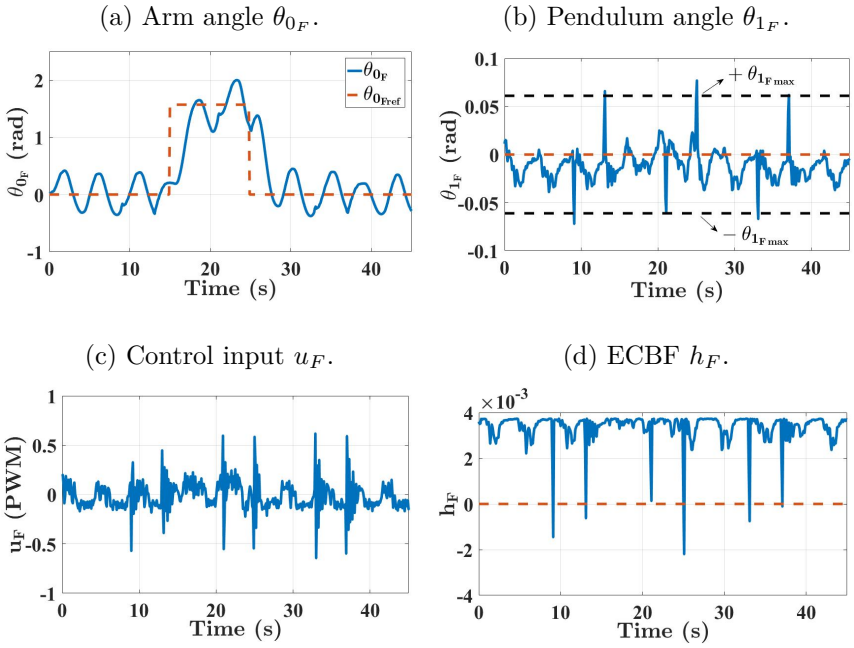

Source: Author.

Posteriorly, the CBF is considered to guarantee the safety constraint; thus, we apply the controller $u_F = u_{no_F} + u_{cbf_F}$, where u_{no_F} is the nominal LQR and u_{cbf_F} is given by (3.10), i.e., the safety constraint is expressed as an ECBF. We consider the following relative-degree two safety constraint:

$$h_F(x_F) = \theta_{1_{Fmax}}^2 - \theta_{1_F}^2. \tag{6.40}$$

We set $K_{b_F} = [1100 \;\; 50]$ and $C_{e_F} = 0$. Considering these values and the nominal system dynamics, i.e., without the increase in the mass m_{0_F}, the safety constraint is respected, as shown in Fig. 16. We observed that $|\theta_{1_F}|$ never exceeds $\theta_{1_{Fmax}}$ and the ECBF h_F respects the safe set (2.2). However, when we considered the real system dynamics, i.e., with the increase in the mass m_{0_F}, the safety constraint is not respected, as shown in Fig. 17. We observed that $|\theta_{1_F}|$ exceeds $\theta_{1_{Fmax}}$ and the ECBF h_F does not respect the safe set (2.2). Therefore, when the ECBF is applied, the safety constraint is not robustly satisfied.

Figure 16: LQR with the ECBF considering the nominal system dynamics (Furuta pendulum).

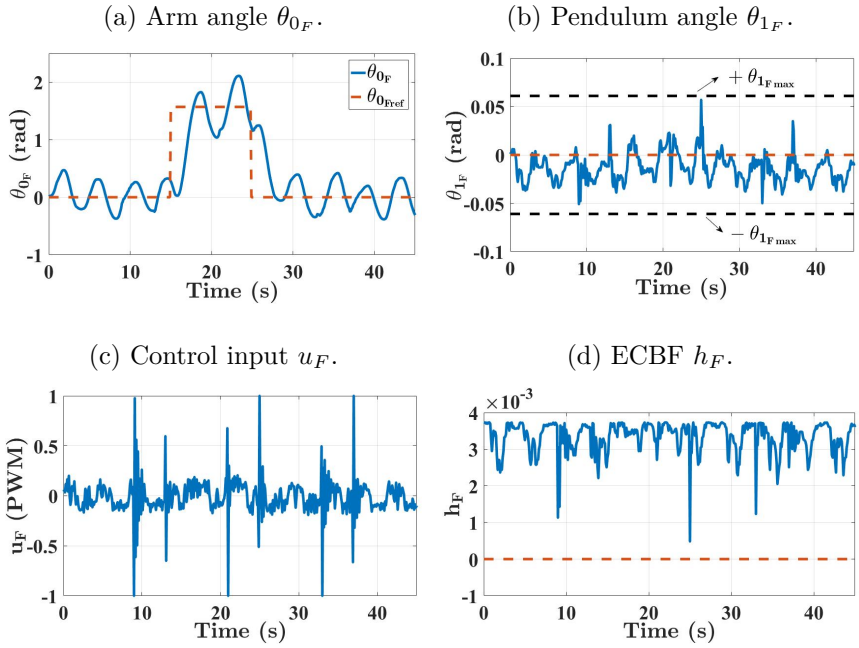

Source: Author.

Figure 17: LQR with the ECBF considering the real system dynamics (Furuta pendulum).

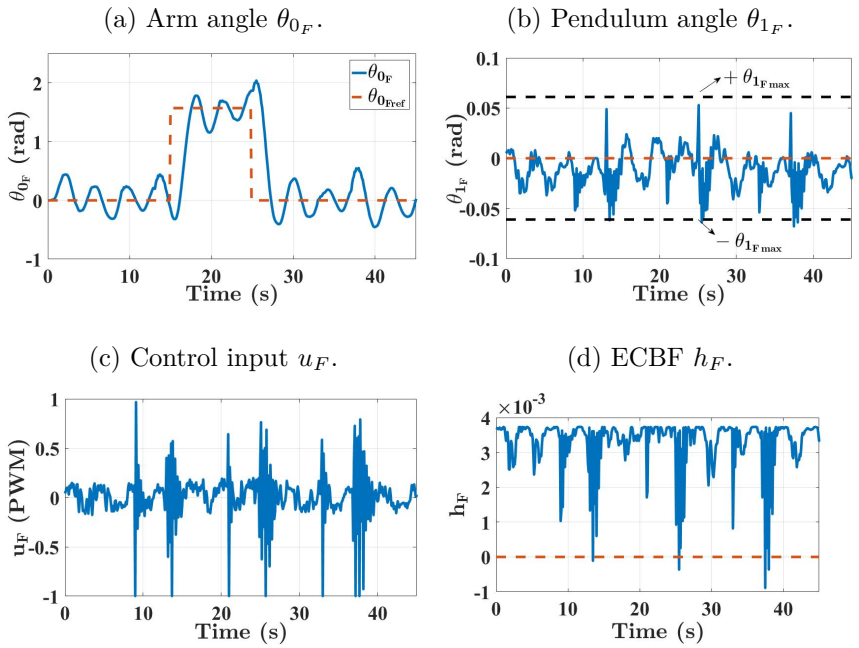

Source: Author.

6.2.3 SMCBF - Explicit Solution

Finally, to deal with the model uncertainties, we apply the controller $u_F = u_{no_F} + u_{cbf_F}$, where u_{no_F} is the nominal LQR and u_{cbf_F} is given by (4.21), i.e., the safety constraint is expressed as a SMCBF. We considered the same safety constraint h_F described in (6.40). The design parameters are $\lambda_{cbf_F} = 10$, $\eta_{cbf_F} = 5$ and the boundary layer thickness $\Phi_F = 0.1$. K_{smc_F}, defined in (4.14), is chosen in order to satisfy (4.16) and considering the uncertainty bounded, i.e., $\Delta_F = \Delta_{F_{max}}$, such as described in (4.9). We empirically set $\Delta_{F_{max}} = 1$. The uncertainty bound is chosen to increase the controller robustness. Several experimental tests were performed with different design parameters, and the design parameters considered here presented the best results. The experimental results are presented in Fig. 18, considering the nominal system dynamics and in Fig. 19, considering the real system dynamics. We observed that $|\theta_{1_F}|$ never exceeds $\theta_{1_{Fmax}}$ and the SMCBF h_F respects the safe set (2.2). Therefore, when the SMCBF is applied, the safety constraint is robustly satisfied.

Figure 18: LQR with the SMCBF considering the nominal system dynamics (Furuta pendulum).

(a) Arm angle θ_{0_F}. (b) Pendulum angle θ_{1_F}.

(c) Control input u_F. (d) SMCBF h_F.

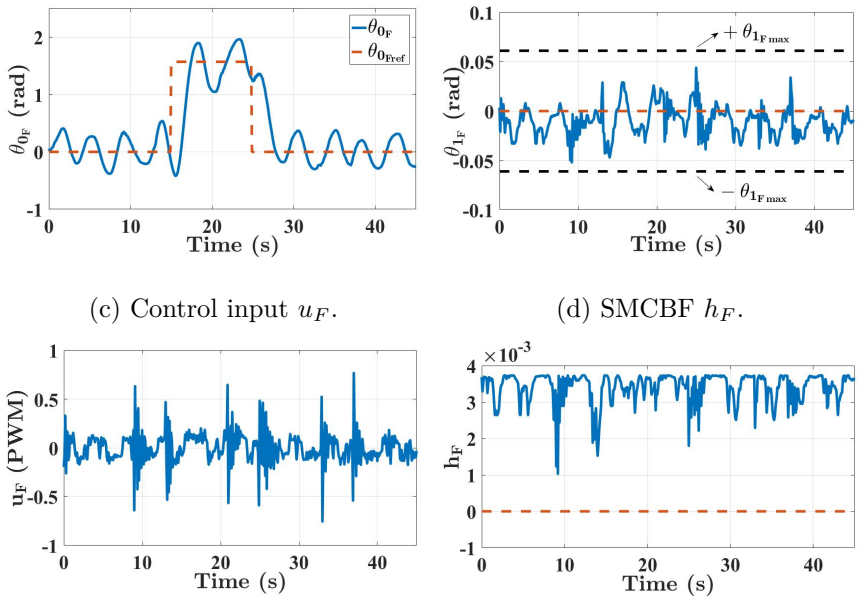

Source: Author.

Figure 19: LQR with the SMCBF considering the real system dynamics (Furuta pendulum).

(a) Arm angle θ_{0_F}. (b) Pendulum angle θ_{1_F}.

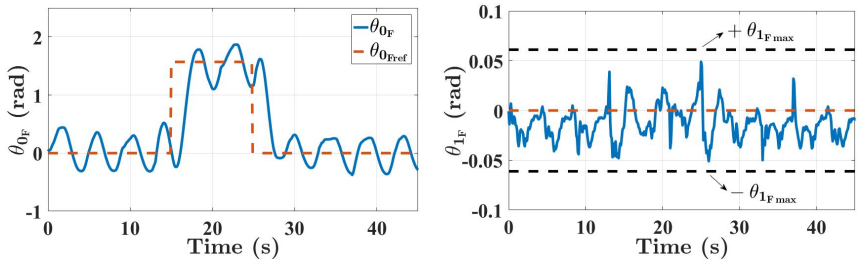

(c) Control input u_F. (d) SMCBF h_F.

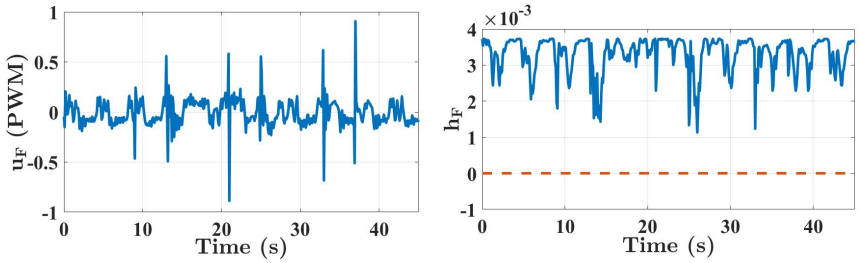

Source: Author.

6.3 MIMO MAGLEV system

For the MIMO MAGLEV system, a SMC is applied as a nominal control law to satisfy the tracking objectives. The SMC is described in Appendix F. Initially, the safety constraints are represented as multiple ECBFs. The control framework is applied as described in (3.9). Posteriorly, model uncertainties are considered and the safe robust controllers with RECBFs and SMCBFs, proposed in (4.6) and (4.20) respectively, are applied. The results are presented numerically.

6.3.1 System Modeling

MAGLEV systems can be used in several engineering applications such as magnetic bearings, high precision positioning platforms, aerospace shuttles, maglev trains, steel and semiconductor manufacturing plants and educational purposes (YU; LI, 2014). The most popular and widely used scheme for the MAGLEV system consists of a metal body, such as a ball, plate or disk suspended by a voltage-controlled magnetic field obtained from an electromagnet (HAJJAJI; OULADSINE, 2001). The objective is to keep the metal body at a prescribed reference level. The electromagnet current may be increased until the magnetic force produced compensates the gravitational force acting on the metal body.

This system is nonlinear and Single-Input-Single-Output (SISO) (BARIE; CHIASSON, 1996).

The MAGLEV system scheme analyzed in this work is based on the experimental apparatus described in (FUJII et al., 1994) and (TSUJINO; NAKASHIMA; FUJII, 1999). The system is constituted by a Y shape metal plate that must be levitated by electromagnetic attractive forces. A controller must be designed so that the plate positions track reference inputs with adequate performance. The system is also nonlinear, however, it is a MIMO system.

The schematic diagram of the MAGLEV system is presented in Fig. 20. The system is constituted by a Y shape plate made of aluminum with small pieces of iron mounted at the edges and that must be levitated by electromagnetic forces. The attractive forces are generated from three electromagnets. The controller provides voltage command signals V_1, V_2 and V_3 that are converted to proportional current signals i_1, i_2 and i_3 by power amplifiers in order to generate the corresponding attractive forces F_1, F_2 and F_3. The outputs are represented by three plate positions r_1, r_2 and r_3, measured by gap sensors mounted below the edges of the plate.

Figure 20: Schematic diagram of the MAGLEV system.

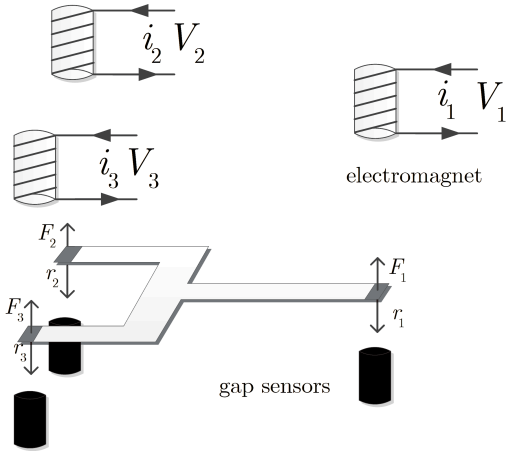

Source: Adapted from (TSUJINO; NAKASHIMA; FUJII, 1999).

The coordinate axis of the plate X_v, X_p and X_r are presented in Fig. 21. x_v is the vertical gap length between the electromagnet and the plate at the origin O, right above the center of gravity, while θ_p and θ_r are the pitching and rotating angles respectively. The parameters of the MAGLEV are the mass of the plate M, the moments of inertia around the origin O in pitching direction J_{pm} and in rolling direction J_{rm}, and the distance d_{ml} between the origin O and the center of gravity. The distances l_{1g}, l_{2g} and l_{3g} are presented in Fig. 22.

Figure 21: Coordinate axis of the plate.

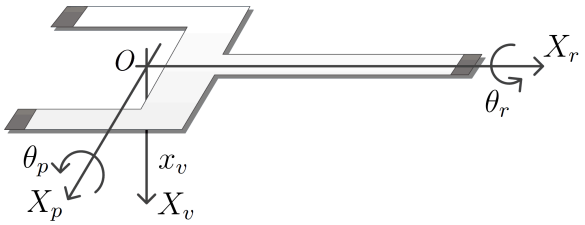

Source: Adapted from (TSUJINO; NAKASHIMA; FUJII, 1999).

Figure 22: Parameters of the MAGLEV system.

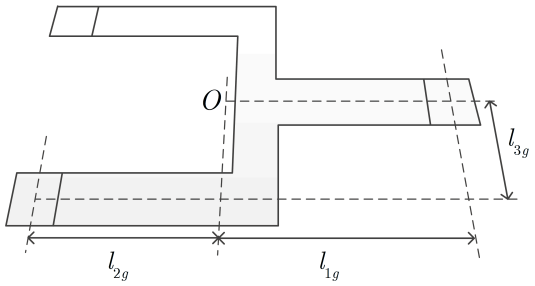

Source: Adapted from (TSUJINO; NAKASHIMA; FUJII, 1999).

The equations of vertical, pitching and rotating motions can be described respectively as (TSUJINO; NAKASHIMA; FUJII, 1999)

$$M\ddot{x}_v = Mg - (F_1 + F_2 + F_3), \tag{6.41}$$

$$J_{pm}\ddot{\theta}_p = F_1 l_{1g} - (F_2 + F_3) l_{2g} - Mgd_{ml} \sin\theta_p, \tag{6.42}$$

$$J_{rm}\ddot{\theta}_r = (F_2 - F_3) l_{3g} - Mgd_{ml} \sin\theta_r. \tag{6.43}$$

The plate positions r_1, r_2 and r_3 have the same directions as x_v and are given by

$$r_1 = x_v - l_{1g} \tan\theta_p, \tag{6.44}$$

$$r_2 = x_v + l_{2g} \tan\theta_p - l_{3g} \tan\theta_r, \tag{6.45}$$

$$r_3 = x_v + l_{2g} \tan\theta_p + l_{3g} \tan\theta_r, \tag{6.46}$$

and the electromagnets attractive forces can be written as a nonlinear function of the input voltages V_j and the plate positions r_j (TSUJINO; NAKASHIMA; FUJII, 1999):

$$F_j := k_j \left(\frac{V_j}{r_j}\right)^2 \quad j = 1, 2, 3, \tag{6.47}$$

where k_1, k_2 and k_3 are constants related to each electromagnet.

The system can be represented by:

$$\dot{x}_{ml} = f_{ml}(x_{ml}) + g_{ml}(x_{ml})w_{ml}, \tag{6.48}$$

$$y_{ml} = o_{ml}(x_{ml}), \tag{6.49}$$

where $x_{ml} = \begin{bmatrix} x_v & \theta_p & \theta_r & \dot{x}_v & \dot{\theta}_p & \dot{\theta}_r \end{bmatrix}^T$ is the state vector, $w_{ml} = [V_1^2 \;\; V_2^2 \;\; V_3^2]^T$ is the input vector, $y_{ml} = [r_1 \;\; r_2 \;\; r_3]^T$ is the output vector,

$$f_{ml}(x_{ml}) = \begin{bmatrix} \dot{x}_v & \dot{\theta}_p & \dot{\theta}_r & g & \dfrac{-Mgd_{ml}\sin\theta_p}{J_{pm}} & \dfrac{-Mgd_{ml}\sin\theta_r}{J_{rm}} \end{bmatrix}^T, \tag{6.50}$$

$$g_{ml}(x_{ml}) = \begin{bmatrix} 0 & 0 & 0 \\ 0 & 0 & 0 \\ 0 & 0 & 0 \\ -\frac{k_1}{Mr_1^2} & -\frac{k_2}{Mr_2^2} & -\frac{k_3}{Mr_3^2} \\ \frac{l_{1g}k_1}{J_{pm}r_1^2} & -\frac{l_{2g}k_2}{J_{pm}r_2^2} & -\frac{l_{2g}k_3}{J_{pm}r_3^2} \\ 0 & \frac{l_{3g}k_2}{J_{rm}r_2^2} & -\frac{l_{3g}k_3}{J_{rm}r_3^2} \end{bmatrix}, \tag{6.51}$$

and

$$o_{ml}(x_{ml}) = \begin{bmatrix} x_v - l_{1g}\tan\theta_p \\ x_v + l_{2g}\tan\theta_p - l_{3g}\tan\theta_r \\ x_v + l_{2g}\tan\theta_p + l_{3g}\tan\theta_r \end{bmatrix}. \tag{6.52}$$

It is important to highlight that the voltage command signals are given by

$$u_{ml} = \begin{bmatrix} \sqrt{w_{ml_{11}}} & \sqrt{w_{ml_{12}}} & \sqrt{w_{ml_{13}}} \end{bmatrix}^T = [V_1 \;\; V_2 \;\; V_3]^T. \tag{6.53}$$

The numerical values of the parameters, described in (TSUJINO; NAKASHIMA; FUJII, 1999), are $l_{1g} = 0.306$m, $l_{2g} = 0.203$m, $l_{3g} = 0.120$m, $M = 1.93$kg, $g = 9.81$m/s^2, $J_{pm} = 6.43 \times 10^{-2}$kg $\cdot$ m^2, $J_{rm} = 1.82 \times 10^{-2}$kg $\cdot$ m^2, $d_{ml} = 3.24 \times 10^{-3}$m, $k_1 = 3.70 \times 10^{-4}$Nm^2/V, $k_2 = 1.03 \times 10^{-4}$Nm^2/V and $k_3 = 1.36 \times 10^{-4}$Nm^2/V.

6.3.2 ECBFs

The works related to the control of MAGLEV systems typically are proposed to satisfy tracking objectives, i.e, to track reference inputs. Several control techniques are proposed and applied in the literature, such as SMC (AL-MUTHAIRI; ZRIBI, 2004), Fuzzy logic (BENOMAIR; TOKHI, 2015), MPC (KARAMPOORIAN; MOHSENI, 2010), backstepping (LIU; ZHOU, 2013), neural network (ALIASGHARY et al., 2008) and H_∞ (TSUJINO; NAKASHIMA; FUJII, 1999). However, safety constraints are not considered.

So, the control framework described in this work is applied to simultaneously satisfy tracking objectives and safety constraints.

The behavior of the MAGLEV with the proposed control framework is verified through numerical simulations with MATLAB/Simulink. We considered a simulation experiment where the plate positions r_j $(j = 1, 2, 3)$ should track the reference inputs r_{j_d} and the safety constraints must be respected. A SMC is applied as the nominal control law $w_{no_{ml}}$ for tracking the reference inputs, as described in Appendix F. The safety constraints are considered to ensure that the plate positions r_j never exceed predetermined bounds and satisfy the safe set (2.2). We considered the bounds $\pm r_{j_{\max}} = r_{j_{rs}} \pm r_{j_b}$, where $r_{1_{rs}} = -0.05$m, $r_{2_{rs}} = -0.07$m, $r_{3_{rs}} = -0.09$m and $r_{1_b} = r_{2_b} = r_{3_b} = 0.01$m. The mass of the plate M is increased 50%.

The design parameters for the nominal control $w_{no_{ml}}$, defined in (F.22), are

$$\lambda_{ml_c} = \begin{bmatrix} 50 & 0 & 0 \\ 0 & 50 & 0 \\ 0 & 0 & 50 \end{bmatrix} \tag{6.54}$$

for the sliding surface (F.16), $\eta_{ml_c} = [30 \;\; 30 \;\; 30]^T$ for the sliding condition (F.17) and $\Phi_{ml_c} = [0.05 \;\; 0.05 \;\; 0.05]^T$ for the boundary layer thickness. The gain K_{ml_c} is set in order to satisfy (F.21).

Initially, only the SMC is applied as the nominal control law and the safety constraints are not considered. The simulation results are presented in Fig. 23. In all numerical simulations, the MAGLEV is assumed to start at an initial position $r_{1_0} = r_{2_0} = r_{3_0} = -0.05$m. The results show that the SMC is able to track the reference inputs even with the increase in the mass of the plate M.

Figure 23: SMC without CBFs (MAGLEV).

(a) Outputs y_{ml}.

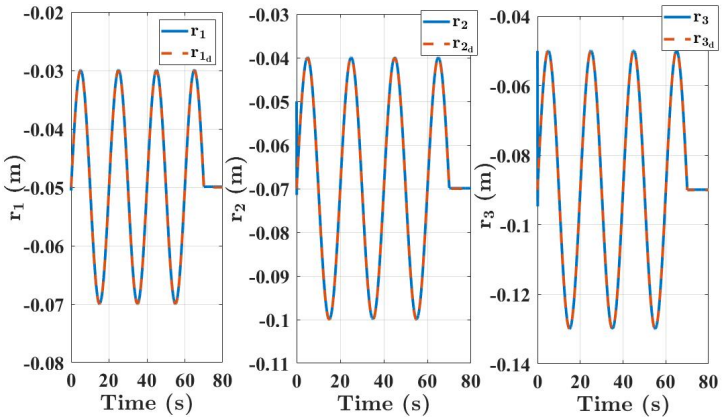

(b) States x_{ml}.

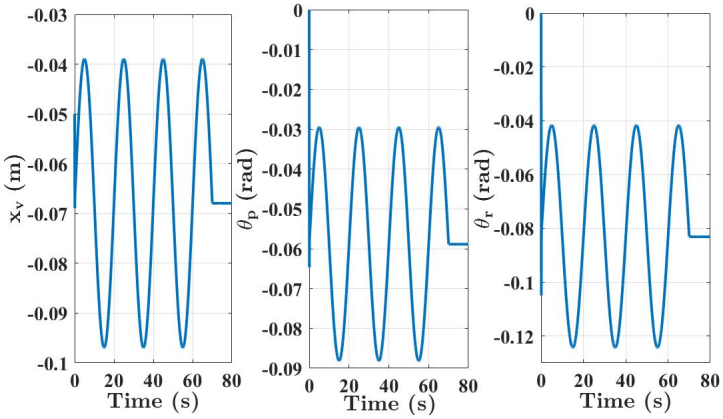

(c) Voltage signals u_{ml}.

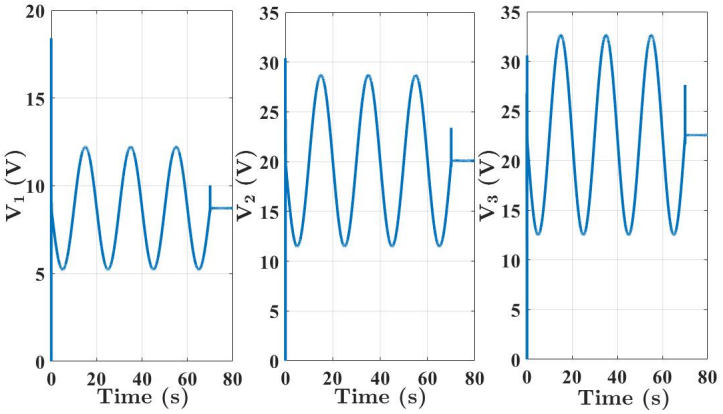

Source: Author.

Posteriorly, the safety constraints are considered; thus, the QP-based controller (3.9) that unifies the nominal control law $w_{no_{ml}}$ and the safety constraints, expressed as ECBFs,

is applied. The controller is adapted to multiple safety constraints, such that

$$\begin{aligned}
\mathbf{w_{ml}}^*(x_{ml}) = & \underset{(w_{ml},\mu_{b_{ml}})\in\mathbb{R}^6}{\arg\min} \; w_{ml}^T w_{ml} - 2w_{no_{ml}}^T w_{ml} \\
s.t. \; & \left[L_{g_{ml}}L_{f_{ml}}h_1(x_{ml}) \;\; L_{g_{ml}}L_{f_{ml}}h_2(x_{ml}) \;\; L_{g_{ml}}L_{f_{ml}}h_3(x_{ml})\right] w_{ml} \\
& + \left[L_{f_{ml}}^2 h_1(x_{ml}) \;\; L_{f_{ml}}^2 h_2(x_{ml}) \;\; L_{f_{ml}}^2 h_3(x_{ml})\right]^T = \mu_{b_{ml}}, \\
& \mu_{b_{ml}} = \left[\mu_{b_1} \;\; \mu_{b_2} \;\; \mu_{b_3}\right]^T \geq -\left[K_{b_1}\eta_{b_1}(x_{ml}) \;\; K_{b_2}\eta_{b_2}(x_{ml}) \;\; K_{b_3}\eta_{b_3}(x_{ml})\right]^T, \quad (6.55)
\end{aligned}$$

where we consider the following relative-degree two safety constraints, expressed as the ECBFs

$$h_j(x_{ml}) = (r_{j_b})^2 - (r_j - r_{j_{rs}})^2, \quad j = 1, 2, 3. \tag{6.56}$$

The QP is implemented using Hildreth's QP procedure (HILDRETH, 1957). We set $K_{b_1} = [2000 \;\; 200]$, $K_{b_2} = [2000 \;\; 200]$ and $K_{b_3} = [2000 \;\; 500]$. Considering these values and the nominal system dynamics, i.e., without the increase in the mass of the plate M, the safety constraints are respected, as shown in Fig. 24. We observed that $|r_j|$ never exceeds $\pm r_{j_{\max}}$ and the safe set (2.2) is respected. Initially $|r_2|$ and $|r_3|$ exceed $+r_{2_{\max}}$ and $+r_{3_{\max}}$ since the ECBFs are programmed to act only after the transient time due to the initial condition. However, when the mass of the plate M is increased, the safety constraints are not respected, as shown in Fig. 25. Therefore, the ECBFs are not robustly satisfied.

Figure 24: SMC with ECBFs considering the nominal system dynamics (MAGLEV).

(a) Outputs y_{ml}.

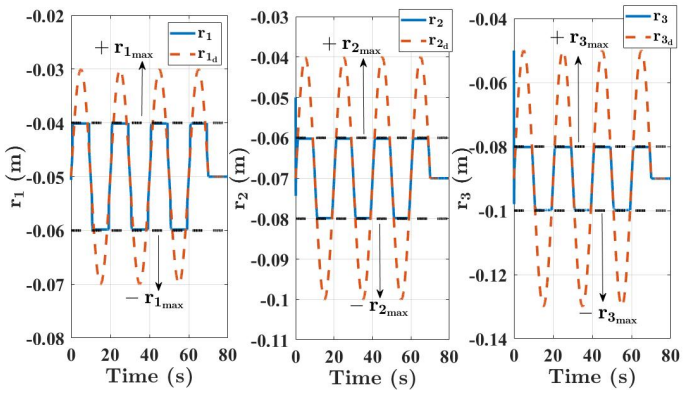

(b) States x_{ml}.

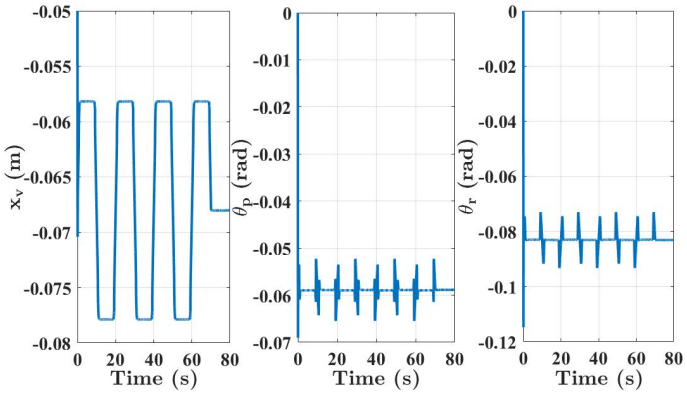

(c) Voltage signals u_{ml}.

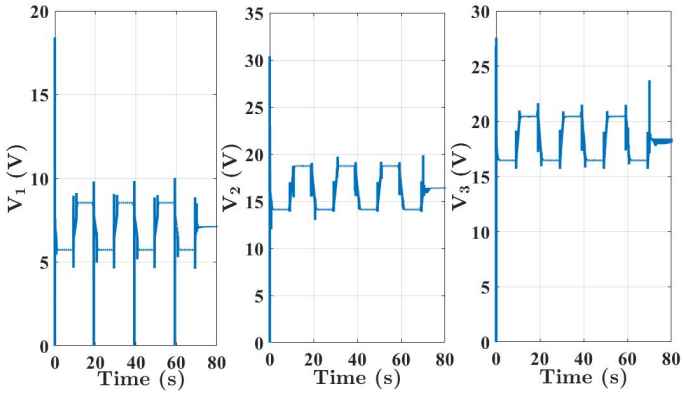

(d) ECBFs h_{ml}.

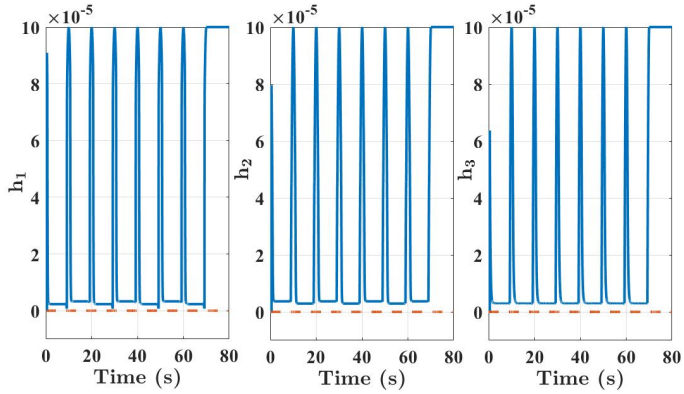

Source: Author.

Figure 25: SMC with ECBFs considering the real system dynamics (MAGLEV).

(a) Outputs y_{ml}.

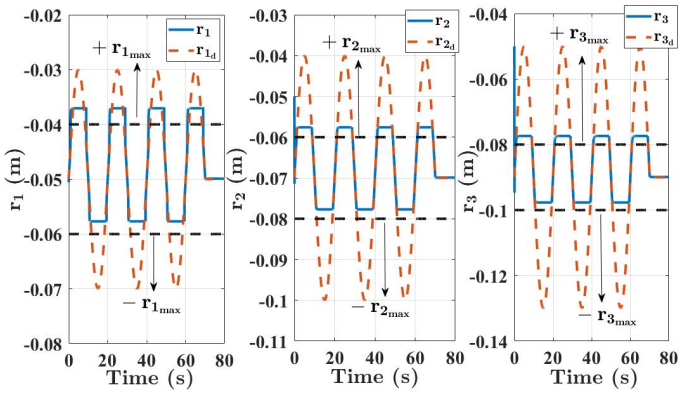

(b) States x_{ml}.

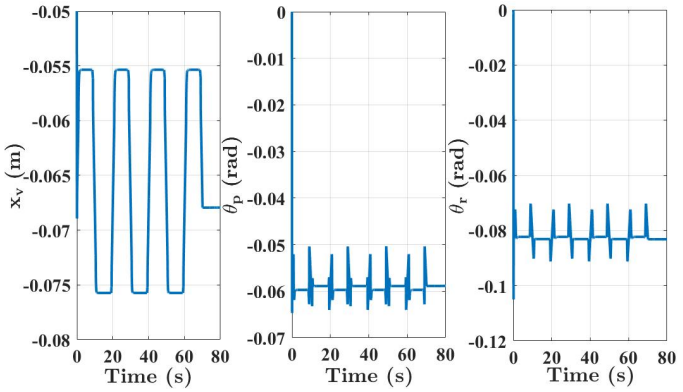

(c) Voltage signals u_{ml}.

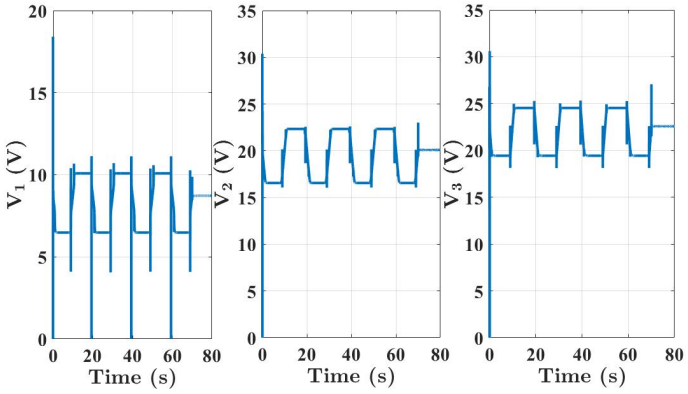

(d) ECBFs h_{ml}.

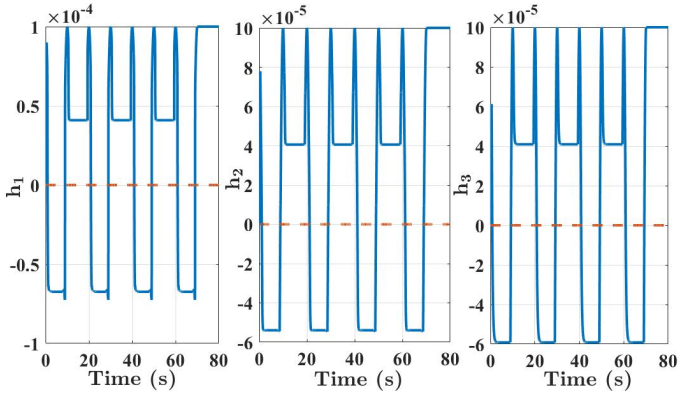

Source: Author.

6.3.3 RECBFs

The model uncertainties can be considered applying the QP-based controller (4.6) that unifies the nominal control law $w_{no_{ml}}$ and the safety constraints, expressed as RECBFs. The controller is adapted to multiple safety constraints, such that

$$
\begin{aligned}
\mathbf{w_{ml}}^*(x_{ml}) = & \underset{(w_{ml},\mu_{b_{ml}})\in\mathbb{R}^6}{\arg\min} \; w_{ml}^T w_{ml} - 2w_{no_{ml}}^T w_{ml} \\
s.t. \;\; & A_{r_1}(x_{ml})w_{ml} + b_{r_1}(x_{ml}) = \mu_{b_1}, \\
& A_{r_2}(x_{ml})w_{ml} + b_{r_2}(x_{ml}) = \mu_{b_2}, \\
& A_{r_3}(x_{ml})w_{ml} + b_{r_3}(x_{ml}) = \mu_{b_3}, \\
& \psi_{0,bv_1}^{max}(x_{ml}) + \psi_{1,bv_1}^{p}(x_{ml})\mu_{b_1} \geq 0, \\
& \psi_{0,bv_1}^{max}(x_{ml}) + \psi_{1,bv_1}^{n}(x_{ml})\mu_{b_1} \geq 0, \\
& \psi_{0,bv_2}^{max}(x_{ml}) + \psi_{1,bv_2}^{p}(x_{ml})\mu_{b_2} \geq 0, \\
& \psi_{0,bv_2}^{max}(x_{ml}) + \psi_{1,bv_2}^{n}(x_{ml})\mu_{b_2} \geq 0, \\
& \psi_{0,bv_3}^{max}(x_{ml}) + \psi_{1,bv_3}^{p}(x_{ml})\mu_{b_3} \geq 0, \\
& \psi_{0,bv_3}^{max}(x_{ml}) + \psi_{1,bv_3}^{n}(x_{ml})\mu_{b_3} \geq 0,
\end{aligned}
\tag{6.57}
$$

where $A_{r_j}(x_{ml})$, $b_{r_j}(x_{ml})$, $\psi_{0,bv_j}^{max}(x_{ml})$, $\psi_{1,bv_j}^{p}(x_{ml})$ and $\psi_{1,bv_j}^{n}(x_{ml})$, with $j = 1, 2, 3$, are described in (4.2)-(4.6). K_{b_j} are the same applied in subsection 6.3.2 and we considered $\Delta_{1_j,max}^{b} = 0.05$ and $\Delta_{2_j,max}^{b} = 0.9$. The simulation results are presented in Fig. 26. We observed that $|r_j|$ never exceeds $\pm r_{j_{\max}}$ and the RECBFs $h_j(x_{ml})$ respect the safe set (2.2). Initially $|r_2|$ and $|r_3|$ exceed $+r_{2max}$ and $+r_{3max}$ since the RECBFs are programmed to act only after the transient time due to the initial condition. Therefore, the RECBFs are robustly satisfied.

Figure 26: SMC with RECBFs considering the real system dynamics (MAGLEV).

(a) Outputs y_{ml}.

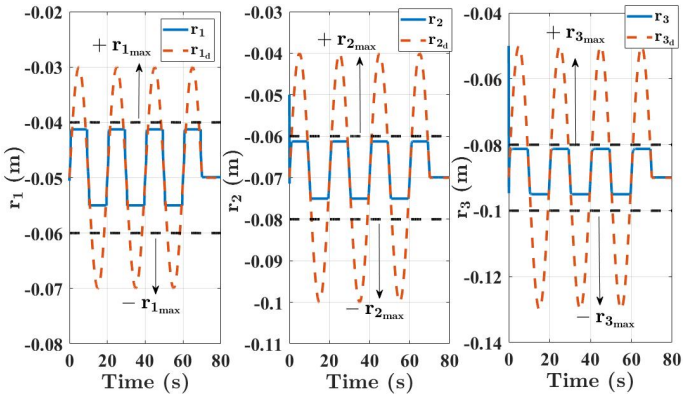

(b) States x_{ml}.

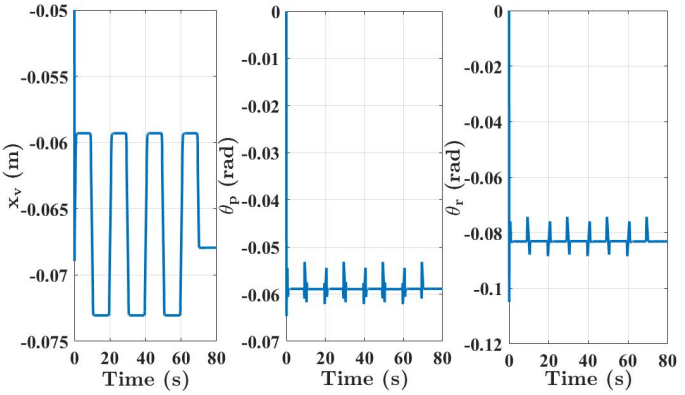

(c) Voltage signals u_{ml}.

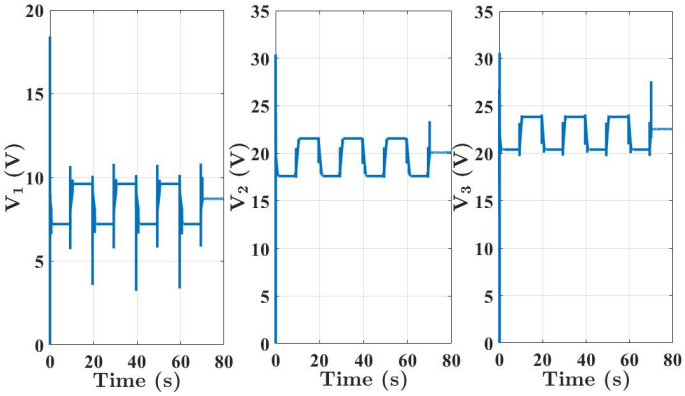

(d) RECBFs h_{ml}.

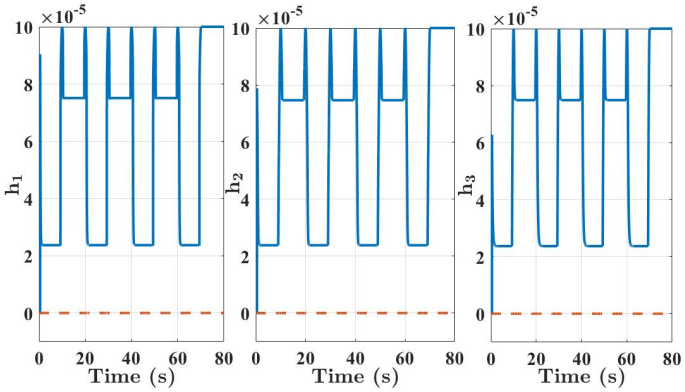

Source: Author.

6.3.4 SMCBFs

The model uncertainties can be considered again applying the QP-based controller (4.20) that unifies the nominal control law $w_{no_{ml}}$ and the safety constraints, expressed as SMCBFs. The controller is adapted to multiple safety constraints, such that

$$
\begin{aligned}
\mathbf{w_{ml}}^*(x_{ml}) = & \underset{(w_{ml},\mu_{b_{ml}})\in\mathbb{R}^6}{\arg\min} \; w_{ml}^T w_{ml} - 2w_{no_{ml}}^T w_{ml} \\
s.t. \;\; & \left[L_{g_{ml}}L_{f_{ml}}h_1(x_{ml}) \;\; L_{g_{ml}}L_{f_{ml}}h_2(x_{ml}) \;\; L_{g_{ml}}L_{f_{ml}}h_3(x_{ml})\right] w_{ml} \\
& + \left[L_{f_{ml}}^2 h_1(x_{ml}) \;\; L_{f_{ml}}^2 h_2(x_{ml}) \;\; L_{f_{ml}}^2 h_3(x_{ml})\right]^T = \mu_{b_{ml}}, \\
& \mu_{b_{ml}} = \left[\mu_{b_1} \;\; \mu_{b_2} \;\; \mu_{b_3}\right]^T \geq \left[\mu_{eq_1} \;\; \mu_{eq_2} \;\; \mu_{eq_3}\right]^T - K_{ml_s}\mathrm{sat}(\mathrm{s_{ml_s}}/\Phi_{\mathrm{ml_s}}), \quad (6.58)
\end{aligned}
$$

where the sliding surface s_{ml_s} is given by (4.10) considering $h_{ml} = \left[h_1 \;\; h_2 \;\; h_3\right]^T$,

$$
\lambda_{ml_s} = \begin{bmatrix} 50 & 0 & 0 \\ 0 & 50 & 0 \\ 0 & 0 & 50 \end{bmatrix},
$$

$\eta_{ml_s} = \left[200 \;\; 200 \;\; 200\right]^T$ for the sliding condition (4.11) and $\Phi_{ml_s} = \left[0.003 \;\; 0.003 \;\; 0.003\right]^T$ for the boundary layer thickness. The gain K_{ml_s} is chosen in order to satisfy (4.16) and we also assumed that $\Delta_{ml_{\max}} = \left[10 \;\; 10 \;\; 10\right]^T$ in (4.9). Several numerical tests were performed with different design parameters, and the design parameters considered here presented the best results. Simulation results are presented in Fig. 27. We observed that $|r_j|$ never exceeds $\pm r_{j_{\max}}$ and the safe set (2.2) is respected. Therefore, the SMCBFs are robustly satisfied.

Figure 27: SMC with SMCBFs considering the real system dynamics (MAGLEV).

(a) Outputs y_{ml}.

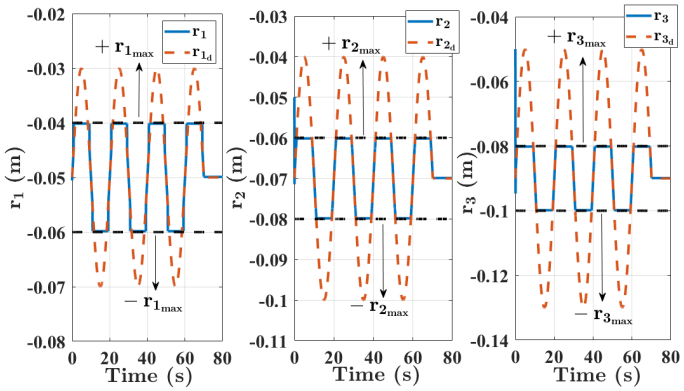

(b) States x_{ml}.

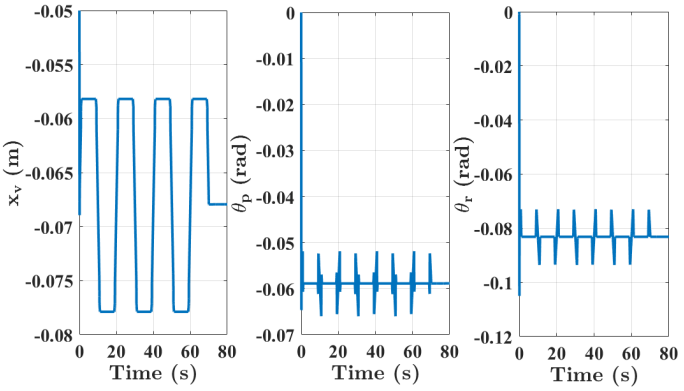

(c) Voltage signals u_{ml}.

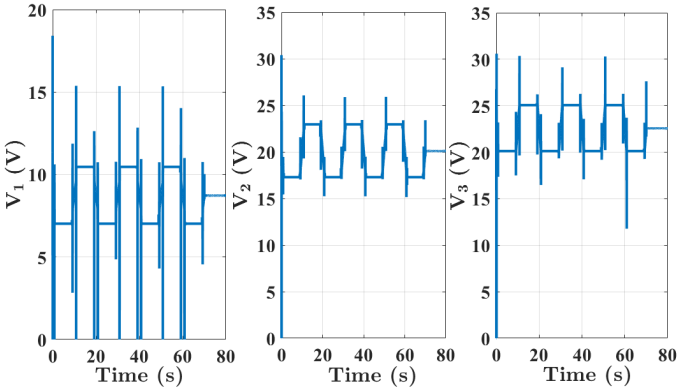

(d) SMCBFs h_{ml}.

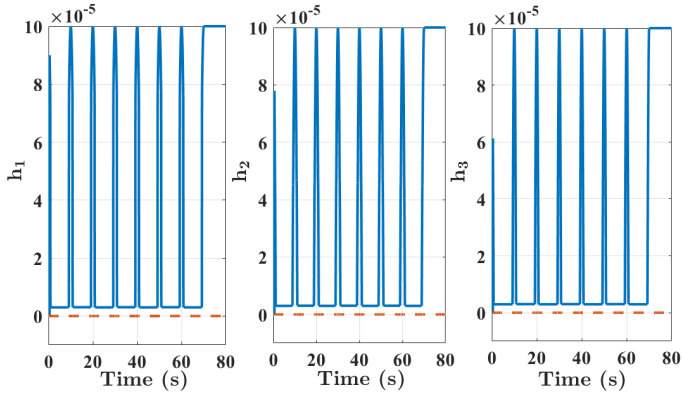

Source: Author.

6.4 ACC - Automotive Vehicle

As previously described, adaptive cruise control (ACC) is applied to an automotive vehicle available at EPUSP considering a Smith predictor to compensate an input delay and to a generic automotive vehicle considering an upper level controller (outer loop) and a lower level controller (inner loop). The control framework described in this work has already been applied to the ACC problem. However, the works presented in the literature related to this control strategy do not deal with input delay for the ACC problem and only consider the ACC upper level controller that will be described posteriorly.

6.4.1 ACC - Introduction

Advanced driver assistance systems (ADAS) is related to technologies that aim to reduce the risk of accidents, improve safety, and enhance comfort and performance for drivers (MOON; MOON; YI, 2009). These technologies are ACC, lane keeping, collision avoidance (CA) and automated parking assistance. In this work, we considered ACC. ACC is an extension of cruise control (CC), which is a very widespread feature in some modern vehicles (NAUS et al., 2010), (XIAO; GAO, 2010). The first researches with ACC were developed in the late 90s and nowadays some cars and trucks are equipped with ACC (IOANNOU; CHIEN, 1993), (VAHIDI; ESKANDARIAN, 2003). The CC objective is to control an ego (host) vehicle speed aiming to track a desired speed (cruise speed) provided by the driver. In CC, only the throttle is used as actuator. The ACC must adapt the host vehicle speed to maintain a safe distance to a target (leader) vehicle, i.e., the ACC objective is to control the host vehicle speed aiming to track a desired distance between the vehicles. When there is no leader vehicle, the host vehicle enters in CC mode and only tracks the cruise speed provided by the driver. In CA, the objective is to avoid a collision between the leader and the host vehicle. In ACC and CA, throttle and brake are used as actuators (NAUS et al., 2010). Usually, sensors like radars are applied to detect the leader vehicle and to measure the relative distance and the relative speed between the vehicles.

The schematic diagram of the ACC is described in Fig. 28. The host vehicle, with speed v_h and acceleration a_h, is equipped with ACC and therefore maintains a safe distance to the leader vehicle, with speed v_l. A radar measures the relative distance x_r and the relative speed $v_r = v_l - v_h$ between the vehicles. v_c is the cruise speed provided by the driver in CC mode.

Figure 28: Schematic diagram of the ACC. Adapted from (NAUS et al., 2010).

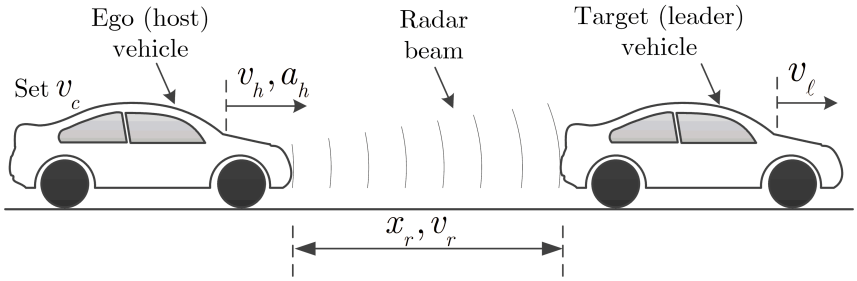

Source: Author.

The schematic diagram of the ACC control loop is described in Fig. 29. The control loop is divided in two parts: upper level controller (outer loop) and lower level controller (inner loop). The upper level controller provides a desired acceleration/deceleration a_h^* to the host vehicle to maintain a safe distance to the leader vehicle. The lower level controller receives a_h and a_h^* as inputs, compares these inputs and provides the control signal u_{th} to the throttle pedal and u_{br} to the brake pedal aiming that a_h tracks a_h^*. The driver can enable or disable the ACC. When ACC is disabled, the system enters in CC mode, i.e., tracks the cruise speed v_c provided by the driver.

Figure 29: Schematic diagram of the ACC control loop. Adapted from (NAUS et al., 2010).

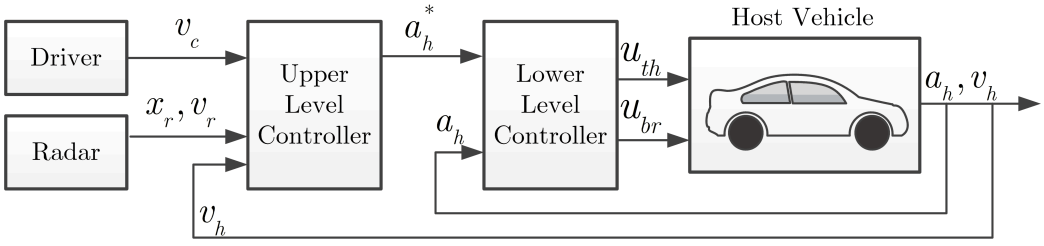

Source: Author.

The main objective of upper level controller is to maintain a safe distance between the vehicles. However, in some works, other characteristics are considered, such as safety, comfort, fuel economy and traffic-flow efficiency (VAHIDI; ESKANDARIAN, 2003). These characteristics impose conflicting control objectives and introduce constraints, complicating the controller design. For example, if safety is a priority, the system must be agile, requiring high acceleration and deceleration levels, which is not desirable concerning comfort or fuel economy (NAUS et al., 2010). The upper level controller of the ACC can be designed considering these multiple conflicting objectives using MPC. Some works describe the ACC design with MPC, such as (NAUS et al., 2010), (LI et al., 2011), (CORONA;

SCHUTTER, 2008), (LI et al., 2017) and (MAGDICI; ALTHOFF, 2017). As ACC works very similarly to the driver's behavior in a practical situation, its control and logic need to work similarly to the decision-making process and characteristics of the driver. So, several researches focus on modeling and understanding the driver's behavior and design the ACC based on these characteristics, such as (GOODRICH; BOER, 2003), (PENG, 2002) and (FANCHER; BAREKET; ERVIN, 2000).

Some works describe cooperative adaptive cruise control (CACC) to improve traffic throughput, fuel efficiency, and vehicle safety (SAWANT; CHASKAR; GINOYA, 2021; WU; LIN; ESKANDARIAN, 2019; ZHU; HE; ZHAO, 2020). The CACC utilizes onboard sensors and a wireless communication to detect more information of the surrounding vehicles and road infrastructure (SAWANT; CHASKAR; GINOYA, 2021).

The work (MOON; MOON; YI, 2009) describes a control scheme for ACC with CA aiming safety and comfort. The scheme has three control modes. The mode 1 or comfort-mode only presents ACC, the mode 2 or large-deceleration mode presents ACC and CA and the mode 3 or severe-braking mode only presents CA. These modes are selected according to two indexes: warning index and inverse time-to-collision. When the warning index is high and the inverse time-to-collision is low, the driving situation is in a safe region. However, if the warning index decreases or the inverse time-to-collision gradually increases, the danger of a collision increases and the vehicle needs to quickly decelerate to avoid a warning region. When the warning index is low and the inverse time-to-collision is high, the driving situation is critical and therefore an emergency brake should be applied (MOON; MOON; YI, 2009).

Other control strategies are applied to the ACC problem, such as intelligent control with neural networks in (KUYUMCU; SENGOR, 2016) and SMC in (GANJI et al., 2014).

It is important to highlight that the comfort of a driving action is often related to the number, size and frequency of vibrations or oscillations in the longitudinal acceleration of the vehicle due to, for example, external disturbances, engine torque peaks, driveline characteristics, etc. Therefore, in ACC, the maximum values or peaks of acceleration and derivative of acceleration (jerk) must be bounded (NAUS et al., 2010). The work (MOON; MOON; YI, 2009) describes that, in tests performed with drivers, 98% of accelerations/decelerations were between -2.17 and 1.77 m/s^2. Most drivers and passengers feel significantly uncomfortable when the vehicle deceleration is greater than 3-4 m/s^2. Drivers use large deceleration (greater than 4 m/s^2) only when they really need to apply severe braking to prevent an unsafe distance between the leader and the host vehi-

cle. According to legislation, the maximum deceleration is limited to 3 m/s^2 (ISO15622, 2002). The work (MOON; MOON; YI, 2009) also describes that, according to tests performed with drivers, the maximum and minimum values of acceleration to provide comfort vary with the vehicle speed. Finally, (MOON; MOON; YI, 2009) considers $a_h > 2m/s^2$ for the comfort-mode (ACC), $-2m/s^2 \geqslant a_h > -4m/s^2$ for the large-deceleration mode (ACC+CA) and $-4m/s^2 \geq a_h$ for the severe-braking mode (CA). The work (NAUS et al., 2010) considers a maximum jerk of 3 m/s^3.

The ACC problem involves a tracking objective (track a desired cruise speed provided by the driver), a safety constraint (maintain a safe distance between the leader and the host vehicle) and comfort constraints (maximum values or peaks of acceleration and jerk must be bounded). The tracking objective and, the safety and comfort constraints can conflict in certain situations and the control must set priority for safety and comfort constraints. Therefore, the control framework described in this work is a reasonable choice for solving the upper level controller.

The control framework described in this work has already been considered to the ACC problem. In (AMES et al., 2017), it is applied to ACC and lane keeping problems separately and the results are presented through numerical simulations. In (HU; WANG, 2021) and (SON; NGUYEN, 2019), CBF is considered to ACC and the results are presented using the simulators Carsim and Amesim respectively. In (XU et al., 2017), the control framework is applied to ACC and lane keeping problems simultaneously and the results are obtained experimentally on robot testbeds. In (MEHRA et al., 2015), it is applied to ACC and the results are obtained experimentally on scale-model cars. It is important to highlight that these works do not consider the lower level controller. However, in this work, we apply the control framework with CBF considering the upper level controller and the lower level controller simultaneously.

6.4.2 Application 1

The first application considers ACC applied to an automotive vehicle available at EPUSP considering a Smith predictor to compensate an input delay. The host vehicle considered is a Volkswagen Polo Sedan model with spark-ignition engine 2.0 L. The vehicle is controlled by an open-source electronic control unit and was tested on an inertial dynamometer from NAPRO company (BRUGNOLLI et al., 2019).

Although the vehicle has a customized electronic control unit, it does not have an electronic brake system. Thus, the brake action u_{br} was discarded as a control input.

The control input u_{th} is equivalent to the throttle pedal, where the range varies from 0% (not pushed) to 100% (fully pushed) (BRUGNOLLI et al., 2019). The system output is the host vehicle speed v_h. This same vehicle is controlled with ACC in (BRUGNOLLI et al., 2019) and (BRUGNOLLI; ANGÉLICO; LAGANÁ, 2019) using Dahlin Control and MPC respectively. It is important to highlight that, in this application, the lower level controller, described in Fig. 29, is not considered and the output of the upper level controller is u_{th}.

The system identification, obtained in (BRUGNOLLI et al., 2019) and considering a sampling time $T_{d_{acc}} = 0.5s$, and the vehicle in third gear, is given by:

$$\frac{V_h(s)}{U_{th}(s)} = \frac{0.1788}{s + 0.2041} e^{-0.5s}, \tag{6.59}$$

for continuous-time and by:

$$\frac{V_h(z)}{U_{th}(z)} = \frac{0.085}{z - 0.903} z^{-1}, \tag{6.60}$$

for discrete-time. The vehicle dynamics presents an input time-delay of 0.5s or one sampling time (z^{-1}). This input time-delay can degrade performance and stability. Thus, a Smith predictor is considered to compensate this input time-delay. Smith predictor will be described next.

6.4.2.1 Smith Predictor

Control systems with time-delay is a topic analyzed by engineers and scientists for decades. Time-delay is commonly seen in engineering applications, such as thermic and chemical. The delay can be found in system states, control input or system output and can be generated by sensors and actuators in the control loop. Time-delay, in general, degrades performance and stability of control systems.

A common alternative to design control systems with time-delay is to use Padé approximation to represent time-delay. This can generate considerable increase in system order and sensibility to perturbations. One of the most traditional structures and widely used in industry to compensate time-delay is the Smith predictor, proposed by O. J. Smith (SMITH, 1957).

Smith predictor is a control structure that shifts the delay outside the control loop, so that the controller acts on the process as if the closed-loop dynamics is not delayed (NORMEY-RICO; CAMACHO, 2008). When Smith predictor was developed, a constant time-delay and an exact system model were supposed. Therefore, Smith predictor is very

sensitive to model uncertainties.

Fig. 30 shows a block diagram of the Smith predictor. $K_{sm}(s)$ is the controller, $G_n(s)$ is the nominal system model without time-delay, $e^{-\tau_d s}$ represents the time-delay τ_d and $G(s)$ is the real system model. $r_e(t)$ is the reference input, $u(t)$ is the control input, $y(t)$ is the system output, $\hat{y}(t+\tau_d)$ and $\hat{y}(t)$ are the predicted values for the system output.

Figure 30: Block diagram of the Smith predictor.

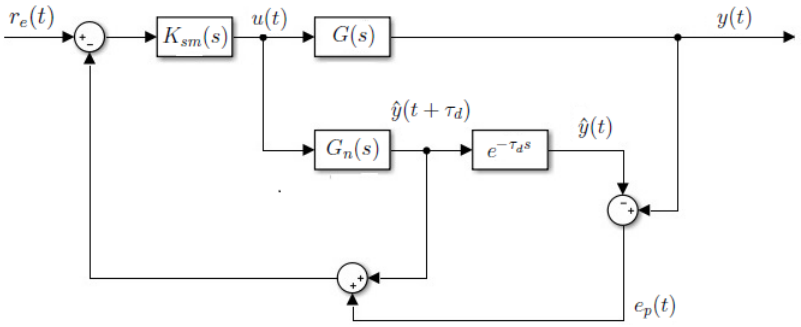

Source: Author.

The closed-loop transfer function is given by:

$$\frac{Y(s)}{R_e(s)} = \frac{K_{sm}(s)G(s)}{1 + K_{sm}(s)\left[G(s) - G_n(s)e^{-\tau_d s} + G_n(s)\right]}. \tag{6.61}$$

If there is no error between nominal system model and real system model, i.e., $G_n(s)e^{-\tau_d s} = G(s)$, the prediction error $e_p(t)$ will be zero. Therefore, (6.61) becomes:

$$\frac{Y(s)}{R_e(s)} = \frac{K_{sm}(s)G(s)}{1 + K_{sm}(s)G_n(s)} \tag{6.62}$$

and the delay is compensated. Thus, the feedback signal will be a prediction of the process output and the controller $K_{sm}(s)$ can be designed considering the process without time-delay. This design procedure can be easily extended to discrete-time.

6.4.2.2 Control Framework

As previously described, the vehicle dynamics presents an input time-delay. Using the Smith predictor, the controller can be designed disregarding delay. The design procedure is done considering the system in structure (2.1) for continuous-time and in structure (5.1) for discrete-time. Thus, the system is represented in continuous-time without delay,

such as

$$\begin{aligned} \dot{x}_{acc} &= f_{acc}(x_{acc}) + g_{acc}(x_{acc})u_{acc}, \\ y_{acc} &= x_{acc}, \end{aligned} \tag{6.63}$$

where $x_{acc} = [v_h \;\; x_r]^T$, $f_{acc}(x_{acc}) = [-0.2041 v_h \;\; v_l - v_h]^T$, $g_{acc}(x_{acc}) = [0.1788 \;\; 0]^T$ and $u_{acc} = u_{th}$, and in discrete-time without delay, such as

$$\begin{aligned} x_{acc_{k+1}} &= f_{acc_d}(x_{acc_k}) + g_{acc_d}(x_{acc_k})u_{acc_k}, \\ y_{acc_k} &= x_{acc_k}, \end{aligned} \tag{6.64}$$

where $x_{acc_k} = [v_{h_k} \;\; x_{r_k}]^T$, $f_{acc_d}(x_{acc_k}) = [0.903 v_{h_k} \;\; v_{l_k} - v_{h_k}]^T$, $g_{acc_d}(x_{acc_k}) = [0.085 \;\; 0]^T$ and $u_{acc_k} = u_{th_k}$.

In ACC, the host vehicle speed v_h must track a cruise speed v_c provided by the driver. This problem can be expressed as a tracking objective and related to a CLF V_{acc} or a nominal control law $u_{no_{acc}}$. However, when the leader vehicle with lower speed v_l is encountered, ACC must adapt the host vehicle speed v_h to maintain a safe distance x_r between the vehicles. Sensors like radars are applied to measure x_r. This problem can be expressed as a safety constraint and related to a CBF h_{acc}. If the leader vehicle increases its speed v_l or leaves the lane and there is no conflict between the safe distance x_r and the desired cruise speed v_c, ACC automatically increases the host vehicle speed v_h to track the cruise speed v_c. The comfort constraints are not considered in this application.

The control framework is considered in continuous-time and in discrete-time. In continuous-time, the tracking objective is satisfied by the CLF V_{acc} and the safety constraint is represented by the CBF h_{acc}. The control framework is applied as described in (2.15) and the block diagram is presented in Fig. 31a. In discrete-time, the tracking objective is satisfied by the proportional-integral (PI) nominal control law $u_{no_{acc}}$ and the safety constraint is represented by the DCBF h_{acc_k}. A DCLF also could be considered to satisfy the tracking objective, however we considered a PI nominal control law aiming to show different approaches. The control framework is applied as described in (5.7) and the block diagram is presented in Fig. 31b.

Figure 31: Block diagram of the control framework applied to the ACC problem on application 1.

(a) Continuous-time. (b) Discrete-time.

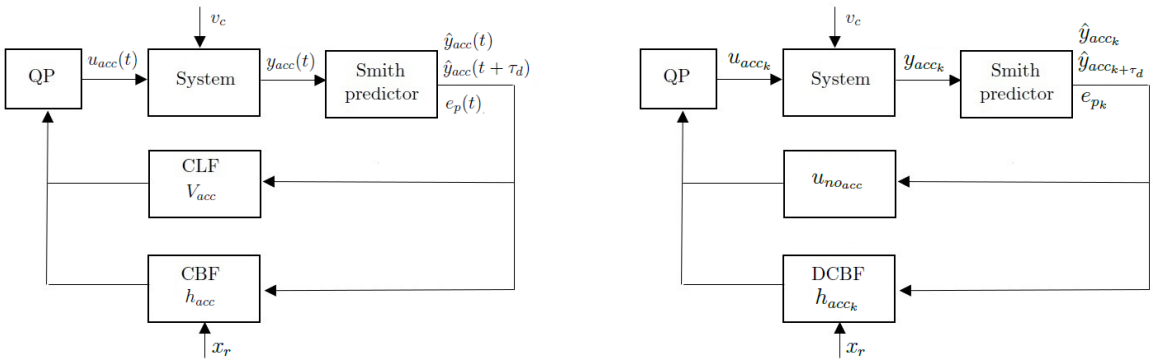

Source: Author.

The CLF V_{acc}, for the continuous-time, is given by:

$$V_{acc} = e_{acc}^2, \tag{6.65}$$

where $e_{acc} = v_c - (\hat{y}_{acc}(t+\tau_d) + e_p(t))$, $\hat{y}_{acc}(t+\tau_d)$, $e_p(t)$ and $v_c = r_e(t)$ are shown in Figs. 30 and 31a.

The PI nominal control law $u_{no_{acc}}$, for the discrete-time, is implemented using the incremental/velocity algorithm, where the output of the controller represents the increments of the control signal. This can reduce numerical precision problems. The controller is given by:

$$u_{no_{acc}} = u_{acc_{k-1}} + K_{P_{acc}}(e_{acc_k} - e_{acc_{k-1}}) + K_{I_{acc}} T_{d_{acc}} e_{acc_k}, \tag{6.66}$$

where $e_{acc_k} = v_c - (\hat{y}_{acc_{k+\tau_d}} + e_{p_k})$, $\hat{y}_{acc_{k+\tau_d}}$, e_{p_k} and $v_c = r_{e_k}$ are shown in Figs. 30 and 31b. $K_{P_{acc}}$ and $K_{I_{acc}}$ are the proportional and integral gains respectively.

The CBF h_{acc} is given by:

$$h_{acc} = x_r - \tau_{th} e_{acc}, \tag{6.67}$$

where τ_{th} is the desired time headway, which is an estimation of the human driver reaction time (AMES et al., 2017), (MOON; MOON; YI, 2009). In discrete-time, the DCBF h_{acc_k} is considered with the same formulation described in (6.67).

It is important to highlight that the CBF (6.67) and the discrete-time system (6.64) are both linear, so the general NLP (5.7) can be described as a QP.

6.4.2.3 Continuous-Time Results

For the evaluation of the control framework in continuous-time, numerical results are obtained with MATLAB/Simulink. Three simulation experiments are considered, shown in Figs. 32, 33 and 34.

The QP-based controller (2.15) is applied considering $\alpha_{h_{acc}}(h_{acc}) = \gamma_{acc} h_{acc}$ and the numerical values of the parameters used in all simulations are $\tau_{th} = 1.8$s (AMES et al., 2017), $\gamma_{acc} = 10$, $c_{V_{acc}} = 5$, $F_{acc} = \begin{bmatrix} 0 \\ 0 \end{bmatrix}$ and $H_{acc} = \begin{bmatrix} 1 & 0 \\ 0 & p_{\delta_{acc}} \end{bmatrix}$, where $p_{\delta_{acc}} = 100$ is the weight on the relaxation parameter δ_{acc}. The QP (2.15) is solved using a closed-form solution demonstrated in (AMES et al., 2017).

In simulation 1, the initial conditions adopted are $x_{l_0} = 30$m (leader vehicle initial position), $x_{h_0} = 0$m (host vehicle initial position) and $v_{h_0} = 0$m/s (host vehicle initial speed). The cruise speed is $v_c = 15$m/s and the leader vehicle speed v_l is shown in Fig. 32. The simulation results show that the host vehicle reaches the cruise speed, respecting the CLF constraint, and when the leader vehicle speed reduces, the CBF constraint acts in the QP and reduces the host vehicle speed, so that the safety constraint is satisfied. It is also important to highlight the influence of the weight $p_{\delta_{acc}}$ on the relaxation parameter δ_{acc} so that the CLF becomes a soft constraint and the CBF a hard constraint. The parameter $c_{V_{acc}}$ exerts influence on the convergence rate to the cruise speed when the CBF is not active and the parameter γ_{acc} specifies how far from the barrier limit the CBF acts to satisfy the safety constraint when the CBF is active. h_{acc} always satisfies the safe set (2.2) and the safe distance x_r between the vehicles is ensured.

Figure 32: Numerical simulation 1 (ACC) - Continuous-time.

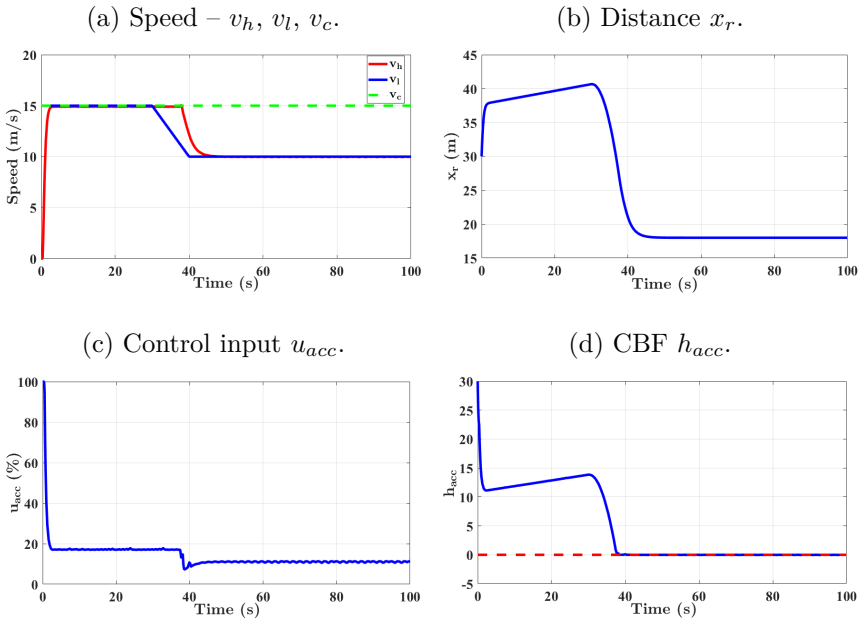

Source: Author.

In simulation 2, the initial conditions are the same for simulation 1, except that $x_{l_0} = 20$m, the cruise speed is the same and the leader vehicle speed is shown in Fig. 33. The simulation results show that the host vehicle speed increases progressively to reach the cruise speed due to the CLF constraint. Posteriorly, the host vehicle speed never exceeds the leader vehicle speed due to the CBF constraint. When the leader vehicle speed reaches the cruise speed, the host vehicle speed does not increase, because it cannot exceed the cruise speed. h_{acc} always satisfies the safe set (2.2) and the safe distance x_r between the vehicles is ensured.

Figure 33: Numerical simulation 2 (ACC) - Continuous-time.

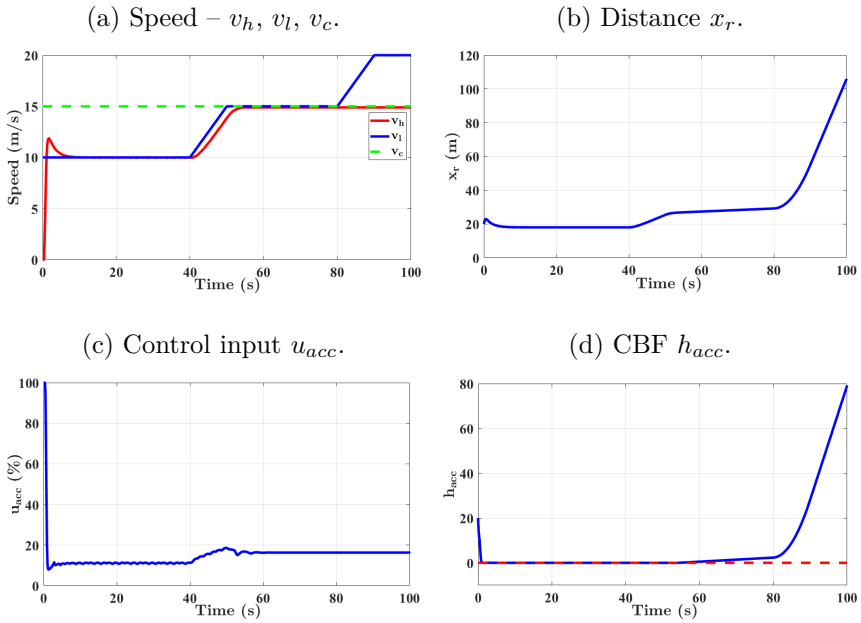

Source: Author.

In simulation 3, the initial conditions adopted are $x_{l_0} = 170$m, $x_{h_0} = 0$m and $v_{h_0} = 0$m/s. The cruise speed is $v_c = 22$m/s and the leader vehicle speed is shown in Fig. 34. The simulation results show that, between 0s and 10s, the host vehicle reaches the cruise speed due to the CLF constraint. Between 10s and 20s, the host vehicle speed decreases in order to satisfy the CBF constraint. Between 20s and 80s, the host vehicle reaches the cruise speed again, but does not exceed it. Finally, after 80s, the host vehicle speed decreases again to satisfy the CBF constraint. h_{acc} always satisfies the safe set (2.2) and the safe distance x_r between the vehicles is ensured.

Figure 34: Numerical simulation 3 (ACC) - Continuous-time.

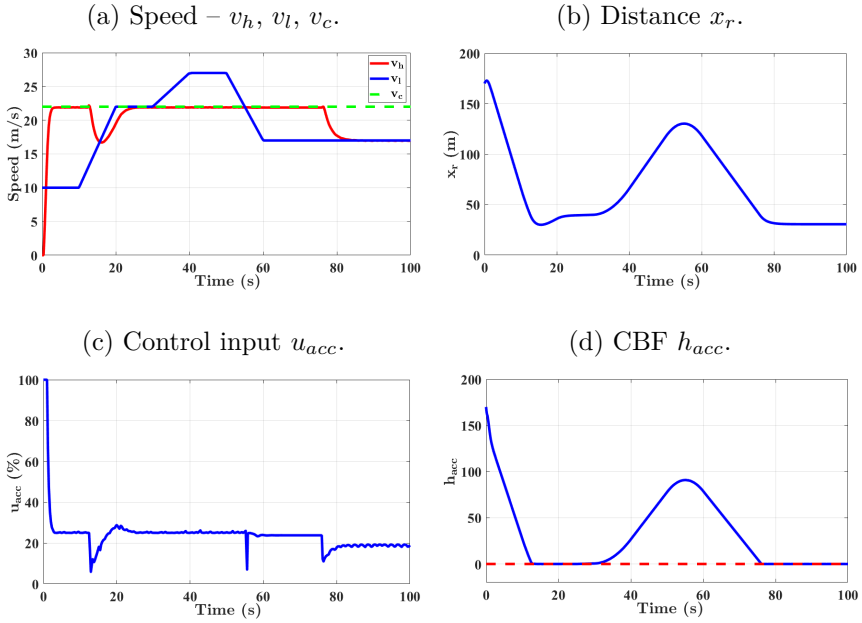

Source: Author.

6.4.2.4 Discrete-Time Results

For the evaluation of the control framework in discrete-time, numerical results are obtained with MATLAB/Simulink again. We consider the same simulation experiments applied for continuous-time, shown in Figs. 35, 36 and 37.

The controller (5.7) is applied considering a sampling time $T_{d_{acc}} = 0.5s$, $\tau_{th} = 1.8$s (AMES et al., 2017), $\gamma_{d_{acc}} = 0.1$, $K_{P_{acc}} = 10$ and $K_{I_{acc}} = 5$ for the PI nominal control law $u_{no_{acc}}$ described in (6.66). As mentioned previously, the NLP (5.7) is described as a QP. The QP is solved using Hildreth's QP procedure (HILDRETH, 1957).

The results are very similar to the continuous-time results. The proportional gain $K_{P_{acc}}$ exerts influence on the convergence rate to the cruise speed and the integral gain $K_{I_{acc}}$ exerts influence on the steady-state error when the DCBF is not active. The parameter $\gamma_{d_{acc}}$ specifies how far from the barrier limit the DCBF acts to satisfy the safety constraint when the DCBF is active. h_{acc_k} always satisfies the safe set (5.5) and the safe distance x_r between the vehicles is ensured.

Figure 35: Numerical simulation 1 (ACC) - Discrete-time.

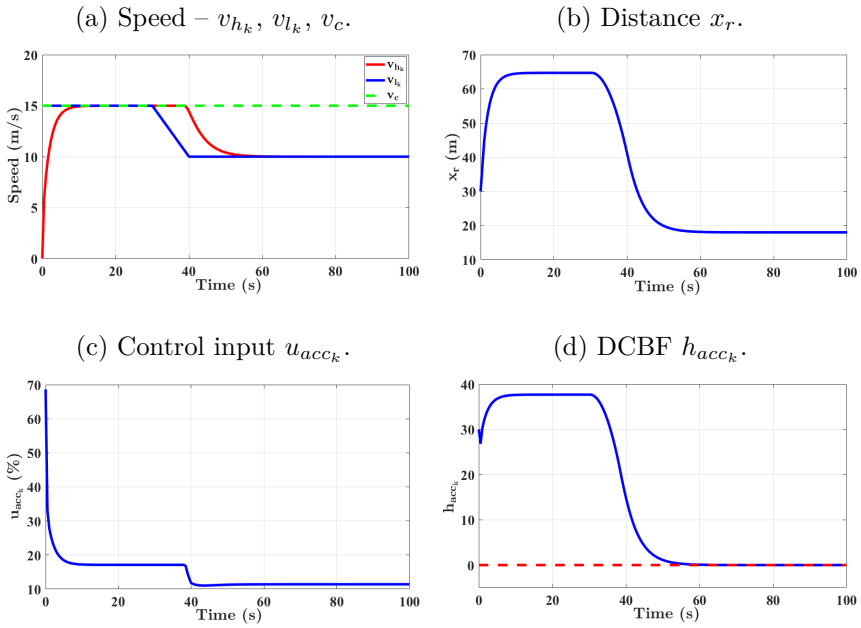

Source: Author.

Figure 36: Numerical simulation 2 (ACC) - Discrete-time.

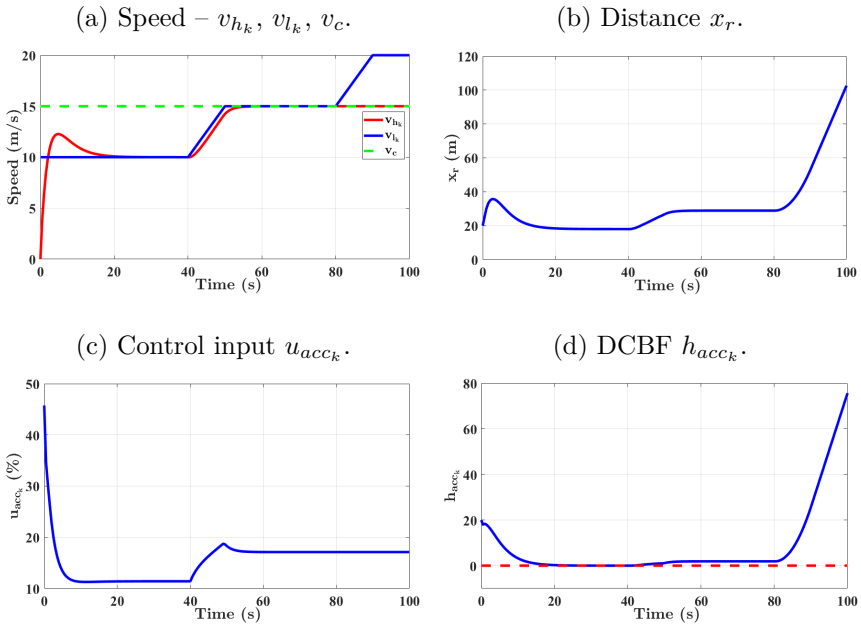

Source: Author.

Figure 37: Numerical simulation 3 (ACC) - Discrete-time.

(a) Speed – v_{h_k}, v_{l_k}, v_c.

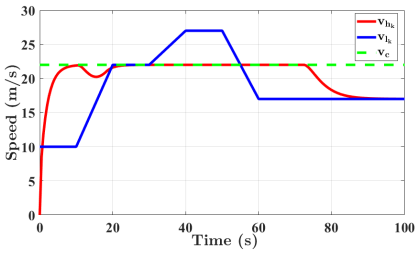

(b) Distance x_r.

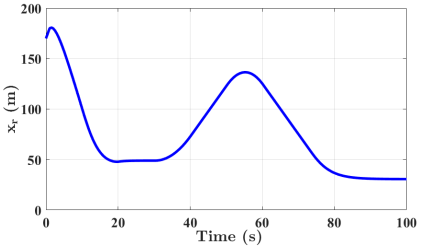

(c) Control input u_{acc_k}.

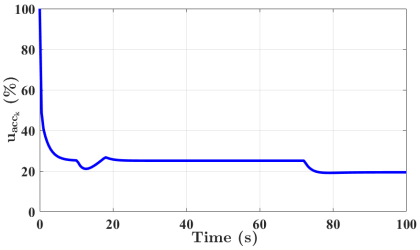

(d) DCBF h_{acc_k}.

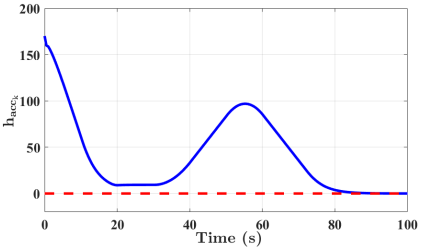

Source: Author.

6.4.3 Application 2

The second application demonstrates ACC applied to a generic automotive vehicle considering the complete ACC control loop described in Fig. 29, i.e., the upper level controller and the lower level controller.

6.4.3.1 Upper Level Controller - Control Framework

The design procedure for the upper level controller is done considering the system in structure (2.1). Thus, the upper level controller is described as

$$\dot{x}_{acc} = f_{acc}(x_{acc}) + g_{acc}(x_{acc})u_{acc} = \begin{bmatrix} -F_r(v_h)/M_h \\ v_l - v_h \end{bmatrix} + \begin{bmatrix} 1 \\ 0 \end{bmatrix} u_{acc}, \tag{6.68}$$

where $x_{acc} = [v_h \;\; x_r]^T$, M_h is the host vehicle mass, $F_r(v_h)$ is the aerodynamic drag that will be described posteriorly, $u_{acc} = F_w/M_h$, where F_w is the wheel force, and $a_h^* = u_{acc} - F_r(v_h)/M_h$. It is important to highlight that a_h^* will be applied as a reference input for the lower level controller, where the host vehicle acceleration a_h must track a_h^* through the actuation of the throttle control u_{th} and brake control u_{br}.

In the upper level controller, the host vehicle speed v_h must track a cruise speed v_c provided by the driver. This problem can be expressed as a tracking objective and related

to a CLF V_{acc}. However, when the leader vehicle with lower speed v_l is encountered, ACC must adapt the host vehicle speed v_h to maintain a safe distance x_r between the vehicles. Sensors like radars are applied to measure x_r. This problem can be expressed as a safety constraint and related to a CBF h_{acc}. If the leader vehicle increases its speed v_l or leaves the lane and there is no conflict between the safe distance x_r and the desired cruise speed v_c, ACC automatically increases the host vehicle speed v_h to track the cruise speed v_c. The control framework is applied as described in (2.15) considering $\alpha_{h_{acc}}(h_{acc}) = \gamma_{acc} h_{acc}$ and the block diagram is presented in Fig. 38.

Figure 38: Block diagram of the control framework applied to the upper level controller on application 2.

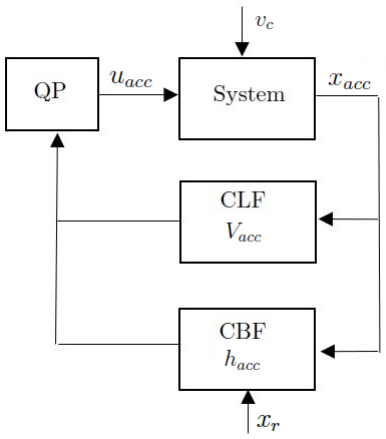

Source: Author.

The CLF V_{acc} is given by:

$$V_{acc} = (v_h - v_c)^2. \tag{6.69}$$

The CBF h_{acc} is given by:

$$h_{acc} = x_r - \tau_{th} v_h, \tag{6.70}$$

where τ_{th} is the desired time headway, which is an estimation of the human driver reaction time (AMES et al., 2017), (MOON; MOON; YI, 2009). We also considered a comfort constraint given by $-2\text{m/s}^2 \leq a_h^* \leq 2\text{m/s}^2$.

The cost function in the QP (2.15) is selected in view of achieving the control objective encoded in the CLF and the relaxation parameter (AMES et al., 2017). Initially, the system is linearized through the feedback $u_{acc} = F_r/M_h + \mu_{acc}$. As a result, the cost function is chosen as

$$\mu_{acc}^T \mu_{acc} = u_{acc}^2 - 2u_{acc}\frac{F_r}{M_h} + \frac{F_r^2}{M_h^2}. \tag{6.71}$$

This can then be converted into the form

$$H_{acc} = 2\begin{bmatrix} 1 & 0 \\ 0 & p_{\delta_{acc}} \end{bmatrix}, F_{acc} = -2\begin{bmatrix} F_r/M_h \\ 0 \end{bmatrix}, \tag{6.72}$$

where $p_{\delta_{acc}}$ is the weight on the relaxation parameter δ_{acc}.

6.4.3.2 Upper Level Controller - Simulation Results

Initially, simulation results are presented considering a simplified model of the vehicle and only the upper level controller. These simulations aim to validate and to understand the behavior of the proposed control framework analyzing a simpler model. Then, posteriorly, the control framework can be applied to a more complex model. The implementation in MATLAB/Simulink is described in Fig. 39. This implementation is related to the ACC control loop described in Fig. 29 disregarding the lower level controller. The Simulink library Vehicle Dynamics Blockset is used.

Figure 39: Implementation of the upper level controller in MATLAB/Simulink considering a simplified model of the vehicle for the application 2.

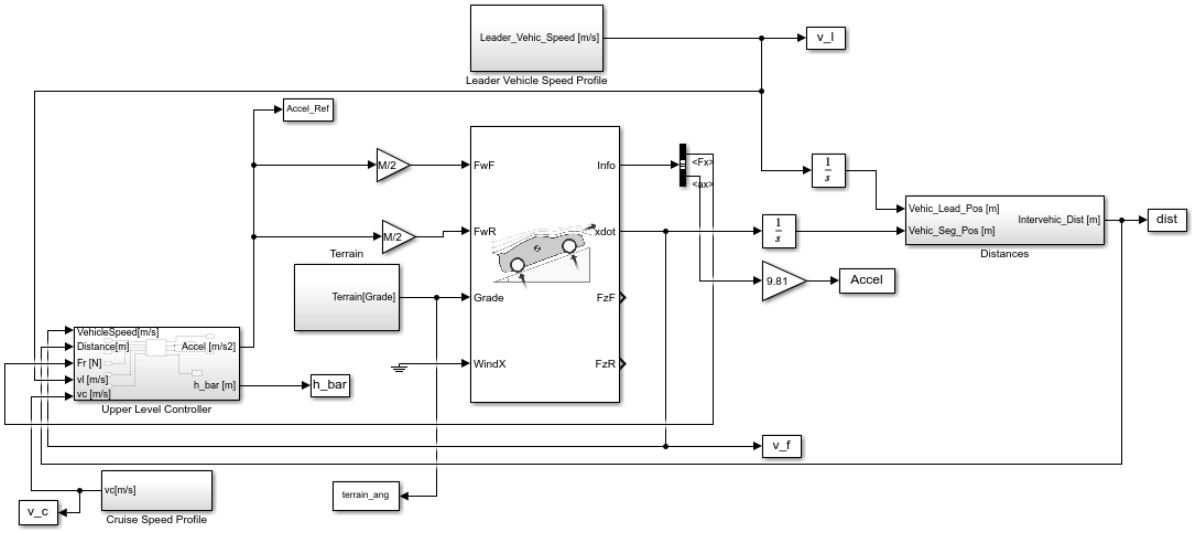

Source: Author.

The block Upper Level Controller implements the control framework described in subsection 6.4.3.1 and provides the desired acceleration/deceleration a_h^* (`Accel_Ref` in Simulink). The block Leader Vehicle Speed Profile provides the leader vehicle speed v_l (`v_l` in Simulink). The relative distance between the vehicles x_r (`dist` in Simulink) is determined in the block Distances. The cruise speed v_c (`v_c` in Simulink) is provided by the block Cruise Speed Profile. The block Vehicle Body 1DOF Longitudinal from the Simulink library Vehicle Dynamics Blockset represents the simplified model of the

vehicle. This block implements an one DOF rigid vehicle body with constant mass M_h undergoing longitudinal motion. The inputs are the longitudinal force on the front axle (`FwF` in Simulink) and the longitudinal force on the rear axle (`FwR` in Simulink). It is important to highlight that the desired acceleration/deceleration a_h^* or the output of the block Upper Level Controller is multiplied by the vehicle mass M_h (`M` in Simulink) to obtain the longitudinal forces. The outputs are the aerodynamic drag F_r (`Fr` in Simulink), the host vehicle acceleration a_h (`Accel` in Simulink) and the host vehicle speed v_h (`v_f` in Simulink). The block Terrain provides a road inclination (`terrain_ang` in Simulink).

The numerical values adopted for the controller are $\tau_{th} = 1.8$s (AMES et al., 2017), $\gamma_{acc} = 1$, $c_{V_{acc}} = 5$ e $p_{\delta_{acc}} = 100$. The QP is implemented using Hildreth's QP procedure (HILDRETH, 1957). The aerodynamic drag is calculated using $F_r = \frac{1}{2T_a} C_{ad} A_f P_{abs} (v_h - w_x)^2$ (GILLESPIE, 1992), where T_a is the air temperature, C_{ad} is the air drag coefficient, A_f is the effective vehicle cross-sectional area, P_{abs} is the environmental air absolute pressure and w_x is the longitudinal wind speed along earth-fixed X-axis. The numerical values adopted for the host vehicle are $M_h = 1500$kg, $T_a = 273$K, $C_{ad} = 0.3$, $A_f = 4\text{m}^2$, $P_{abs} = 101325$Pa and $w_x = 0$m/s.

The simulation results, presented in Fig. 40, show that the host vehicle speed v_h reaches the cruise speed v_c, respecting the CLF constraint, and when the leader vehicle speed v_l reduces, the CBF constraint acts in the QP and reduces v_h, so that the safety constraint is satisfied. It is also important to highlight the influence of the weight $p_{\delta_{acc}}$ on the relaxation parameter δ_{acc} so that the CLF becomes a soft constraint and the CBF a hard constraint. The parameter $c_{V_{acc}}$ exerts influence on the convergence rate to the cruise speed when the CBF is not active and the parameter γ_{acc} specifies how far from the barrier limit the CBF acts to satisfy the safety constraint when the CBF is active. h_{acc} always satisfies the safe set (2.2) and the safe distance x_r between the vehicles is ensured.

Figure 40: Numerical simulation (ACC) - Upper level controller.

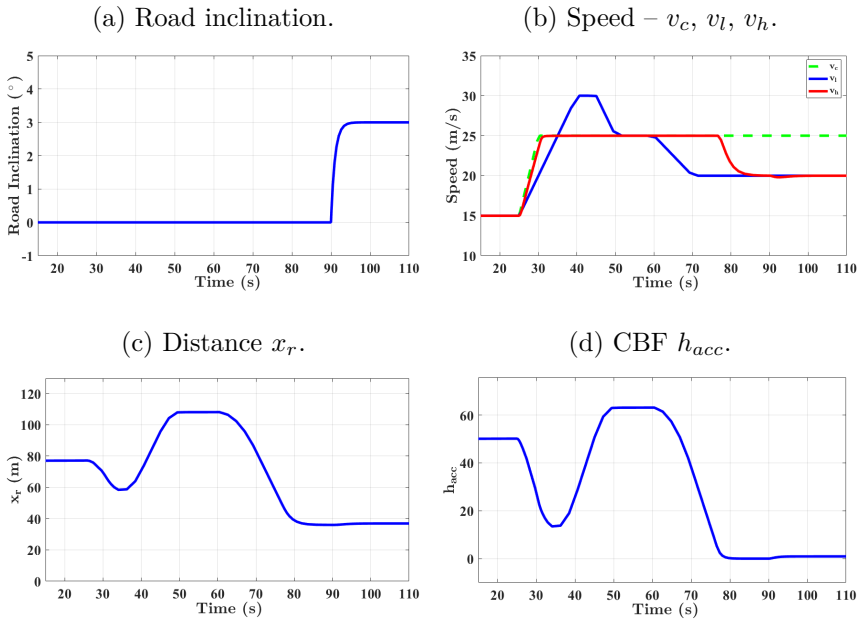

Source: Author.

6.4.3.3 Lower Level Controller - Control Framework

As previously described, the lower level controller calculates the throttle (u_{th}) and the brake (u_{br}) actuation, both within the range from 0 to 100%, to track the desired acceleration (a_h^*) demanded by the upper level controller. Some works described the lower level controller. In (YI; KWON, 2001), (HAN et al., 2006) and (MOON; YI, 2008), PID controllers are considered for throttle and brake control. In (YI; KWON, 2001), a throttle/brake switching map is provided based on experimental data. In this work, we considered the approach proposed in (FLIESS; JOIN, 2013) denominated model-free control. It consists in defining an ultra-local model and apply algebraic estimators for the unknown ultra-local dynamics. Some automotive applications with model-free control can be seen in (POLACK; DELPRAT; NOVEL, 2019) and (WANG; WANG, 2020). Model-free control is described in Appendix G. The lower level controller is implemented considering the model-free approach, being one controller for u_{th} and another one for u_{br}. In both cases, the ultra-local model is approximated by a first order system, as described in (G.5), such that

$$\dot{u}_{th} = \phi_{th} + \alpha_{th}\, a_h, \tag{6.73}$$

and,

$$\dot{u}_{br} = \phi_{br} + \alpha_{br}\, a_h, \tag{6.74}$$

for the throttle and brake, respectively, where α_{th} and α_{br} are constant parameters chosen by the designer and, ϕ_{th} and ϕ_{br} represent the unknown parts of the plant, including possible disturbances, which are obtained by (G.12).

The control signals u_{th} and u_{br} are given by

$$u_{th} = \frac{-\phi_{th} + \dot{a}_h^* - K_{P_{th}} e_{th}}{\alpha_{th}}, \tag{6.75}$$

and

$$u_{br} = \frac{-\phi_{br} + \dot{a}_h^* - K_{P_{br}} e_{br}}{\alpha_{br}}, \tag{6.76}$$

being $e_{th} = a_h - a_h^*$ and $e_{br} = a_h^* - a_h$. $K_{P_{th}}$ and $K_{P_{br}}$ are the proportional gains related to the throttle and brake signals respectively.

In order to avoid undesired switching between the control signals u_{th} and u_{br}, a dead-zone was imposed. If $|a_h^*| < 2 \times 10^{-5}$, then $u_{th} = 0$ and $u_{br} = 0$. In addition, a low-pass filter with unitary gain and time constant of 0.5s was added at each output of the lower level controller, such that the acceleration and braking responses could behave closer to human action. We stress that the model-free parameters were adjusted taking into account this filter.

6.4.3.4 Upper and Lower Level Controllers - Simulation Results

Finally, simulation results are presented considering a complex model of the vehicle and, the upper and lower level controllers simultaneously. The implementation in MATLAB/Simulink is described in Fig. 41. This implementation is related to the ACC control loop described in Fig. 29 and is adapted from (MATHWORKS, 2021). The Simulink library Vehicle Dynamics Blockset is used.

Figure 41: Implementation of the upper level and lower level controllers in MATLAB/Simulink considering a complex model of the vehicle for the application 2.

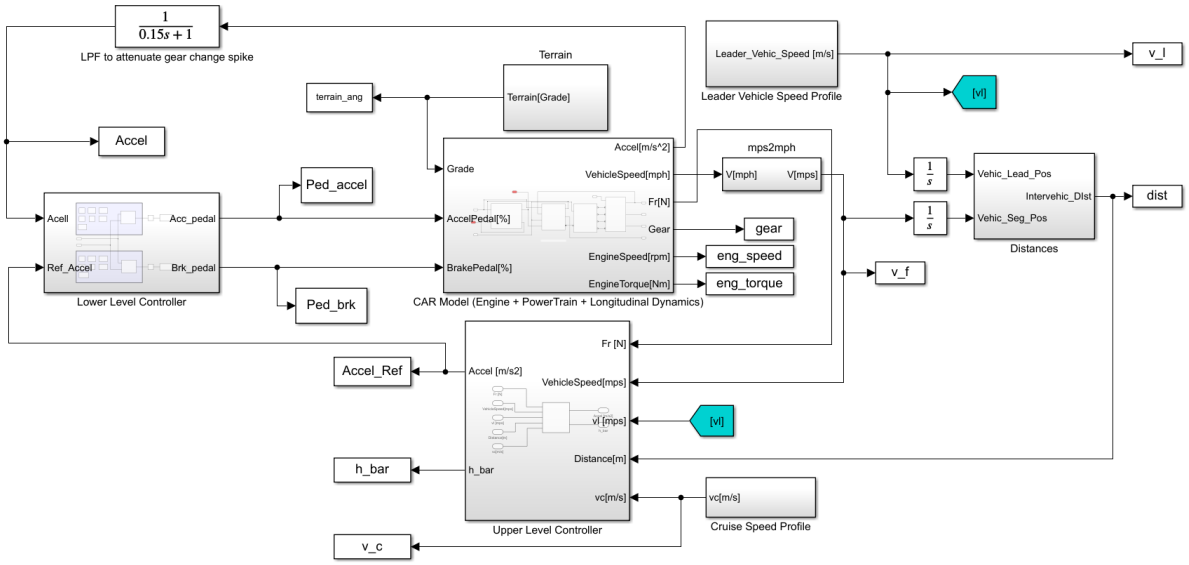

Source: Author.

The blocks and signals for the upper level controller are the same described in Fig. 39. However, in this implementation, the block Lower Level Controller implements the model-free control quoted in subsection 6.4.3.3. This block receives a_h (`Accel` in Simulink) and a_h^* (`Accel_Ref` in Simulink) as inputs, compares these inputs and provides the control signal u_{th} (`Ped_accel` in Simulink) to the throttle pedal and u_{br} (`Ped_brk` in Simulink) to the brake pedal aiming that a_h tracks a_h^*. The block CAR Model (Engine + PowerTrain + Longitudinal Dynamics) implements the complex model of the vehicle considering engine, driveline, wheels and brakes. More details about this block are described in Appendix H. It is important to highlight that the gear change mechanism was implemented with a state machine and the clutch model was not accurate, so pulses (spikes) were observed in the vehicle acceleration at the time of gear change. A low-pass filter was applied to attenuate gear change spike.

The numerical values adopted for the upper level controller and for the vehicle are the same applied for the simulation results presented in subsection 6.4.3.2, however, here we adopted $\gamma_{acc} = 3$.

For the lower level controller we considered $\alpha_{th} = 0.005$, $K_{P_{th}} = 0.6$, $\alpha_{br} = 0.1$, $K_{P_{br}} = 10$ and, $N = 50$ and $T_s = 0.02s$ for (G.12).

The simulation results, presented in Fig. 42, are very similar to the results presented in Fig. 40. The acceleration a_h tracks a_h^* with good performance applying moderate u_{th}

and u_{br} commands. Therefore, the objective of the upper level controller is satisfied using the controller (2.15) and the objective of the lower level controller is satisfied using model-free control. The comfort constraint given by $-2\text{m/s}^2 \leq a_h^* \leq 2\text{m/s}^2$ is respected. Note, however, that this constraint is imposed over a_h^* and there is a small violation of a_h. This violation could be avoided by setting a ramp acceleration trajectory to get the desired cruise speed. Finally, the gear position and the engine speed follow the host vehicle speed v_h.

Fig. 43 shows that h_{acc} always satisfies the safe set (2.2) and the safe distance x_r between the vehicles is ensured.

Fig. 44 presents the estimated values of ϕ_{th} and ϕ_{br}, showing that the algebraic estimators are in action when acceleration/deceleration is demanded.

Figure 42: Numerical simulation (ACC) - Upper level and lower level controllers.

(a) Road inclination.

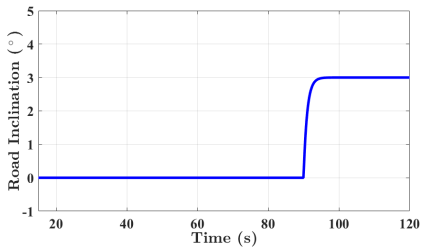

(b) Speeds – v_c, v_l, v_h.

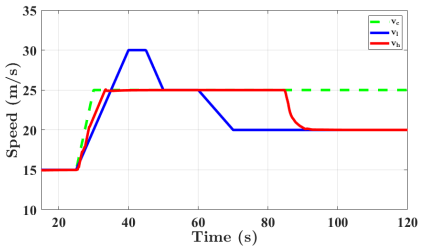

(c) Distance x_r.

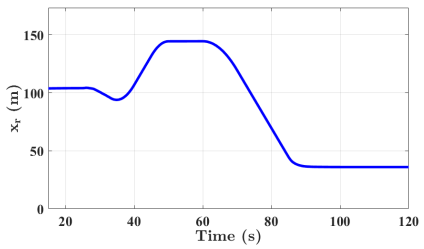

(d) Accelerations a_h^* and a_h.

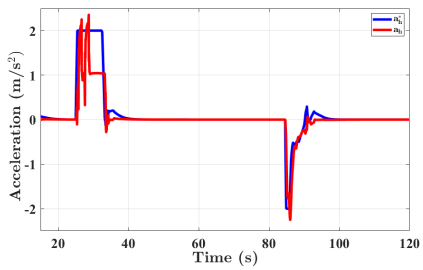

(e) Control signals u_{th} and u_{br}.

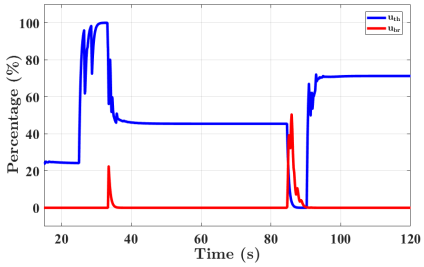

(f) Gear position and engine speed.

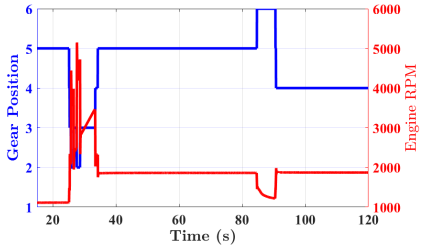

Source: Author.

Figure 43: CBF h_{acc}.

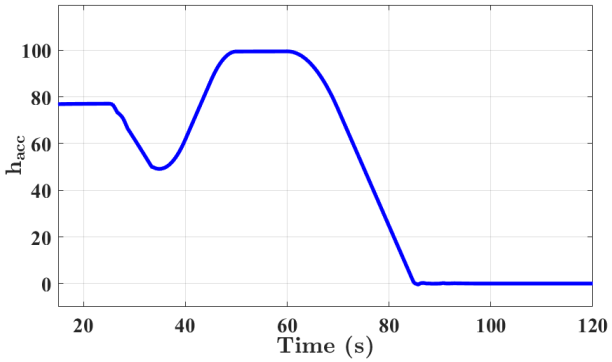

Source: Author.

Figure 44: Estimated values of ϕ_{th} and ϕ_{br}.

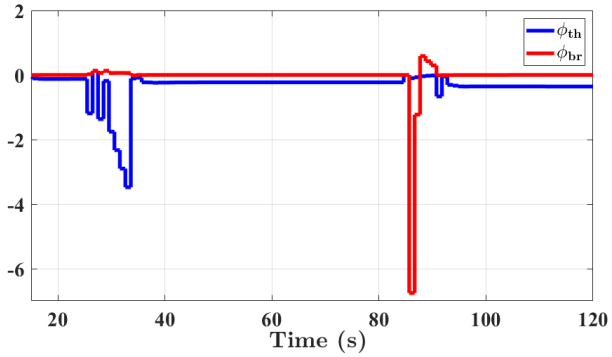

Source: Author.

7 CONCLUSIONS

This work presented approaches for the safe control of dynamical systems with CBFs. The system must satisfy stability/tracking objectives and safety constraints. Stability/tracking objectives can be satisfied through a CLF or a nominal control law. Safety constraints are specified in terms of a set invariance and verified through CBFs. The control framework considered unifies stability/tracking objectives and safety constraints through QP. If stability/tracking objectives and safety constraints are in conflict, the control framework mediates these requirements, in the sense that safety is always prioritized.

Initially, a literature review with works related to the safety of dynamical systems and CBF was presented and the basic formulation of the considered control framework was described by CBFs represented by relative-degree one safety constraints. Posteriorly, advanced topics were presented, such as CBFs represented by high relative-degree safety constraints, robust CBFs, an explicit solution without QP and DCBFs. The main contributions of this work were new formulations for robust CBFs, where RECBFs and SMCBFs were proposed, the experimental application of an explicit solution to deal with high relative-degree and robust safety constraints, and practical applications not explored in the literature so far.

The experiments were organized so that all the topics described in the literature review and the work contributions were covered. The results were presented experimentally in a reaction wheel pendulum and a Furuta pendulum, and numerically in a MIMO MAGLEV system and ACC applied to automotive vehicles.

For the reaction wheel pendulum, the stability objective and the safety constraint were satisfied. The safety constraint was described, initially by a relative-degree one CBF and, posteriorly by a relative-degree two ECBF. In both cases, the safety constraint was satisfied. Since ECBF is a generalization of the definition of CBF for higher relative-degree safety constraints, as described in Remark 3.1, the results must be very similar. In discrete-time, the stability objective and the safety constraint were satisfied again. It is important to highlight that the results with DCBFs described in (AGRAWAL; SREENATH,

2017) and (TAKANO; OYAMA; YAMAKITA, 2018) were verified only numerically while here the results were verified numerically and experimentally.

For the Furuta pendulum, the stability objective and the safety constraint were satisfied with the ECBF just when the nominal system dynamics was considered. When the model uncertainties were considered, the safety constraint was not respected with the ECBF. To deal with the model uncertainties, the safe robust controller with SMCBF was applied. Then, the safety constraint was respected. In both cases, the control framework was applied using the explicit solution without QP as described in (3.10) and (4.21). The numerical and experimental results demonstrated that the explicit solution without QP presented results similar to the QP-based control framework.

For the MIMO MAGLEV system, the tracking objectives and the safety constraints were satisfied with the ECBFs just when the nominal system dynamics was considered. When model uncertainties were considered, the safety constraints were not respected with the ECBFs. To deal with the model uncertainties, the safe robust controllers with RECBFs and SMCBFs, proposed in (4.6) and (4.20) respectively, were applied. Then, the safety constraints were respected. After several numerical tests, we observed that the safe robust controller with SMCBFs (4.20) presented better results than the safe robust controller with RECBFs (4.6) in terms of precision, performance, robustness and feasibility. In (4.6), the bounds of the model uncertainties $\Delta^b_{1,max}$ and $\Delta^b_{2,max}$, defined in (4.3), are design parameters, as described in (NGUYEN; SREENATH, 2020). We observed a tradeoff between robustness and feasibility of the controller. Small values for the bounds $\Delta^b_{1,max}$ and $\Delta^b_{2,max}$ can deteriorate stability/tracking performance and violate safety constraints because less model uncertainties are tolerated. Otherwise, higher values for the bounds $\Delta^b_{1,max}$ and $\Delta^b_{2,max}$ can make the QP infeasible (NGUYEN; SREENATH, 2020). Feasibility problems were not verified with the controller (4.20).

For the automotive vehicles with ACC, the tracking objective and the safety constraints were satisfied in both cases. In application 1, i.e., ACC applied to an automotive vehicle available at EPUSP, the Smith predictor compensated the input time-delay adequately and the results were presented in continuous-time and in discrete-time. In application 2, i.e., ACC applied to a generic automotive vehicle, the upper level controller and the lower level controller satisfied the tracking objective and the safety constraints.

Therefore the new formulations of robust CBFs proposed in this work ensured the safety of the dynamical systems when the model uncertainties were considered. Besides that, the explicit solution without QP presented results similar to the QP-based control

framework. However, the explicit solution is computationally advantageous because the QP does not need to be solved at each sampling time. The disadvantage is that the explicit solution cannot be applied to multiple CBFs. It is important to highlight that the results with the explicit solution presented in (IGARASHI; TEZUKA; NAKAMURA, 2019) were verified only numerically and, in this work, the results were verified numerically and experimentally.

Several variations of the control framework were validated numerically and experimentally and, in all cases, stability/tracking objectives and safety constraints were satisfied. Thus, the effectiveness, versatility and robustness of the control framework were verified.

Some future works can be developed, such as:

- Numerical and experimental results of the control framework applied to a two DOF helicopter. The two DOF helicopter is a MIMO system that allows the study of advanced control techniques that can be applied in real situations of flight control, behavior of rigid bodies helicopters and aircrafts. This system is chosen because the LCA-EPUSP has an experimental prototype of the two DOF helicopter. Numerical results have already been obtained considering ECBFs and SMCBFs. In the future, these results can be verified experimentally;
- Experimental results with ACC applied on automotive vehicles available at EPUSP considering the proposed control framework, as described in applications 1 and 2 of subsections 6.4.2 and 6.4.3 respectively;
- Numerical and experimental results considering CBFs integrated with model-free control, described in Appendix G. The basic idea is that the Lie derivatives related to the CBF can be computed based on the estimated ultra-local dynamics. Numerical results have already been obtained considering the two DOF helicopter.

7.1 Publications

The list of submitted and published papers are presented below:

- “Safe Adaptive Cruise Control with Control Barrier Function and Smith Predictor”, published and presented at the XXIII Congresso Brasileiro de Automática (CHINELATO; ANGÉLICO, 2020b). This publication is related to the results presented in the subsection 6.4.2.3;

- "Control of a MIMO Magnetic Levitation System using Exponential Control Barrier Function", published and presented at the XXIII Congresso Brasileiro de Automática (CHINELATO; ANGÉLICO, 2020a). This publication is related to numerical results with ECBFs applied to the MIMO MAGLEV system;

- "Safe Control of a Reaction Wheel Pendulum Using Control Barrier Function", published at the Journal IEEE Access (CHINELATO; NEVES; ANGÉLICO, 2020). This publication is related to the results presented in the subsection 6.1;

- "Robust Exponential Control Barrier Functions for Safety-Critical Control", published and presented at the 2021 American Control Conference (CHINELATO; ANGÉLICO, 2021a). This publication is related to the safe robust controller described in the subsection 4.1. The results are obtained numerically considering the Furuta pendulum and the MIMO MAGLEV system;

- "Safe Control of a 2DOF Helicopter Using Exponential Control Barrier Function", published and presented at the 2021 Simpósio Brasileiro de Automação Inteligente (CHINELATO; ANGÉLICO, 2021b). This publication is related to numerical results with ECBFs applied to the two DOF helicopter available at LCA-EPUSP;

- "A Sliding Mode Approach for High Relative-Degree Control Barrier Function", submitted to the Journal Asian Journal of Control. At this moment, the submission status is "under review". This publication is related to the safe robust controller described in the subsection 4.2. The results are obtained numerically considering the MIMO MAGLEV system;

- "Practical Application of Robust Control Barrier Function Using Sliding Modes", submitted to the International Journal of Control. At this moment, the submission status is "under review". This publication is related to the results presented in the subsection 6.2;

- "Design of Adaptive Cruise Control with Control Barrier Function and Model-Free Control", submitted to the Journal of Control, Automation and Electrical Systems. At this moment, the submission status is "under review". This publication is related to the results presented in the subsection 6.4.3.4;

- "Vehicle Lateral Stability Regions for Control Applications", submitted as a co-author to the Journal of Intelligent Transportation Systems: Technology, Planning, and Operations. At this moment, the submission status is "under review". This

publication is related to the application of control-dependent barrier functions, proposed in (HUANG; YONG; CHEN, 2021) and (HUANG; YONG; CHEN, 2019), to the problem of vehicle lateral stability.

REFERENCES

AGRAWAL, A.; SREENATH, K. Discrete control barrier functions for safety-critical control of discrete systems with application to bipedal robot navigation. In: *Robotics: Science and Systems (RSS)*. Massachusetts, USA: [s.n.], 2017.

AL-MUTHAIRI, N.; ZRIBI, M. Sliding mode control of a magnetic levitation system. *Mathematical Problems in Engineering*, v. 2, p. 93–107, Jun 2004.

ALIASGHARY, M.; SHOOREHDELI, M.; JALILVAND, A.; TESHNEHLAB, M. Magnetic levitation control based-on neural network and feedback error learning approach. In: *IEEE International Power and Energy Conference*. Johor Bahru, Malaysia: [s.n.], 2008. p. 1426–1430.

ALPERN, B.; SCHNEIDER, F. Defining liveness. *Information Processing Letters*, p. 181–185, Oct 1985.

AMES, A.; COOGAN, S.; EGERSTEDT, M.; NOTOMISTA, G.; SREENATH, K.; TABUADA, P. Control barrier functions: theory and applications. In: *European Control Conference (ECC)*. Naples, Italy: [s.n.], 2019. p. 3420–3431.

AMES, A.; GALLOWAY, K.; SREENATH, K.; GRIZZLE, J. Rapidly exponentially stabilizing control lyapunov functions and hybrid zero dynamics. *IEEE Transactions on Automatic Control*, v. 59, n. 4, p. 876–891, Apr 2014.

AMES, A.; GRIZZLE, J.; TABUADA, P. Control barrier function based quadratic programs with application to adaptive cruise control. In: *IEEE Conference on Decision and Control (CDC)*. California, USA: [s.n.], 2014. p. 6271–6278.

AMES, A.; XU, X.; GRIZZLE, J.; TABUADA, P. Control barrier function based quadratic programs for safety critical systems. *IEEE Transactions on Automatic Control*, v. 62, n. 8, p. 3861–3876, Aug 2017.

ANGÉLICO, B.; BRUGNOLLI, M.; NEVES, G. Digital h_∞ robust control of mechanical system with implicit observer. In: *IEEE Conference on Decision and Control (CDC)*. Nice, France: [s.n.], 2019. p. 1171–1176.

ARTSTEIN, Z. Stabilization with relaxed controls. *Nonlinear Analysis: Theory, Methods and Applications*, v. 7, n. 11, p. 1163–1173, 1983.

AVELAR, C.; VALENZUELA, J. New feedback linearization-based control for arm trajectory tracking of the furuta pendulum. *IEEE/ASME Transactions on Mechatronics*, v. 21, n. 2, p. 638–648, Apr 2016.

BARIE, W.; CHIASSON, J. Linear and nonlinear state-space controllers for magnetic levitation. *International Journal of Systems Science*, v. 27, n. 11, p. 1153–1163, Nov 1996.

BENOMAIR, A.; TOKHI, M. Control of single axis magnetic levitation system using fuzzy logic control. In: *Science and Information Conference (SAI)*. London, UK: [s.n.], 2015. p. 514–518.

BLANCHINI, F. Set invariance in control. *Automatica*, v. 35, n. 11, p. 1747–1767, Nov 1999.

BLOCK, D.; ASTROM, K.; SPONG, M. *The reaction wheel pendulum*. [S.l.]: Morgan and Claypool, 2007.

BOYD, S.; VANDENBERGHE, L. *Convex Optimization*. [S.l.]: Cambridge University Press, 2004.

BROWN, T.; SCHMIEDELER, J. Reaction wheel actuation for improving planar biped walking efficiency. *IEEE Transactions on Robotics*, v. 32, n. 5, p. 1290–1297, Oct 2016.

BRUGNOLLI, M.; ANGÉLICO, B.; LAGANÁ, A. Predictive adaptive cruise control using a customized ecu. *IEEE Access*, v. 7, p. 55305–55317, May 2019.

BRUGNOLLI, M.; PEREIRA, B.; ANGÉLICO, B.; LAGANÁ, A. Adaptive cruise control with a customized electronic control unit. *Journal of Control, Automation and Electrical Systems*, v. 30, p. 9–15, 2019.

CHINELATO, C.; ANGÉLICO, B. Control of a mimo magnetic levitation system using exponential control barrier function. In: *Congresso Brasileiro de Automática (CBA)*. Online: [s.n.], 2020.

CHINELATO, C.; ANGÉLICO, B. Safe adaptive cruise control with control barrier function and smith predictor. In: *Congresso Brasileiro de Automática (CBA)*. Online: [s.n.], 2020.

CHINELATO, C.; ANGÉLICO, B. Robust exponential control barrier functions for safety-critical control. In: *American Control Conference (ACC)*. New Orleans, USA: [s.n.], 2021. p. 2342–2347.

CHINELATO, C.; ANGÉLICO, B. Safe control of a 2dof helicopter using exponential control barrier function. In: *Simpósio Brasileiro de Automação Inteligente (SBAI)*. Online: [s.n.], 2021. p. 500–505.

CHINELATO, C.; NEVES, G.; ANGÉLICO, B. Safe control of a reaction wheel pendulum using control barrier function. *IEEE Access*, v. 8, p. 160315–160324, Aug 2020.

CHOU, M.; LIAW, C.; CHIEN, S.; SHIEH, F.; TSAI, J.; CHANG, H. Robust current and torque controls for pmsm driven satellite reaction wheel. *IEEE Transactions on Aerospace and Electronic Systems*, v. 47, n. 1, p. 58–74, Jan 2011.

CORONA, D.; SCHUTTER, B. D. Adaptive cruise control for a smart car: A comparison benchmark for mpc-pwa control methods. *IEEE Transactions on Control Systems Technology*, v. 16, n. 2, p. 365–372, Mar 2008.

DANG, Q.; ALLOUCHE, B.; VERMEIREN, L.; DEQUIDT, A.; DAMBRINE, M. Design and implementation of a robust fuzzy controller for a rotary inverted pendulum using the takagi-sugeno descriptor representation. In: *IEEE Symposium on Computational Intelligence in Control and Automation (CICA)*. Orlando, USA: [s.n.], 2014.

FANCHER, P.; BAREKET, Z.; ERVIN, R. Human-centered design of an acc-with-braking and forward-crash-warning system. In: *International Symposium on Advanced Vehicle Control (AVEC)*. Michigan, USA: [s.n.], 2000.

FLIESS, M.; JOIN, C. Model-free control. *International Journal of Control*, v. 86, n. 12, p. 2228–2252, Jul 2013.

FREEMAN, R.; KOKOTOVIC, P. Inverse optimality in robust stabilization. *SIAM Journal on Control and Optimization*, v. 34, n. 4, p. 1365–1391, 1996.

FUJII, T.; TSUJINO, T.; SUEMATU, K.; SASAKI, K.; MURATA, Y. Multivariable control of a magnetic levitation system with a y shape iron plate. In: *IFAC Symposium on Advances in Control Education*. Tokyo, Japan: [s.n.], 1994. p. 25–28.

FURUTA, K.; YAMAKITA, M.; KOBAYASHI, S. Swing-up control of inverted pendulum using pseudo-state feedback. *Proceedings of the Institution of Mechanical Engineers, Part I: Journal of Systems and Control Engineering*, v. 206, n. 4, p. 263–269, Nov 1992.

GALLOWAY, K.; SREENATH, K.; AMES, A.; GRIZZLE, J. Torque saturation in bipedal robotic walking through control lyapunov function-based quadratic programs. *IEEE Access*, v. 3, p. 323–332, Apr 2015.

GANJI, B.; KOUZANI, A.; KHOO, S.; SHAMS-ZAHRAEI, M. Adaptive cruise control of a hev using sliding mode control. *Expert Systems with Applications*, v. 41, n. 2, p. 607–615, Feb 2014.

GILLESPIE, T. *Fundamentals of Vehicle Dynamics*. [S.l.]: Society of Automotive Engineers, Inc., 1992.

GOODRICH, M.; BOER, E. Model-based human-centered task automation: A case study in acc system design. *IEEE Transactions on Systems, Man and Cybernetics Part A: Systems and Humans*, v. 33, n. 3, p. 325–335, May 2003.

GRONWALL, T. Note on the derivatives with respect to a parameter of the solutions of a system of differential equations. *Annals of Mathematics, Second Series*, v. 20, n. 4, p. 292–296, Jul 1919.

GURRIET, T.; SINGLETARY, A.; REHER, J.; CIARLETTA, L.; FERON, E.; AMES, A. Towards a framework for realizable safety critical control through active set invariance. In: *ACM/IEEE International Conference on Cyber-Physical Systems*. Porto, Portugal: [s.n.], 2018. p. 98–106.

HAJJAJI, A.; OULADSINE, M. Modeling and nonlinear control of magnetic levitation systems. *IEEE Transactions on Industrial Electronics*, v. 48, n. 4, p. 831–838, Aug 2001.

HAN, D.; YI, K.; LEE, J.; KIM, B.; YI, S. Design and evaluation of intelligent vehicle cruise control systems using a vehicle simulator. *International Journal of Automotive Technology*, v. 7, n. 3, p. 377–383, 2006.

HAN, S.; LEE, J. Balancing and velocity control of a unicycle robot based on the dynamic model. *IEEE Transactions on Industrial Electronics*, v. 62, n. 1, p. 405–413, Jan 2015.

HERA, P. L.; FREIDOVICH, L.; SHIRIAEV, A.; METTIN, U. New approach for swinging up the furuta pendulum: Theory and experiments. *Mechatronics*, v. 19, n. 8, p. 1240–1250, Dec 2009.

HILDRETH, C. A quadratic programming procedure. *Naval Research Logistics Quarterly*, v. 4, n. 1, p. 79–85, Mar 1957.

HSU, S.; XU, X.; AMES, A. Control barrier function based quadratic programs with application to bipedal robotic walking. In: *American Control Conference (ACC)*. Chicago, USA: [s.n.], 2015.

HU, C.; WANG, J. Trust-based and individualizable adaptive cruise control using control barrier function approach with prescribed performance. *IEEE Transactions On Intelligent Transportation Systems*, p. 1–11, 2021.

HUANG, Y.; YONG, S.; CHEN, Y. Guaranteed vehicle safety control using control-dependent barrier functions. In: *American Control Conference (ACC)*. Philadelphia, USA: [s.n.], 2019. p. 983–988.

HUANG, Y.; YONG, S.; CHEN, Y. Stability control of autonomous ground vehicles using control-dependent barrier functions. *IEEE Transactions on Intelligent Vehicles*, v. 6, n. 4, p. 699–710, Dec 2021.

IGARASHI, M.; TEZUKA, I.; NAKAMURA, H. Time-varying control barrier function and its application to environment-adaptive human assist control. *IFAC papers online*, v. 52, n. 16, p. 735–740, Jan 2019.

IOANNOU, P.; CHIEN, C. Autonomous intelligent cruise control. *IEEE Transactions on Vehicular Technology*, v. 42, n. 4, p. 657–672, Nov 1993.

ISO15622. International organization for standardization—transport information and control systems—adaptive cruise control systems—performance requirements and test procedures. NEN-ISO 15622, 2002.

JANKOVIC, M. Robust control barrier functions for constrained stabilization of nonlinear systems. *Automatica*, v. 96, p. 359–367, Oct 2018.

JEPSEN, F.; SOBORG, A.; PEDERSEN, A.; YANG, Z. Development and control of an inverted pendulum driven by a reaction wheel. In: *International Conference on Mechatronics and Automation (ICMA)*. Changchun, China: [s.n.], 2009. p. 2829–2834.

KARAMPOORIAN, H.; MOHSENI, R. Control of a nonlinear magnetic levitation system by using constraint generalized model predictive control. In: *International Conference on Control, Automation and Systems (ICCAS)*. Gyeonggi-do, South Korea: [s.n.], 2010. p. 48–51.

KHALIL, H. *Nonlinear Systems*. [S.l.]: Prentice Hall, 2002.

KOLATHAYA, S.; AMES, A. Input-to-state safety with control barrier functions. *IEEE Control Systems Letters*, v. 3, n. 1, p. 108–113, Jan 2019.

KONG, H.; HE, F.; SONG, X.; HUNG, W.; GU, M. Exponential-condition-based barrier certificate generation for safety verification of hybrid systems. In: *Computer Aided Verification (CAV)*. Saint Petersburg, Russia: [s.n.], 2013. p. 242–257.

KUYUMCU, A.; SENGOR, N. Effect of neural controller on adaptive cruise control. In: *Artificial Neural Networks and Machine Learning (ICANN)*. Barcelona, Spain: [s.n.], 2016. p. 515–522.

LAMPORT, L. Proving the correctness of multiprocess programs. *IEEE Transactions on Control Engineering*, v. 3, n. 2, p. 125–143, Mar 1977.

LI, S.; GUO, Q.; XU, S.; DUAN, J.; LI, S.; LI, C.; SU, K. Performance enhanced predictive control for adaptive cruise control system considering road elevation information. *IEEE Transactions on Intelligent Vehicles*, v. 2, n. 3, p. 150–160, Sep 2017.

LI, S.; LI, K.; RAJAMANI, R.; WANG, J. Model predictive multi-objective vehicular adaptive cruise control. *IEEE Transactions on Control Systems Technology*, v. 19, n. 3, p. 556–566, May 2011.

LIU, B.; ZHOU, W. Backstepping based nonlinear adaptive control of magnetic levitation system with unknown disturbances. In: *International Conference on Intelligent Human-Machine Systems and Cybernetics*. Hangzhou, China: [s.n.], 2013. p. 11–14.

MAGDICI, S.; ALTHOFF, M. Adaptive cruise control with safety guarantees for autonomous vehicles. *IFAC-PapersOnLine*, v. 50, n. 1, p. 5774–5781, Jul 2017.

MATHWORKS. Mathworks student competitions team - matlab and simulink racing lounge: Vehicle modeling. 2021. Available in: <https://github.com/mathworks/vehicle-modeling/releases/tag/v4.1.1>. Accessed in: 28 Sep. 2021.

MATTINGLEY, J.; BOYD, S. Cvxgen: a code generator for embedded convex optimization. *Optimization and Engineering*, v. 13, n. 1, p. 1–27, Mar 2012.

MEHRA, A.; MA, W.; BERG, F.; TABUADA, P.; GRIZZLE, J.; AMES, A. Adaptive cruise control: experimental validation of advanced controllers on scale-model cars. In: *American Control Conference (ACC)*. Chicago, USA: [s.n.], 2015. p. 1411–1418.

MOON, S.; MOON, I.; YI, K. Design, tuning, and evaluation of a full-range adaptive cruise control system with collision avoidance. *Control Engineering Practice*, v. 17, n. 4, p. 442–455, Apr 2009.

MOON, S.; YI, K. Human driving data-based design of a vehicle adaptive cruise control algorithm. *Vehicle System Dynamics*, v. 46, n. 8, p. 661–690, Jun 2008.

MUEHLEBACH, M.; D'ANDREA, R. Nonlinear analysis and control of a reaction-wheel-based 3-d inverted pendulum. *IEEE Transactions on Control Systems Technology*, v. 25, n. 1, p. 235–246, Jan 2017.

NAGUMO, M. Uber die lage der integralkurven gewohnlicher differentialgleichungen. *Proceedings of the Physico-Mathematical Society of Japan. 3rd Series*, v. 24, p. 551–559, May 1942.

NAUS, G.; PLOEG, J.; MOLENGRAFT, M.; HEEMELS, W.; STEINBUCH, M. Design and implementation of parameterized adaptive cruise control: An explicit model predictive control approach. *Control Engineering Practice*, v. 18, n. 8, p. 882–892, Apr 2010.

NEVES, G.; ANGÉLICO, B.; AGULHARI, C. Robust h_2 controller with parametric uncertainties applied to a reaction wheel unicycle. *International Journal of Control*, p. 1–11, Jan 2019.

NGUYEN, Q.; SCREENATH, K. Safety-critical control for dynamical bipedal walking with precise footstep placement. *IFAC papers online*, v. 48, n. 27, p. 147–154, 2015.

NGUYEN, Q.; SREENATH, K. Exponential control barrier functions for enforcing high relative-degree safety-critical constraints. In: *American Control Conference (ACC)*. Boston, USA: [s.n.], 2016. p. 322–328.

NGUYEN, Q.; SREENATH, K. Optimal robust control for constrained nonlinear hybrid systems with application to bipedal locomotion. In: *American Control Conference (ACC)*. Boston, USA: [s.n.], 2016. p. 4807–4813.

NGUYEN, Q.; SREENATH, K. Optimal robust safety-critical control for dynamic robotics. *preprint arXiv:2005.07284*, p. 1–16, May 2020.

NORMEY-RICO, J.; CAMACHO, E. Dead-time compensators: A survey. *Control Engineering Practice*, v. 16, n. 4, p. 407–428, Apr 2008.

OGATA, K. *Discrete-time Control Systems*. [S.l.]: Prentice Hall, 1995.

OGATA, K. *Modern Control Engineering*. [S.l.]: Prentice Hall, 2009.

PARK, M.; CHWA, D. Swing-up and stabilization control of inverted-pendulum systems via coupled sliding-mode control method. *IEEE Transactions on Industrial Electronics*, v. 56, n. 9, p. 3541–3555, Sep 2009.

PENG, H. Evaluation of driver assistance systems - a human centered approach. In: *International Symposium on Advanced Vehicle Control (AVEC)*. Hiroshima, Japan: [s.n.], 2002.

POLACK, P.; DELPRAT, S.; NOVEL, B. Brake and velocity model-free control on an actual vehicle. *Control Engineering Practice*, v. 92, n. 8, p. 1–35, Nov 2019.

PRAJNA, S. Barrier certificates for nonlinear model validation. *Automatica*, v. 42, n. 1, p. 117–126, Jan 2006.

PRAJNA, S.; JADBABAIE, A. Safety verification of hybrid systems using barrier certificates. In: *International Workshop on Hybrid Systems: Computation and Control*. Philadelphia, USA: [s.n.], 2004. p. 477–492.

PRAJNA, S.; RANTZER, A. On the necessity of barrier certificates. *IFAC Proceedings Volumes*, v. 38, n. 1, p. 526–531, Jan 2005.

RAUSCHER, M.; KIMMEL, M.; HIRCHE, S. Constrained robot control using control barrier functions. In: *IEEE Conference on Decision and Control (CDC)*. Las Vegas, USA: [s.n.], 2016. p. 279–285.

RIZAL, Y.; MANTALA, R.; RACHMAN, S.; NURMAHALUDIN, N. Balance control of reaction wheel pendulum based on second-order sliding mode control. In: *International Conference on Applied Science and Technology (ICAST)*. Manado, Indonesia: [s.n.], 2018. p. 51–56.

ROMDLONY, M.; JAYAWARDHANA, B. Stabilization with guaranteed safety using control lyapunov–barrier function. *Automatica*, v. 66, p. 39–47, Apr 2016.

ROSOLIA, U.; AMES, A. Multi-rate control design leveraging control barrier functions and model predictive control policies. *IEEE Control Systems Letters*, v. 5, n. 3, p. 1007–1012, Jul 2021.

SAWANT, J.; CHASKAR, U.; GINOYA, D. Robust control of cooperative adaptive cruise control in the absence of information about preceding vehicle acceleration. *IEEE Transactions on Intelligent Transportation Systems*, v. 22, n. 9, p. 5589–5598, Sep 2021.

SLOTINE, J.; LI, W. *Applied Nonlinear Control*. [S.l.]: Prentice Hall, 1991.

SMITH, O. Closer control of loops with dead-time. *Chemical Engineering Process*, v. 53, n. 5, p. 217–219, 1957.

SON, T.; NGUYEN, Q. Safety-critical control for non-affine nonlinear systems with application on autonomous vehicle. In: *IEEE Conference on Decision and Control (CDC)*. Nice, France: [s.n.], 2019. p. 7623–7628.

SONTAG, E. A universal construction of artstein's theorem on nonlinear stabilization. *Systems and Control Letters*, v. 13, n. 2, p. 117–123, Aug 1989.

SPONG, M.; CORKE, P.; LOZANO, R. Nonlinear control of the reaction wheel pendulum. *Automatica*, v. 37, n. 11, p. 1845–1851, Nov 2001.

TAKANO, R.; OYAMA, H.; YAMAKITA, M. Application of robust control barrier function with stochastic disturbance model for discrete time systems. *IFAC papers online*, v. 51, n. 31, p. 46–51, Jan 2018.

TAYLOR, A.; SINGLETARY, A.; YUE, Y.; AMES, A. Learning for safety-critical control with control barrier functions. *Proceedings of Machine Learning Research*, p. 1–12, 2020.

TEE, K.; GE, S.; TAY, E. Barrier lyapunov functions for the control of output-constrained nonlinear systems. *Automatica*, v. 45, n. 4, p. 918–927, Apr 2009.

TRENTIN, J.; SILVA, S.; RIBEIRO, J.; SCHAUB, H. Inverted pendulum nonlinear controllers using two reaction wheels: design and implementation. *IEEE Access*, v. 8, p. 74922–74932, Apr 2020.

TSUJINO, T.; NAKASHIMA, K.; FUJII, T. Application of h_∞ control and closed loop identification to a magnetic levitation system. *Asian Journal of Control*, v. 1, n. 4, p. 283–296, Dec 1999.

TÜRKMEN, A.; KORKUT, M.; ERDEM, M.; GÖNÜL, O.; SEZER, V. Design, implementation and control of dual axis self balancing inverted pendulum using reaction wheels. In: *International Conference on Electrical and Electronics Engineering (ELECO)*. Bursa, Turkey: [s.n.], 2017. p. 717–721.

UTKIN, V.; GULDNER, J.; SHI, J. *Sliding Mode Control in Electro-Mechanical Systems*. [S.l.]: CRC Press, 2009.

VAHIDI, A.; ESKANDARIAN, A. Research advances in intelligent collision avoidance and adaptive cruise control. *IEEE Transactions on Intelligent Transportation Systems*, v. 4, n. 3, p. 143–153, Sep 2003.

VALENZUELA, J.; AVELAR, C.; GUZMÁN, S.; SANTIBÁNEZ, V. Adaptive neural network control for the trajectory tracking of the furuta pendulum. *IEEE Transactions on Cybernetics*, v. 46, n. 12, p. 3439–3452, Dec 2016.

WANG, L.; AMES, A.; EGERSTEDT, M. Safety barrier certificates for collisions-free multirobot systems. *IEEE Transactions on Robotics*, v. 33, n. 3, p. 661–674, Feb 2017.

WANG, Z.; WANG, J. Ultra-local model predictive control: A model-free approach and its application on automated vehicle trajectory tracking. *Control Engineering Practice*, v. 101, n. 2, p. 1–14, Aug 2020.

WIELAND, P.; ALLGOWER, F. Constructive safety using control barrier functions. *IFAC Proceedings Volumes*, v. 40, n. 12, p. 462–467, Aug 2007.

WU, C.; LIN, Y.; ESKANDARIAN, A. Cooperative adaptive cruise control with adaptive kalman filter subject to temporary communication loss. *IEEE Access*, v. 7, p. 93558–93568, Jul 2019.

WU, G.; SCREENATH, K. Safety-critical and constrained geometric control synthesis using control lyapunov and control barrier functions for systems evolving on manifolds. In: *American Control Conference (ACC)*. Chicago, USA: [s.n.], 2015. p. 2038–2044.

WU, G.; SREENATH, K. Safety-critical control of a planar quadrotor. In: *American Control Conference (ACC)*. Boston, USA: [s.n.], 2016. p. 2252–2258.

XIAO, L.; GAO, F. A comprehensive review of the development of adaptive cruise control systems. *Vehicle System Dynamics*, v. 48, n. 10, p. 1167–1192, Apr 2010.

XIAO, W.; BELTA, C. Control barrier functions for systems with high relative degree. In: *IEEE Conference on Decision and Control (CDC)*. Nice, France: [s.n.], 2019. p. 474–479.

XU, X. Constrained control of input–output linearizable systems using control sharing barrier functions. *Automatica*, v. 87, p. 195–201, Jan 2018.

XU, X.; TABUADA, P.; GRIZZLE, J.; AMES, A. Robustness of control barrier functions for safety critical control. *IFAC papers online*, v. 48, n. 27, p. 54–61, Oct 2015.

XU, X.; WATERS, T.; PICKEM, D.; GLOTFELTER, P.; EGERSTEDT, M.; TABUADA, P.; GRIZZLE, J.; AMES, A. Realizing simultaneous lane keeping and adaptive speed regulation on accessible mobile robot testbeds. In: *IEEE Conference on Control Technology and Applications (CCTA)*. Mauna Lani, USA: [s.n.], 2017. p. 1769–1775.

YANG, Y. Spacecraft attitude and reaction wheel desaturation combined control method. *IEEE Transactions on Aerospace and Electronic Systems*, v. 53, n. 1, p. 286–295, Feb 2017.

YI, K.; KWON, Y. Vehicle-to-vehicle distance and speed control using an electronic-vacuum booster. *JSAE Review*, v. 22, n. 4, p. 403–412, Oct 2001.

YU, W.; LI, X. A magnetic levitation system for advanced control education. In: *World Congress The International Federation of Automatic Control*. Cape Town, South Africa: [s.n.], 2014. p. 9032–9037.

ZENG, J.; ZHANG, B.; SCREENATH, K. Safety-critical model predictive control with discrete-time control barrier function. In: *American Control Conference (ACC)*. New Orleans, USA: [s.n.], 2021.

ZENG, J.; ZHANG, B.; SREENATH, K. Safety-critical model predictive control with discrete-time control barrier function. In: *American Control Conference (ACC)*. New Orleans, USA: [s.n.], 2021. p. 3882–3889.

ZHU, Y.; HE, H.; ZHAO, D. Lmi-based synthesis of string-stable controller for cooperative adaptive cruise control. *IEEE Transactions on Intelligent Transportation Systems*, v. 21, n. 11, p. 4516–4525, Nov 2020.

APPENDIX A – SONTAG'S UNIVERSAL CONTROL FORMULA

(ARTSTEIN, 1983) has given necessary and sufficient conditions for the existence of a CLF, which has been used to design a universal control law for nonlinear systems in (SONTAG, 1989).

Given a CLF $V(x)$, the system (2.1) has the small-control property w.r.t. $V(x)$ if for every $\varepsilon_{clf} > 0$ there exists a $\delta_{clf} > 0$ such that for every $0 < \|x\| < \delta_{clf}$ $\exists u \in \mathbb{R}^m$ such that $\|u\| < \varepsilon_{clf}$ and $L_f V(x) + L_g V(x)u < 0$ (SONTAG, 1989), (ROMDLONY; JAYAWARDHANA, 2016).

Using the notion of CLF, small-control property and considering the function $k_{so} : \mathbb{R} \times \mathbb{R} \times \mathbb{R}^m \to \mathbb{R}^m$ defined by

$$k_{so}(\gamma_{clf}, a, b) = \begin{cases} -\frac{a+\sqrt{a^{2}+\gamma_{clf}\|b\|^{4}}}{b^{T}b} b & if \quad b \neq 0 \\ 0 & otherwise, \end{cases} \tag{A.1}$$

Sontag has proposed an universal control law as summarized in the following theorem (SONTAG, 1989):

Theorem A.1. *Assume that the system (2.1) has a CLF $V(x)$ and satisfies the small-control property w.r.t. $V(x)$. Then the feedback law*

$$u = k_{so}(\gamma_{clf}, L_f V(x), (L_g V(x))^T) \quad \gamma_{clf} > 0, \tag{A.2}$$

is continuous and ensures that the closed-loop system is globally asymptotically stable.

APPENDIX B – RECIPROCAL CBF (RCBF)

Typically, $B(x)$ and $h(x)$ are related using (AMES et al., 2017)

$$B(x) = -log\left(\frac{h(x)}{1+h(x)}\right), \tag{B.1}$$

or

$$B(x) = \frac{1}{h(x)}. \tag{B.2}$$

Besides that, it is important to highlight that

$$\inf_{x\in Int(C)} B(x) \geq 0, \qquad \lim_{x\to\partial C} B(x) = \infty. \tag{B.3}$$

After the set C and safety have been defined, the RCBF $B(x)$ can formally be defined.

Definition B.1. *Consider the control system (2.1) and a set C defined by (2.2). A continuously differentiable function $B(x) : Int(C) \to \mathbb{R}$ is called a RCBF if there exist class κ functions $\alpha_1, \alpha_2, \alpha_B$, such that, for all $x \in Int(C)$ (AMES et al., 2017),*

$$\frac{1}{\alpha_1(h(x))} \leq B(x) \leq \frac{1}{\alpha_2(h(x))}, \tag{B.4}$$

$$\inf_{u\in U} \left[L_f B(x) + L_g B(x)u - \alpha_B(B(x))\right] \leq 0. \tag{B.5}$$

The class κ function is given in Definition 2.5.

Given a RCBF $B(x)$, for all $x \in Int(C)$, define the set (AMES et al., 2017)

$$K_{rcbf}(x) = \left\{u \in U : L_f B(x) + L_g B(x)u - \alpha_B(B(x)) \leq 0\right\}. \tag{B.6}$$

Considering control values in this set, the forward invariance of C is guaranteed by the following corollary:

Corollary B.1. *Consider a set C defined by (2.2) and let $B(x)$ be a RCBF for the system (2.1). Then any locally Lipschitz continuous controller $u : Int(C) \to U$ such that $u(x) \in K_{rcbf}(x)$ will render the set $Int(C)$ forward invariant (AMES et al., 2017).*

The controllers defined in (2.15) and (2.18) for the ZCBF $h(x)$, can be defined for the RCBF $B(x)$ respectively as:

$$\begin{aligned} \mathbf{u}^*(x) = & \underset{\mathbf{u}=(u,\delta)\in\mathbb{R}^m\times\mathbb{R}}{\arg\min} \ \tfrac{1}{2}\mathbf{u}^T H(x)\mathbf{u} + F(x)^T\mathbf{u} \\ s.t. \ \ & L_f V(x) + L_g V(x)u + c_V V(x) - \delta \leq 0, \\ & L_f B(x) + L_g B(x)u - \alpha_B(B(x)) \leq 0, \end{aligned} \tag{B.7}$$

$$\begin{aligned} \mathbf{u}^*(x) = & \underset{u\in\mathbb{R}^m}{\arg\min} \ u^T u - 2u_{no}^T u \\ s.t. \ \ & L_f B(x) + L_g B(x)u - \alpha_B(B(x)) \leq 0. \end{aligned} \tag{B.8}$$

Typically, we considered $\alpha_B(B(x)) = \gamma/B(x)$ as described in (2.11).

APPENDIX C – EXPLICIT SOLUTION

The work (IGARASHI; TEZUKA; NAKAMURA, 2019) shows that u_{cbf} can be obtained by:

$$u_{cbf} = \begin{cases} -\frac{I_h(x,u_{no})-J_h(x)}{\|L_gB(x)\|^2}(L_gB(x))^T & if \;\; I_h(x,u_{no}) > J_h(x) \\ 0 & if \;\; I_h(x,u_{no}) \leq J_h(x), \end{cases} \tag{C.1}$$

where functions $I_h : \mathbb{R}^n \times \mathbb{R}^m \to \mathbb{R}$ and $J_h : \mathbb{R}^n \to \mathbb{R}$ are defined by

$$\begin{aligned} I_h(x,u_{no}) &= L_fB(x) + L_gB(x)u_{no}, \\ J_h(x) &= K_hB(x) + C_h, \end{aligned} \tag{C.2}$$

where K_h and C_h are project parameters.

This formulation is obtained based on Gronwall's inequality given by the following theorem (GRONWALL, 1919), (IGARASHI; TEZUKA; NAKAMURA, 2019):

Theorem C.1. *Consider an absolute continuous non-negative function $z_h : [t_0, t_1] \to \mathbb{R}_{\geq 0}$ such that for any $t \in [t_0, t_1]$, the following inequality holds:*

$$z_h(t) \leq k_h(t) + \int_{t_0}^{t} z_h(s_h)v_{he}(s_h)ds_h, \tag{C.3}$$

where $k_h : [t_0, t_1] \to \mathbb{R}_{\geq 0}$ is a non-negative continuous differentiable function, and $v_{he} : [t_0, t_1] \to \mathbb{R}_{\geq 0}$ is a non-negative continuous function. Then, the following inequality holds for all $t \in [t_0, t_1]$:

$$z_h(t) \leq k_h(t_0) \exp\left(\int_{t_0}^{t} v_{he}(s_h)ds_h\right) \tag{C.4}$$

$$+ \int_{t_0}^{t} k_h'(s_h) \exp\left(\int_{s_h}^{t} v_{he}(r_h)dr_h\right) ds_h. \tag{C.5}$$

Particularly in the case of $k_h(t) = K_h(t - t_0) + C_h \geq 0$ and $v_{he}(x) = L_h \geq 0$, the following inequality holds:

$$z_h(t) \leq \left(L_h + \frac{C_h}{K_h}\right) e^{K_h(t-t_0)} - \frac{C_h}{K_h}. \tag{C.6}$$

Using Gronwall's inequality, (C.1) can be proved:

Proof. The derivative of $B(x)$ is calculated as follows:

$$\dot{B}(x) = \frac{dB}{dx}\frac{dx}{dt} = L_f B(x) + L_g B(x)u + L_g B(x)u_{no}. \tag{C.7}$$

Case 1 - $I_h(x, u_{no}) < J_h(x)$: The following inequality holds according to (C.7):

$$\dot{B}(x) = I_h(x, u_{no}) < J_h(x) = K_h B(x) + C_h. \tag{C.8}$$

Then,

$$\dot{B}(x) = L_f B(x) + L_g B(x)u + L_g B(x)u_{no} \leq K_h B(x) + C_h. \tag{C.9}$$

Case 2 - $I_h(x, u_{no}) > J_h(x)$: Substitute (C.1) into (C.7), and the following equality holds:

$$\dot{B}(x) = J_h(x) = K_h B(x) + C_h. \tag{C.10}$$

Then, the following inequality holds according to Gronwall's inequality:

$$B(t) \leq B(t_0)\exp(K_h t) + \frac{C_h}{K_h}\exp(K_h t) - \frac{C_h}{K_h}. \tag{C.11}$$

Therefore for any $t \geq 0$, $B(x) < \infty$. □

APPENDIX D – HIGH ORDER CBF (HOCBF)

Considering a r^{th} order differentiable function $h(x,t) : \mathbb{R}^n \times [t_0, \infty) \to \mathbb{R}$, we define a series of functions $\psi_{h_0} : \mathbb{R}^n \times [t_0, \infty) \to \mathbb{R}, \psi_{h_1} : \mathbb{R}^n \times [t_0, \infty) \to \mathbb{R}, \psi_{h_2} : \mathbb{R}^n \times [t_0, \infty) \to \mathbb{R}, ..., \psi_{h_r} : \mathbb{R}^n \times [t_0, \infty) \to \mathbb{R}$ in the form (XIAO; BELTA, 2019):

$$\begin{aligned} \psi_{h_0}(x,t) &:= h(x,t), \\ \psi_{h_1}(x,t) &:= \dot{\psi}_{h_0}(x,t) + \alpha_{h_1}(\psi_{h_0}(x,t)), \\ &\vdots \\ \psi_{h_r}(x,t) &:= \dot{\psi}_{h_{r-1}}(x,t) + \alpha_{h_r}(\psi_{h_{r-1}}(x,t)), \end{aligned} \tag{D.1}$$

where $\alpha_{h_1}(\cdot), \alpha_{h_2}(\cdot), ..., \alpha_{h_r}(\cdot)$ denote class κ functions of their argument. The class κ functions are given in Definition 2.5.

We further define a series of sets $C_{h_1}(t), C_{h_2}(t), ..., C_{h_r}(t)$ related to (D.1) in the form (XIAO; BELTA, 2019):

$$\begin{aligned} C_{h_1}(t) &:= \{x \in \mathbb{R}^n : \psi_{h_0}(x,t) \geq 0\}, \\ C_{h_2}(t) &:= \{x \in \mathbb{R}^n : \psi_{h_1}(x,t) \geq 0\}, \\ &\vdots \\ C_{h_r}(t) &:= \left\{x \in \mathbb{R}^n : \psi_{h_{r-1}}(x,t) \geq 0\right\}. \end{aligned} \tag{D.2}$$

Definition D.1. *Let $C_{h_1}(t), C_{h_2}(t), ..., C_{h_r}(t)$ be defined by (D.2) and $\psi_{h_0}(x,t), \psi_{h_1}(x,t), ..., \psi_{h_r}(x,t)$ be defined by (D.1). A function $h(x,t) : \mathbb{R}^n \times [t_0, \infty) \to \mathbb{R}$ is a HOCBF of relative-degree r for the system (2.1) if there exist differentiable class κ functions $\alpha_{h_1}(\cdot), \alpha_{h_2}(\cdot), ..., \alpha_{h_r}(\cdot)$ such that (XIAO; BELTA, 2019)*

$$\begin{aligned} &L_f^r h(x,t) + L_g L_f^{r-1} h(x,t) u + \tfrac{\partial^r h(x,t)}{\partial t^r} \\ &+ O_h(h(x,t)) + \alpha_{h_r}(\psi_{h_{r-1}}(x,t)) \geq 0, \end{aligned} \tag{D.3}$$

for all $(x,t) \in C_{h_1}(t) \cap C_{h_2}(t) \cap, ..., \cap C_{h_r}(t) \times [t_0, \infty)$. In the above equation, $O_h(\cdot)$ denotes the remaining Lie derivatives along f and partial derivatives with respect to t with degree

less than or equal to $r-1$.

Given a HOCBF $h(x,t)$, we define the set of all control values that satisfy (D.3) as:

$$K_{hocbf} = \left\{ \begin{array}{l} u \in U : L_f^r h(x,t) + L_g L_f^{r-1} h(x,t) u \\ + \frac{\partial^r h(x,t)}{\partial t^r} + O_h(h(x,t)) + \alpha_{h_r}(\psi_{h_{r-1}}(x,t)) \geq 0 \end{array} \right\}. \tag{D.4}$$

Theorem D.1. *(XIAO; BELTA, 2019) Given a HOCBF* $h(x,t)$ *from Definition D.1 with the associated sets* $C_{h_1}(t), C_{h_2}(t), ..., C_{h_r}(t)$ *defined by (D.2), if* $x(t_0) \in C_{h_1}(t_0) \cap C_{h_2}(t_0) \cap, ...,$
$\cap\, C_{h_r}(t_0)$*, then any Lipschitz continuous controller* $u \in K_{hocbf}$ *renders the set* $C_{h_1}(t) \cap C_{h_2}(t) \cap, ..., \cap C_{h_r}(t)$ *forward invariant for the system (2.1).*

The relationship between HOCBF and ECBF can be described as the following Remark:

Remark D.1. *In the Definition D.1, we set class* κ *functions*

$$\begin{aligned} \alpha_{h_1} &:= k_{b_1} \psi_{h_0}(x,t), \\ \alpha_{h_2} &:= k_{b_2} \psi_{h_1}(x,t), \\ &\vdots \\ \alpha_{h_r} &:= k_{b_r} \psi_{h_{r-1}}(x,t), \end{aligned} \tag{D.5}$$

where $k_{b_1} > 0, k_{b_2} > 0, ..., k_{b_r} > 0$*. If we substitute (D.5) in (D.1), consider the series of sets (D.2) and the condition (D.3), then we can get the same formulation of ECBF (XIAO; BELTA, 2019).*

APPENDIX E – LINEAR QUADRATIC REGULATOR (LQR)

E.1 Continuous-Time LQR

Consider a system represented by:

$$\dot{x} = A_c x + B_c u, \tag{E.1}$$

where A_c is the state matrix and B_c is the input matrix.

LQR is an optimal regulator that, given the system equation (E.1), determines the matrix K_c of the optimal control vector

$$u = -K_c x \tag{E.2}$$

so as to minimize the performance index

$$J_c = \int_0^\infty \left(x^T Q_c x + u^T R_c u \right) dt, \tag{E.3}$$

where Q_c is a positive-semidefinite matrix and R_c is a positive-definite matrix. These matrices are selected to weight the relative importance of the state vector x and the input u on the performance index minimization (OGATA, 2009).

If there exists a positive-definite matrix P_c satisfying the Riccati equation

$$A_c^T P_c + P_c A_c - P_c B_c R_c^{-1} B_c^T P_c + Q_c = 0, \tag{E.4}$$

then the closed-loop system is stable. Thus, the optimal matrix K_c can be obtained by

$$K_c = R_c^{-1} B_c^T P_c. \tag{E.5}$$

E.2 Discrete-Time LQR

In discrete-time, (E.1) is represented as

$$x_{k+1} = G_d x_k + H_d u_k, \tag{E.6}$$

where G_d is the state matrix and H_d is the input matrix.

The discrete-time LQR controller has the form

$$u_k = -K_d x_k \tag{E.7}$$

where the matrix K_d is such that minimizes the performance index

$$J_k = \frac{1}{2} \sum_{k=0}^{\infty} \left[x_k^T Q_d x_k + u_k^T R_d u_k \right], \tag{E.8}$$

where Q_d is a positive-semidefinite matrix and R_d is a positive-definite matrix. These matrices are selected to weight the relative importance of the state vector x_k and the input u_k on the performance index minimization (OGATA, 1995).

If there exists a symmetric matrix P_d satisfying the discrete Riccati equation

$$P_d = Q_d + G_d^T P_d G_d - G_d^T P_d H_d (R_d + H_d^T P_d H_d)^{-1} H_d^T P_d G_d, \tag{E.9}$$

thus, the optimal matrix K_d can be obtained by

$$K_d = (R_d + H_d^T P_d H_d)^{-1} H_d^T P_d G_d. \tag{E.10}$$

APPENDIX F – SLIDING MODE CONTROL (SMC) - MAGLEV SYSTEM

To generate a direct relationship between the output y_{ml} and the input w_{ml}, the output must be differentiated twice and we obtain:

$$\ddot{y}_{ml} = f_{ml_y}(x_{ml}) + g_{ml_y}(x_{ml})w_{ml}, \tag{F.1}$$

where

$$f_{ml_y}(x_{ml}) = \begin{bmatrix} f_{ml_{y11}} & f_{ml_{y12}} & f_{ml_{y13}} \end{bmatrix}^T, \tag{F.2}$$

$$f_{ml_{y11}} = g + l_{1g}\sec^2\theta_p Mgd_{ml}\sin\theta_p/J_{pm} - 2l_{1g}\tan\theta_p\sec^2\theta_p\dot{\theta}_p^2, \tag{F.3}$$

$$\begin{aligned} f_{ml_{y12}} &= g - l_{2g}\sec^2\theta_p Mgd_{ml}\sin\theta_p/J_{pm} + 2l_{2g}\tan\theta_p\sec^2\theta_p\dot{\theta}_p^2 \\ &+ l_{3g}\sec^2\theta_r Mgd_{ml}\sin\theta_r/J_{rm} - 2l_{3g}\tan\theta_r\sec^2\theta_r\dot{\theta}_r^2, \end{aligned} \tag{F.4}$$

$$\begin{aligned} f_{ml_{y13}} &= g - l_{2g}\sec^2\theta_p Mgd_{ml}\sin\theta_p/J_{pm} + 2l_{2g}\tan\theta_p\sec^2\theta_p\dot{\theta}_p^2 \\ &- l_{3g}\sec^2\theta_r Mgd_{ml}\sin\theta_r/J_{rm} + 2l_{3g}\tan\theta_r\sec^2\theta_r\dot{\theta}_r^2, \end{aligned} \tag{F.5}$$

$$g_{ml_y}(x_{ml}) = \begin{bmatrix} g_{ml_{y11}} & g_{ml_{y12}} & g_{ml_{y13}} \\ g_{ml_{y21}} & g_{ml_{y22}} & g_{ml_{y23}} \\ g_{ml_{y31}} & g_{ml_{y32}} & g_{ml_{y33}} \end{bmatrix}, \tag{F.6}$$

$$g_{ml_{y11}} = \left[-1/M - (l_{1g}^2\sec^2\theta_p)/J_{pm}\right](k_1/r_1^2), \tag{F.7}$$

$$g_{ml_{y12}} = \left[-1/M + (l_{1g}l_{2g}\sec^2\theta_p)/J_{pm}\right](k_2/r_2^2), \tag{F.8}$$

$$g_{ml_{y13}} = \left[-1/M + (l_{1g}l_{2g}\sec^2\theta_p)/J_{pm}\right](k_3/r_3^2), \tag{F.9}$$

$$g_{ml_{y21}} = \left[-1/M + (l_{1g}l_{2g}\sec^2\theta_p)/J_{pm}\right](k_1/r_1^2), \tag{F.10}$$

$$g_{ml_{y22}} = \left[-1/M - (l_{2g}^2\sec^2\theta_p)/J_{pm} - (l_{3g}^2\sec^2\theta_r)/J_{rm}\right](k_2/r_2^2), \tag{F.11}$$

$$g_{ml_{y23}} = \left[-1/M - (l_{2g}^2\sec^2\theta_p)/J_{pm} + (l_{3g}^2\sec^2\theta_r)/J_{rm}\right](k_3/r_3^2), \tag{F.12}$$

$$g_{ml_{y31}} = \left[-1/M + (l_{1g}l_{2g}\sec^2\theta_p)/J_{pm}\right](k_1/r_1^2), \tag{F.13}$$

$$g_{ml_{y32}} = \left[-1/M - (l_{2g}^2 \sec^2\theta_p)/J_{pm} + (l_{3g}^2 \sec^2\theta_r)/J_{rm}\right](k_2/r_2^2), \tag{F.14}$$

$$g_{ml_{y33}} = \left[-1/M - (l_{2g}^2 \sec^2\theta_p)/J_{pm} - (l_{3g}^2 \sec^2\theta_r)/J_{rm}\right](k_3/r_3^2). \tag{F.15}$$

Consider a time-varying surface S_{ml_c} defined by the scalar equation

$$s_{ml_c}(y_{ml}, t) = \dot{\tilde{y}}_{ml} + \lambda_{ml_c}\tilde{y}_{ml}, \tag{F.16}$$

where $y_{ml_d} = [r_{1_d} \;\; r_{2_d} \;\; r_{3_d}]^T$ is the output desired values, $\tilde{y}_{ml} = y_{ml} - y_{ml_d}$ and λ_{ml_c} is composed by strictly positive constants. The problem of tracking $y_{ml} = y_{ml_d}$ is equivalent to that of remaining on the surface S_{ml_c} for all $t > 0$. Furthermore, $s_{ml_c} = 0$ represents a linear differential equation whose unique solution is $\tilde{y}_{ml} = 0$; thus, the problem of tracking y_{ml_d} can be reduced to that of keeping the scalar quantity s_{ml_c} to zero (KHALIL, 2002), (SLOTINE; LI, 1991).

The problem of keeping s_{ml_c} at zero can be achieved by choosing a control law such that s_{ml_c} satisfies

$$\frac{1}{2}\frac{d}{dt}s_{ml_c}^2 \leq -\eta_{ml_c}\left|s_{ml_c}\right|, \tag{F.17}$$

being η_{ml_c} composed by strictly positive constants. The condition (F.17), called sliding condition, demonstrates that, once on the surface, the system trajectories remains it, i.e., the surface is an invariant set. Therefore, model uncertainties and disturbances can be tolerated. S_{ml_c} is denominated sliding surface, and the system's behaviour once on the surface is called sliding mode (UTKIN; GULDNER; SHI, 2009), (SLOTINE; LI, 1991).

In the SMC design, a feedback control law, called equivalent control, is determined to maintain the system in sliding mode, i.e., $\dot{s}_{ml_c} = 0$. However, in order to deal with model uncertainties and disturbances, the control law has to be discontinuous across S_{ml_c} (KHALIL, 2002), (SLOTINE; LI, 1991).

Using (F.1), it can be obtained

$$\dot{s}_{ml_c} = \ddot{y}_{ml} - \ddot{y}_{ml_d} + \lambda_{ml_c}\dot{\tilde{y}}_{ml} = f_{ml_y} + g_{ml_y}w_{ml} - \ddot{y}_{ml_d} + \lambda_{ml_c}\dot{\tilde{y}}_{ml}. \tag{F.18}$$

The equivalent control $w_{ml_{eq}}$ designed using the nominal dynamics and that would achieve $\dot{s}_{ml_c} = 0$ is given by

$$w_{ml_{eq}} = \bar{g}_{ml_y}^{-1}(-\bar{f}_{ml_y} + \ddot{y}_{ml_d} - \lambda_{ml_c}\dot{\tilde{y}}_{ml}), \tag{F.19}$$

where f_{ml_y} and g_{ml_y} represent the real dynamics and $\bar{f}_{ml_y}$ and $\bar{g}_{ml_y}$ represent the nominal dynamics.

The control law given by

$$w_{ml} = w_{ml_{eq}} - \bar{g}_{ml_y}^{-1} K_{ml_c} \operatorname{sgn}(s_{ml_c}), \tag{F.20}$$

will drive y_{ml} to y_{ml_d} despite the uncertainties. Using (F.18) and the sliding condition (F.17), we obtain that

$$K_{ml_c} \geq (g_{ml_y}^{-1} \bar{g}_{ml_y})(\eta_{ml_c} + f_{ml_y}) - \bar{f}_{ml_y} + (I - g_{ml_y}^{-1} \bar{g}_{ml_y})(\ddot{y}_{ml_d} - \lambda_{ml_c} \dot{\tilde{y}}_{ml}), \tag{F.21}$$

where I is the identity matrix.

The discontinuous term in (F.20) generates a control switching that is necessarily imperfect, because switching is not instantaneous, and the value of s_{ml_c} is not known with infinite precision and is never exactly zero. This can lead to "chattering", i.e., undesirable high-frequency oscillation. To avoid "chattering", a boundary layer is applied in the neighboring of the sliding surface and the saturation function replaces the sign function (UTKIN; GULDNER; SHI, 2009), (SLOTINE; LI, 1991), such as

$$w_{ml} = w_{ml_{eq}} - \bar{g}_{ml_y}^{-1} K_{ml_c} \operatorname{sat}(s_{ml_c}/\Phi_{ml_c}), \tag{F.22}$$

where Φ_{ml_c} is the boundary layer thickness.

APPENDIX G – MODEL-FREE CONTROL

Consider that the system dynamics can be represented as the generic ultra-local model

$$y^{(\nu)} = \phi_{mf} + \alpha_{mf}\, u \tag{G.1}$$

in a short time window, where y is the system output, ν is the system order, ϕ_{mf} represents the unknown parts of the plant, including possible disturbances and α_{mf} is a constant parameter chosen by the designer. The choice of α_{mf} is obtained by trial and error until a good closed-loop performance is achieved.

Then, considering that α_{mf} is not precisely known ($\hat{\alpha}_{mf}$), an algebraic estimator is considered for obtaining $\hat{\phi}_{mf}$ (FLIESS; JOIN, 2013). With $\hat{\alpha}_{mf}$ and $\hat{\phi}_{mf}$, the ultra-local dynamics is canceled and the desired dynamics is imposed, such that

$$u = \frac{-\hat{\phi}_{mf} + y_d^{(\nu)} - (\text{desired dynamics for } e_{mf})}{\hat{\alpha}_{mf}}, \tag{G.2}$$

where y_d is the set-point and $e_{mf} = y - y_d$.

The following expressions are important to the development of the algebraic estimators:

$$\frac{c_{mf}}{s^{\alpha_{mf}}},\ \alpha_{mf} \geq 1,\ c_{mf} \in \mathbb{C} \ \leftrightarrow\ c_{mf}\frac{t^{\alpha_{mf}-1}}{(\alpha_{mf}-1)!}, \tag{G.3}$$

$$\frac{1}{s^{\alpha_{mf}}}\frac{d^n}{ds^n}Y(s) \ \leftrightarrow\ \frac{(-1)^n}{(\alpha_{mf}-1)!}\int_0^\infty (t-\tau_{mf})^{\alpha_{mf}-1}\tau_{mf}^n y(\tau_{mf})\, d\tau_{mf}. \tag{G.4}$$

Considering the first order system:

$$\dot{y} = \phi_{mf} + \alpha_{mf}\, u, \tag{G.5}$$

the goal is to cancel the ultra-local dynamics and impose a desired performance in the

form:

$$u = \frac{-\phi_{mf} + \dot{y}_d - K_P e_{mf}}{\alpha_{mf}}, \tag{G.6}$$

where K_P is proportional gain.

Note that:

$$sY(s) - y(0) = \frac{\phi_{mf}}{s} + \alpha_{mf} U(s) \tag{G.7}$$

and applying (d/ds) to cancel out $y(0)$, we have that:

$$Y(s) + s\frac{d}{ds}Y(s) = -s^{-2}\phi_{mf} + \alpha_{mf}\frac{d}{ds}U(s). \tag{G.8}$$

Multiplying the result by $1/s^2$, we obtain:

$$\frac{1}{s^2}Y(s) + \frac{1}{s}\frac{d}{ds}Y(s) = -\phi_{mf}\frac{1}{s^4} + \alpha_{mf}\frac{1}{s^2}\frac{d}{ds}U(s). \tag{G.9}$$

Considering the expressions (G.3) and (G.4), it follows that:

$$\phi_{mf} = -\frac{6}{t^3}\int_0^t (t - 2\tau_{mf}) y(\tau_{mf})\, d\tau_{mf} - \frac{6\alpha_{mf}}{t^3}\int_0^t (t\tau_{mf} - \tau_{mf}^2) u(\tau_{mf})\, d\tau_{mf}. \tag{G.10}$$

We consider a trapezoidal approximation within the window $T = NT_s$ and $a_{mf} = t_0 < t_1 < ... < t_{N-1} < t_N = b_{mf}$, i.e.:

$$\int_{a_{mf}}^{b_{mf}} f_{mf}(t)dt \approx \frac{T_s}{2}(f_{mf}(t_0) + 2f_{mf}(t_1) + 2f_{mf}(t_2) + \ldots + 2f_{mf}(t_{N-1}) + f_{mf}(t_N)). \tag{G.11}$$

Hence, for:

$$\phi_{mf} = -\frac{6}{t^3}\underbrace{\int_0^t f_1(\tau_{mf})\, d\tau_{mf}}_{I_1} - \frac{6\alpha_{mf}}{t^3}\underbrace{\int_0^t f_2(\tau_{mf})\, d\tau_{mf}}_{I_2}, \tag{G.12}$$

where $f_1(\tau_{mf}) = (t - 2\tau_{mf}) y(\tau_{mf})$ and $f_2(\tau_{mf}) = (t\tau_{mf} - \tau_{mf}^2) u(\tau_{mf})$, one can see that:

$$I_1 = \frac{T_s}{2}\left(f_1(\tau_0) + 2f_1(\tau_1) + 2f_1(\tau_2) + \ldots + 2f_1(\tau_{N-1}) + f_1(\tau_N)\right), \tag{G.13}$$

$$I_2 = \frac{T_s}{2}\left(f_2(\tau_0) + 2f_2(\tau_1) + 2f_2(\tau_2) + \ldots + 2f_2(\tau_{N-1}) + f_2(\tau_N)\right). \tag{G.14}$$

APPENDIX H – VEHICLE MODEL

The block CAR Model in Fig. 41 implements the complex model of the vehicle and can be obtained in (MATHWORKS, 2021). The internal blocks of the CAR model are presented in Fig. 45. The block Engine, presented in Fig. 46, implements a mapped engine model using power, air mass flow, fuel flow, exhaust temperature, efficiency and emission performance lookup tables. The block Driveline, presented in Fig. 47, implements an idealized fixed-gear transmission without a clutch or synchronization (block Transmission) and a differential as a planetary bevel gear train (block Rear Differential). The gear change mechanism is implemented with the state machine Transmission Shift Logic. The block Wheels & Brakes, presented in Fig. 48, implements the longitudinal behavior of four ideal wheels. Finally, the block Vehicle Dynamics, presented in Fig. 49, implements an one DOF rigid vehicle body with constant mass undergoing longitudinal motion.

Figure 45: Internal blocks of the CAR model in Simulink.

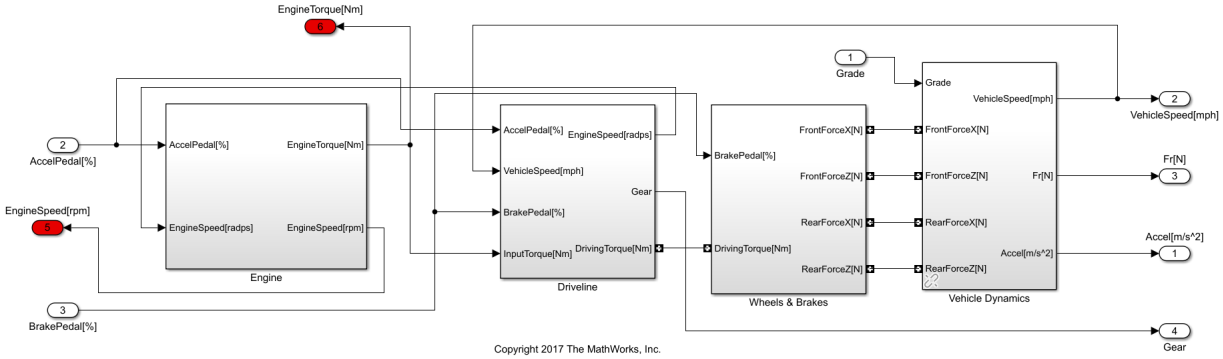

Source: Author.

Figure 46: Block Engine.

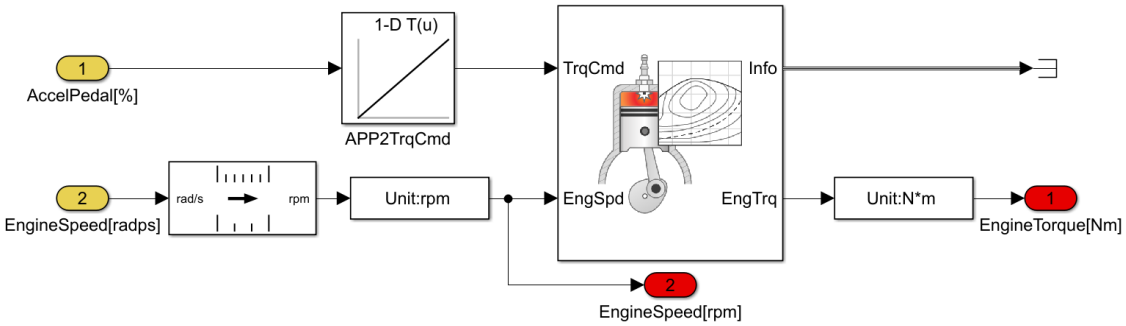

Source: Author.

Figure 47: Block Driveline.

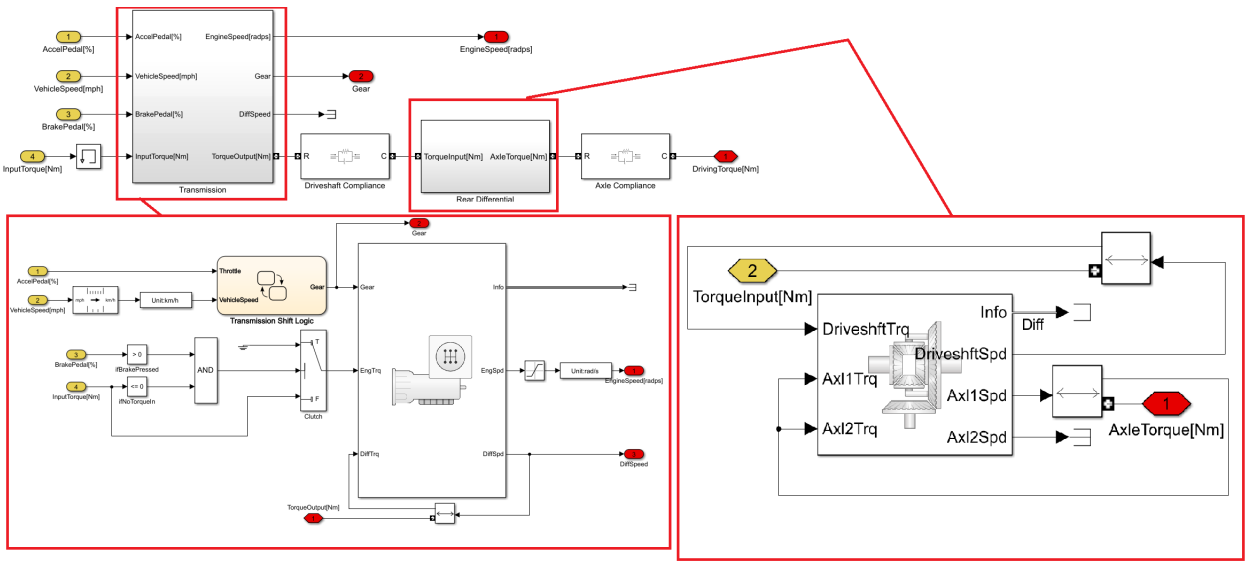

Source: Author.

Figure 48: Block Wheels & Brakes.

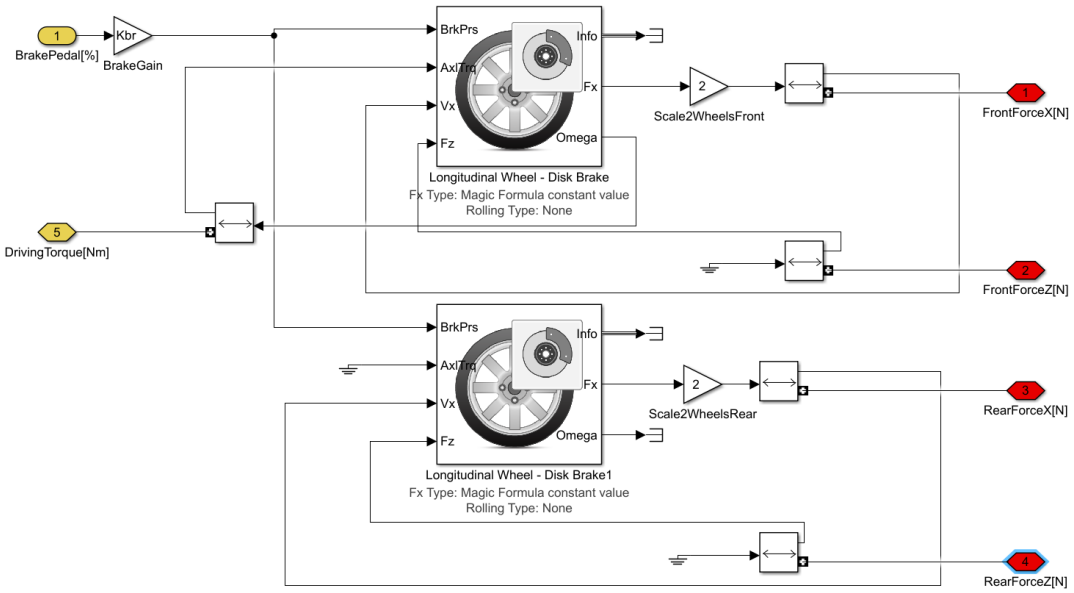

Source: Author.

Figure 49: Block Vehicle Dynamics.

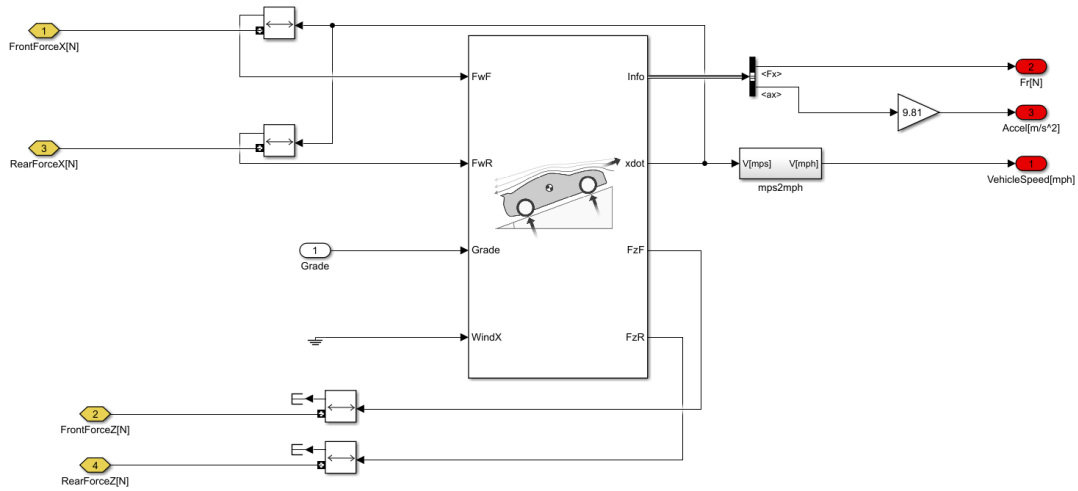

Source: Author.